# SPIRE Mapmaking Algorithm Review Report

Dave Clements, Pierre Chanial, George Bendo, Kevin Xu, Bernhard Schulz,
Tim Waskett, Bruce Sibthorpe, Glenn Laurent

September 16, 2006

## 1   Introduction

One of the key observational modes of the SPIRE instrument is the scan map mode. This will be used for all the imaging observations with SPIRE that require fields larger than a few arcminutes. There are numerous options for producing maps from scan map data ranging from simple rebinning methods to the more complex iterative approaches used by Cosmic Microwave Background experiments.

The original resources for Data Processing were such that the SPIRE ICC would not be able to provide a mapmaking system but would instead provide calibrated bolometer timelines that could then be fed into the user's favourite mapmaker. Over the last year ESA has decided that this is not a good solution, and that maps should be provided as a product produced by the standard data reduction pipeline (the Standard Product Generation (SPG) pipeline). It is therefore necessary for us to develop, code and test mapmaking code for the SPG on a fairly compressed timescale.

We have thus taken the decision to examine already-existing mapmaking algorithms, or simple derivatives thereof, to determine their suitability to be used for making maps from SPIRE scanmap data. We have selected a small number of test cases against which these algorithms can be tested, and have extracted a set of standard metrics that characterise how well a mapmaking algorithm performs when applied to this data. The current document is the result of this testing process and will be the main input for the Mapmaking Review that will select which algorithm(s) goes forward for coding into the DP system, and to become part of the SPG pipeline.

The rest of this report is laid out as follows. Firstly the goals of the Review are discussed. We then detail the three different sets of input models and the simulator that is used to take these input images and produce simulated SPIRE data. The mapmaking codes themselves are then discussed, followed by the metrics against which they will be judged. The results of these metrics are then summarised, with details given in the appendices, including other issues that may influence algorithm selection. Some conclusions are then drawn.

## 2   Goals of the Mapmaking Algorithm Review

This document is the main report that will form the basis for the selection of mapmaking algorithm(s) for SPIRE scan maps. The goal of the mapmaking review is to make this selection. A number of general considerations are also part of the selection process and must be considered alongside the results of the testing presented here.

- The mapping code selected will become part of the SPIRE SPG pipeline. This is a system that will run automatically. The selected algorithm

must therefore be capable of automatic operation with an absolute minimum level of interaction with the user. This is not to say that the algorithm selected should not be able to benefit from interaction with a user, merely that it should be able to perform adequately as part of an automatic pipeline without external assistance.

- The mapping code should produce 'good enough' results in a reasonable run time. Codes that take many hours to produce a wonderful image are appropriate for offline reduction by observers. They are not appropriate for the SPG.

- It is possible that more than one algorithm could be selected which perform well in different circumstances. If this is the case then it must be easy for an observer to specify which code would be better for their observations (eg. point source science vs. very extended source science).

- The selected algorithm should not place substantial constraints on how an observation is performed (eg. frequent calibrations or a large number of repeats should not be required). Such methods might be appropriate for specific observational strategies, but they will not have the general applicability that is needed for the SPG pipeline. Instead, the selected algorithm(s) must be able to cope with a wide variety of possible observing strategies and produce acceptable results for them all.

- The selected algorithm does not need to produce maps of the ultimate quality from the SPG. Optimisations for specific observing strategies or for specific science goals will be left to the observers. It These might be possible through modifying the parameters of the selected algorithm, but this should not be a major selection criterion for the algorithm(s) chosen.

- The ease or difficulty of programming the selected algorithm in Java as part of the SPG should also be considered, especially the need for numerical libraries which might not be available within the Herschel DP system. If an extensive range of new numerical libraries need to be available for a given algorithm this will considerably expand the work required to code it for the DP, and this may be a factor in deciding to select this algorithm.

At the end of the review the panel will select one (possibly two) algorithms which will go forward for development as elements of the SPG pipeline. This will involve their conversion to Java (or Jython) within the Herschel DP system. This work will take place over the next year at Imperial with the aid and assistance of the rest of the mapmaking team.

# 3   The Input Sky Models

## 3.1   The Test Points Field

The test points field consists of an 11x11 grid of point sources separated by 200". All the points in each column have the same flux density. The flux densities range from 0.0001 mJy in the left column to 10 mJy in the right column. The flux densities vary by factors of 100.5. This field is designed to test the effectiveness of the map-making software at reproducing isolated individual point sources.
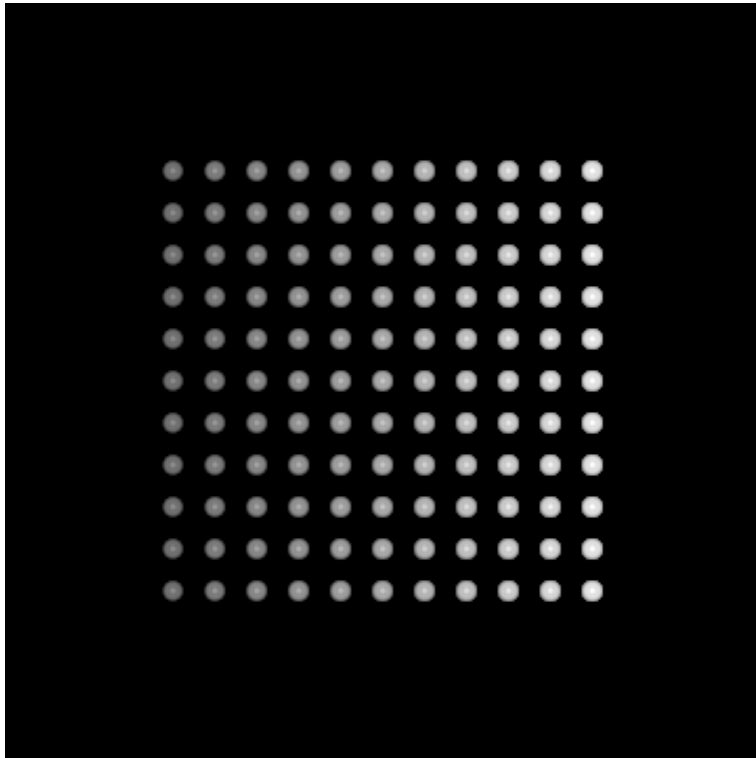
Figure 1: The Test Points Field

## 3.2 Galics Sky Models

The deepest observations that SPIRE is likely to undertake will be the high-redshift extra-galactic surveys to be performed as part of the Guaranteed Time program. To ensure that the map making routines are tested with data approximating this sort of observation a suitably realistic input sky is required for the simulator. To this end the hybrid N-body/semi-analytic model of hierarchical galaxy formation, GALICS (GALaxies In Cosmological Simulations; Hatton, 2003) was selected as a basis for these maps. Ignoring the details, the GALICS model effectively produces a synthetic Universe of galaxies  taking galaxy evolution and cosmology into account  that can be used to create catalogues of sources for any given wavelength. A simple web interface was used to extract a catalogue from GALICS covering a 1 square degree area of sky in the three SPIRE wavebands. In total 58590 sources were extracted down to a PSW flux limit of 2.05 mJy (c.f. a confusion limit of 40 beams per source results in  1000 sources per sq deg.)  This depth was considered to be sufficient to provide realistic confusion noise from faint, unresolved sources, even with ultra-deep SPIRE observations such as those planned for the GT program. Additionally, because the catalogue was extracted directly from the GALICS model the clustering properties of the galaxies are much more realistic than would be achieved if the sources were placed on the sky in a random fashion. This feature acts to increase the confusion noise above what would be expected from a Poisson distribution, and also increases the likelihood of closely separated and blended sources; a desirable consequence since this more closely resembles what the true situation is likely to be.

To double check the validity of the extracted catalogue the total flux provided by all the sources in each band was compared to measurements of the cosmic infra-red background. Although the shape of the IR background was well fit by the extracted GALICS catalogue the absolute level fell short in all three bands by a factor of 1.5. To remedy this situation the fluxes of

all sources were multiplied by 1.5 before the creation of the maps.

The Simulator input maps, created from the catalogue, have 2"x2" pixels. One map for each band was created. Each source in the catalogue has three fluxes, one for each band, and was added to the relevant map as a single pixel to represent a point source. If two or more sources fall into the same map pixel then the flux in that pixel ends up as the sum of the fluxes of all the contributing sources. Because the input maps are limited to 2" the truth list (effectively the catalogue) was also rounded to the nearest 2" so that the two agree.

## 3.3 Resolved Galaxies

These images were designed to test the ability of the map-making software to image resolved source such as debris disks, nearby galaxies, and supernova remnants. Such sources are scientifically-important targets for observation with SPIRE. The images themselves represent a test of the map-making software's ability to deal with extended sources. Some of the simulated targets are designed to be larger than the bolometer arrays so that, during some fraction of the scan-map observations, no background measurements (or measurements of empty sky) are made. Other sources are compact, so background measurements are always made by some part of the bolometer array. Two of the objects are simple axisymmetric structures; the other two are simulations of galaxies based on Spitzer data.

### 3.3.1 Small Exponential Disk

The small exponential disk has a radial profile defined by the function

$$f(r) = e^{-r/20''} \tag{1}$$

The disk is truncated at a radius of 80", so the diameter of the object is 2'.7. The total flux of the object is scaled to equal 100 Jy. The source is placed in the center of a 1 deg. x 1 deg. field, and the background is set to 0. This object should be similar to some small debris disks (such as Vega) and many nearby spiral galaxies with small angular sizes.

### 3.3.2 Large Exponential Disk

The large exponential disk has a radial profile defined by the function

$$f(r) = e^{-r/5'} \tag{2}$$

The disk is truncated at a radius of 20', so the diameter of the object is 40'. The total flux of the object is scaled to equal 1000 Jy. The source is placed in the center of a 1.5 deg. x 1.5 deg. field, and the background is set to 0. This object should be similar to some nearby galaxies with large angular sizes, particularly M81.

### 3.3.3 IC 4710

IC 4710 is a dwarf irregular galaxy with an angular size of 3'.6x2'.8. This source is a representative example of many nearby irregular galaxies.

The image used here is a rescaled version of the background-subtracted 24 $\mu$m Spitzer image of IC 4710. The total flux density of the object in the SPIRE wave bands is determined by fitting a blackbody modified by a $\nu^{-2}$ emissivity function to the 70 and 160 $\mu$m Spitzer flux density measurements and then extrapolating the function to the SPIRE wave bands. A background is calculated in a similar way using the median background levels
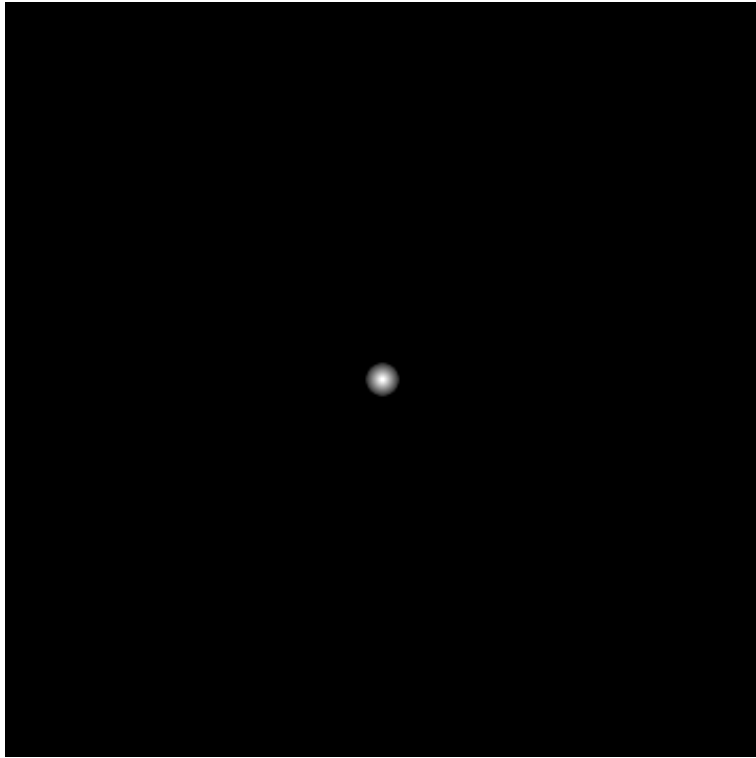
Figure 2: Small Exponential field
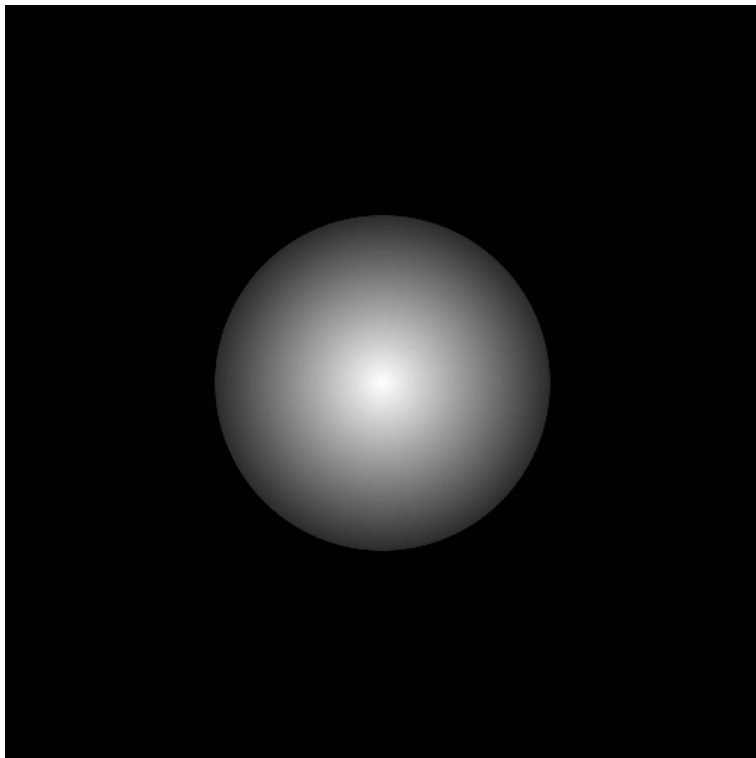


Figure 3: Large Exponential field
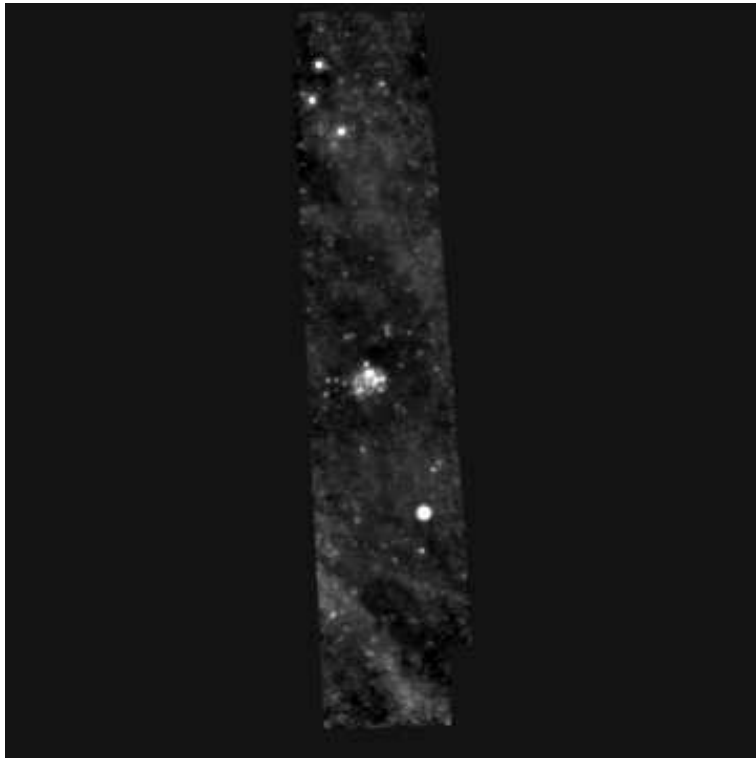
Figure 4: IC4710 field

measured in the 70 and 160 $\mu$m Spitzer data. The flux density of IC 4710 in the images is rescaled to match the values calculated for the SPIRE wave bands. The background expected for the SPIRE bands is then added into the map. The Spitzer scan map has been centered within a 1 deg. x1 deg. field. Pixels outside the Spitzer field but within the 1 deg. x1 deg. field have been set to equal the calculated median background level.

### 3.3.4 NGC 5194

NGC 5194 (M51A) is a well-known nearby spiral galaxy that is interacting with a companion object. The galaxy is 11'.2x6'.9.

The image used here is a rescaled version of the background-subtracted 24$\mu$m Spitzer image of NGC 5194. The image was created in the same way that the IC 4710 image was created. However, because of an error in the scaling process, the image is 3 times brighter than what is expected in Herschel observations.

### 3.4 Galactic Cirrus Sky

There are two forms cirrus sky, both developed by Phillippe André. The first contains only a cirrus cloud structure whose power spectrum has a gradient of 2.9, derived from the analysis of Gautier and Boulanger (1992). The resultant sky shows a flocculent structure on a wide range of scales, and is representative of the distribution of spatial scales expected within a Herschel-SPIRE observation of a star-forming region. The cirrus noise level is approximately 200 mJy/beam (at 250$\mu$m), higher than typical but not unrealistic for a high mass star forming region.

The second map contains the same cirrus structure but in addition contains a range of compact pre-stellar sources. The source models are simple Gaussians of approximately correct width. The mass function (flux distribution) of the sources follows the predicted core mass function derived by Motte et al. (2001), and uses the spatial distribution seen in an observed
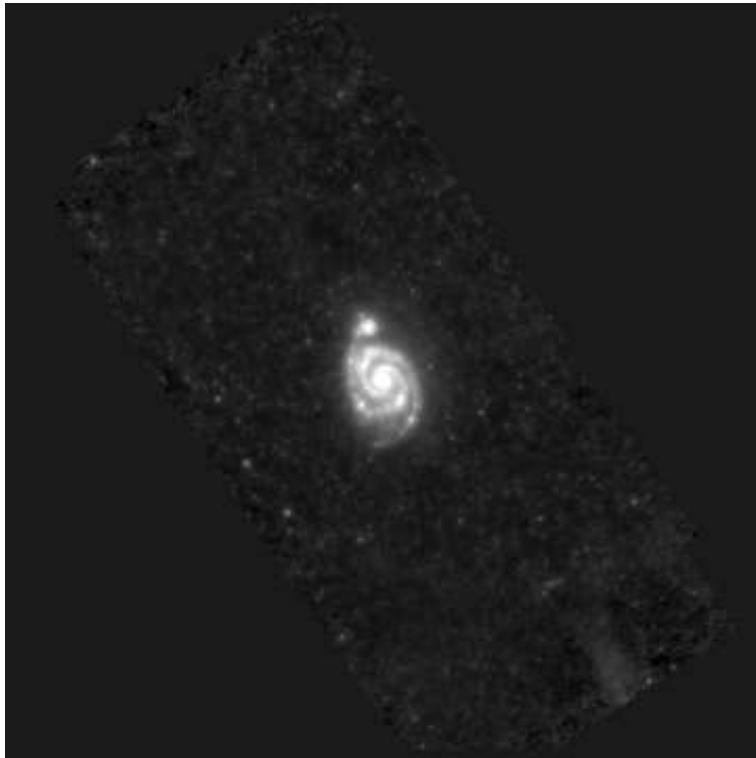
Figure 5: NGC5194 field

star cluster. The flux levels of the cirrus and core images are realistically scaled with respect to each other.

# 4 The Simulator and Simulations

## 4.1 The Simulator

The standard simulations used within this map-making exercise were produced using the SPIRE Photometer Simulator (SPS) V1.01. The SPS takes as an input an input sky in the form of a FITS file. Various instrumental parameters can then be adjusted in order to return a time ordered data set. These data include a telescope bore-sight pointing timeline, and detector voltage timelines for each detector are generated. A variety of photometer observing functions can be implemented with a range of noise conditions and instrument systematics applied. For more information regarding the operation of the SPS see Sibthorpe and Griffin (2006).

## 4.2 Standard Simulations

When producing the standard simulations it was assumed that the input data at the map-making stage would first have passed through some preliminary data cleaning processes. These processes were assumed to have removed all correlated 1/f noise, i.e. noise correlated across all detectors within an array; differences in detector responsivity, i.e. the data had been flat-fielded, and were deglitched to remove cosmic ray hits. As a result none of these attributes were present in the output simulator data.

The simulations all contained uncorrelated 1/f noise, i.e. noise specific to each detector, with a knee frequency of 100 mHz for all detectors. Further correlations were imposed in the data by the low pass filtering which occurs in the sampling phase of the detector readout. The operating temperature of the detectors remained static at 300 mK, resulting in no correlated

temperature variations in the output data.

Three scan map (POF 5) observations were produced for each input sky. A different magic scanning angle was used for each of the three scans, with the array remaining in a fixed orientation with respect to the input sky in all cases. These scans were designated as being in long, short, and diagonal directions with respect to the array, as defined in Waskett and Sibthorpe (2006). The size of scanned area varied depending on the specific input sky. The nominal scan rate of 30"/s was used for all observations.

Once generated, the simulator data were calibrated from V/beam to Jy/pixel, where the pixel size was 6, 10 and 14" for the PSW, PMW, and PLW bands respectively. This calibration was performed using a reference calibration performed during verification of the SPS.

While data was generated for all three SPIRE channels, full tests have only been carried out on PSW, with some additional tests performed on PLW data by way of a 'sanity check'. The reason for this that we do not expect there to be significant differences in mapping the different channels.

## 4.3  GALICS Simulations

The GALICS simulations used the same simulator parameters as the other standard simulations except for the scan pattern. High-z extra-galactic observations are necessarily deep because of the faintness of the sources involved and the three standard simulations do not reach the required sensitivity levels in this case. Therefore 20 simulations were performed instead of three. A different scan strategy was employed for this investigation in order to cover as much of the 1 square degree input map as possible (so that the largest number of sources are detected.) Two cross-linked scan patterns were performed, as shown by the following schematic.

The input map is shown by the black square while the two complementary scan patterns are shown in blue and red. The scan direction was either horizontal (blue) or vertical (red) with the array rotated 12.4 deg. relative to the long axis of the array. Each scan pattern was repeated 10 times so that the combination of all 20 simulations produce an observation that is approximately confusion limited.

For each simulation the length of the individual scan legs was 2740", the scan leg separation was 235" and 14 scan legs were performed. All other parameters were identical to the standard simulations. The scan pattern was designed so that the acceleration/deceleration plus turn-around data is always contained within the input maps. However, this means that the area covered to a uniform depth, with the arrays travelling at the constant scan speed, is only about 0.4 sq deg, as shown by the pale green square in the schematic.

# 5  Mapmaking Codes

## 5.1  Direct (or Naive) Mapmaking

This map-making technique performs no additional data-processing on the timelines. The data is simply re-mapped onto the image plane.

Blank maps of the sky are created to represent the total signal, the total of the squares of the signal, and the coverage. For each bolometer signal at each timestep, the signal measurement is added into the total signal map, the square of the signal is added into the total signal squared map, and 1 is added into the coverage map. After all bolometer signals have been mapped, the total signal map is divided by the coverage map to produce a
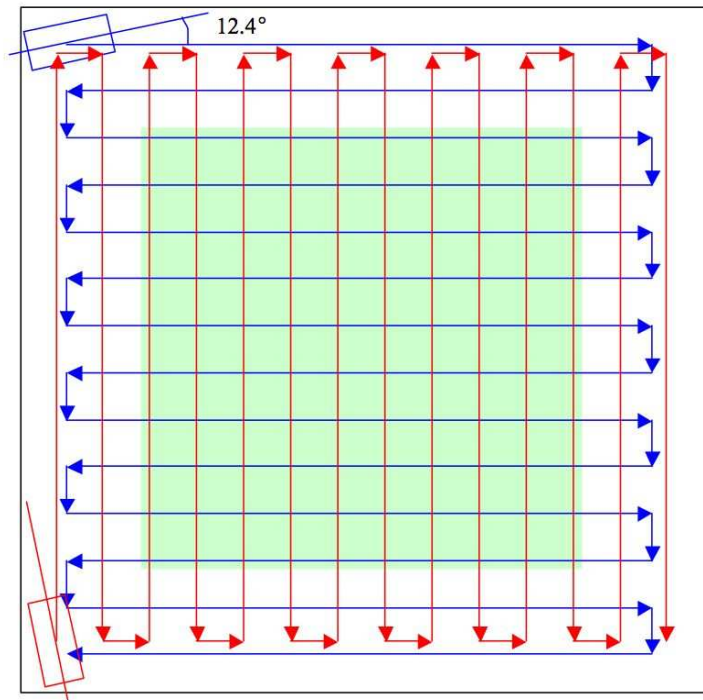
Figure 6: Scanning strategy for the GALICS field

flux density map, and the errors are calculated using the total signal, total signal squared, and coverage map.

## 5.2 Direct Mapping with Fourier 1/f Removal

### 5.2.1 Introduction

This map-making technique includes steps where the 1/f background noise is determined for individual bolometer timelines for each scan leg. These background measurements are then subtracted from the bolometer timelines to produce data without uncorrelated 1/f noise. This method includes a number of iterative steps whereby it attempts to automatically identify extended source emission so that it is not subtracted from the data.

### 5.2.2 Method

**Initial Map Production and Source Identification** A preliminary map is produced using the same method as the direct map-making method. Regions that lie more than 3 sigma above the median signal in the map are identified. These locations are noted in a map mask array.

**Median Timeine Extraction** For every timestep, the median of all bolometers (excluding bolometers where objects have been identified) is determined. This median signal timelime is used in the next step.

**Individual Bolometer Background Determination** Each individual bolometer timeline for each scan leg is Fourier filtered in several steps. First, the median signal timeline is subtracted from the bolometer timeline; this will be referred to as the residual bolometer timeline here. Next, the residual bolometer timeline is masked out where it crosses over bright objects, and then the values are replaced by interpolating over the missing values. Next, the residual bolometer timeline is transformed into Fourier space. The high-frequency portion of the signal is masked out to produce a Fourier-transformed background timeline, which is then transformed back into real space.

If any points in the residual bolometer timeline deviate more than 3 sigma from the background timeline, these deviant points are masked out from the residual signal timeline, new values are determined by interpolation, and the background is recalculated using the method above. This filtering process is repeated until no values in the residual bolometer timeline deviate more than 3 sigma from the background timeline. Once this bolometer signal has been determined, it is subtracted from the bolometer signal.

**Final Map Production** The individual maps are reproduced using the same methods as the direct map-making method.

## 5.3 MADMAP

MADmap is a tool written by Christopher Cantalupo to solve the system of linear equations

$$d_t = A_{tp}s_p + n_t \tag{3}$$

where $d_t$ is the time ordered data set (TOD) ($t$=1..$n$), $s_p$ is the pixelized map ($p$=1..$m$), $A_{tp}$ is the pointing matrix and $n_t$ the noise.

The maximum-likelihood estimate of the map, which is "brute-force" computed by MADmap, is

$$\hat{s} = \left(A^{\mathsf{T}}N^{-1}A\right)^{-1}A^{\mathsf{T}}N^{-1}d \tag{4}$$

where $N$ is the time-time noise covariance matrix.

### 5.3.1 Algorithm

Although MADmap can be used iteratively, in which case every iteration provides a better estimate of the map and by substracting it from the TOD, a better estimate of the time-time noise covariance matrix, we restricted our use of MADmap to only one iteration, by using the calibrated noise power spectrum.

To make Equation 4 computationally tractable, assumptions on $N^{-1}$ ($n \times n$ matrix) are made (piecewise Toeplitz and band-diagonal). It means that $N^{-1}$ acts like a set of convolutions with band limited kernels, which are straightforward operations in Fourier space.

The inversion of $A^{\mathsf{T}} N^{-1} A$ ($m \times m$ matrix) is then done by the preconditioned conjugate gradient method.

MADmap scales as $O(n)$ in time and memory, where n is the number of readouts.

### 5.3.2 Inverse time-time noise correlation matrix

Because we only perform one iteration, $N^{-1}$ is a crucial input. $N^{-1}$ is assumed to be piecewise Toeplitz, so for every chunk, it is represented by its first row, which we will refer as the inverse time-time noise correlation vector. We used the MADDEN utilities (written by Ted Kisner to interface Boomerang data with MADmap) to translate a TOD into a power spectrum and then into an inverse time-time noise correlation vector. An important parameter affecting the execution time and the residual standard deviation is the correlation length which is the number of contiguous correlated readouts.

## 5.4 MOPEX

### 5.4.1 Introduction

MOPEX (MOsaicking and Point source EXtraction) is a Spitzrer data reduction software, developed by David Makovoz. The map-making part of the software is called MOSAIC (http://ssc.spitzer.caltech.edu/postbcd/doc/overview-mosaicker.pdf). As the name implies, the basic function of MOPEX/MOSAIC is to mosaic small maps together and make a big map. It can do:

- Mosaicking with outlier detection

- Background matching

- Pointing refinement

It has the following features:

- Take 2-D FITS maps as input (does not allow data cubes).

- Highly modular. The whole process is divided into several modules, each can be run separately.

- Works with real astrometry. Can make really huge maps (as long as they are smaller than a hemisphere). Spatial information is derived from RA and Dec, calculated using the fits header. Several sky projection algorithms (e.g. TAN, SIN, ZEA, etc. ) are allowed.

- Include many interpolation algorithms. In principle can deal with any kind of pixel shapes, although with high cost in terms of processing time.

- No treatment for 1/f noise.

### 5.4.2 Interface between SPIRE data and MOPEX

In order to process SPIRE photometric scan data with MOPEX, the timeline data cube has to be broken into a set of regular FITS maps, with the spatial information saved in the fits header. One particular issue is that detectors in all three SPIRE photometer arrays are arranged in hexagonal patterns. The image of each frame cannot be directly written into a regular fits map, which assumes the pixels are arranged in a rectangular pattern. The solution we adopted is illustrated in the following figure. Basically we break each SPIRE frame into two FITS maps: one contains the even rows, another the odd rows.

### 5.4.3 1/f noise and high-pass filtering

A high pass filter, which can significantly reduce the 1/f noise, is applied to the time line data cube before it being sent to MOPEX. This is a simple moving-median filter, with high-pass frequency of 0.05, 0.033 and 0.025 Hz for the PSW, PMW and PLW band. With the scan rate of 30 arcsec/sec, this filters out signals on the scale of 600, 900 and 1200 arcsec in the data of the 3 bands, respectively. These scales are much larger than the sizes of corresponding PSFs, therefore will not cause any significant errors in the point source photometry. However, photometry of any extended sources with dimensions comparable or even larger than these spatial scales will lose significant amount of flux.

## 5.5 CM - Constrained Map-maker

### 5.5.1 Introduction

CM (Constrained Map-maker) is a generalized least-square (GLS) map-making code. It derives the least-square solution of the map-making equation

$$d_t = A_{tp} \times m_p + n_t \tag{5}$$

iteratively, with d = time ordered data, A = pointing matrix, m = signal, n = noise, t = time index, p = pointing index. The least squares variance to be minimized is

$$\chi^2 = (d_t - A_{tp}m_p)^T N_{tt'}^{-1}(d_{t'} - A_{t'p}m_p) \tag{6}$$

where the covariance matrix is

$$N_{tt'} = \sum_{i=0}^{n_p}(n_{i+t} - \overline{n})(n_{i+t'} - \overline{n}) \tag{7}$$

Originally, it was developed for CMB observations (e.g. Boomerang). Brendan Crill, one of the authors of CM, provided the code and know-how to NHSC at IPAC.

What CM can do:

- The algorithm derives the GLS estimates for both the signal and noise matrix from data directly (other tools such as Madmap require a-priori knowledge of the noise matrix).

- Can handle time-domain and map-domain constraints, and mode compensation.

Assumptions:

- Noise is piecewise stationary  ie. the noise covariance matrix only depends on the time lag between points t-t' and is therefore circulant.

- Time ordered data are continuous (so that Fourier transforms are meaningful).

If these assumptions hold, the operation $N_{tt'}^{-1}d_t$ is equivalent to filtering the data with the noise power spectrum.

### 5.5.2 Algorithm (iterative solver)

The mapmaking process is started with a naively binned map. Each estimate of the noise filter comes from taking the power spectrum density (PSD) of n = d  s.

For iteration $k$ calculate signal time ordered data:

$$s_i^{(k)} = N_{ii'}^{-1}d_{i'} + (1 - N_{ii'}^{-1})A_{i'p}\Delta_p^{(k)} \tag{8}$$

where $\Delta$ is the current estimate of the map, $A_{ip}$ is the pointing matrix. Next map estimate is:

$$\Delta_p^{k+1} = (A_{pi}^T A_{p'i'})^{-1}A_{pi}s_i \tag{9}$$

### 5.5.3 Interface between SPIRE data and CM

The IDL interface (cmwrap.pro) between the simulator data and the algorithm could be made flexible enough so that it appears to the user as one program, although the CM binary is called inbetween. The needed input parameters are: the names of the simulator files, the size of a skybin, the lowpass cutoff frequency, the number of iterations, and the name of the output FITS file. All other needed parameters are derived from the simulator output. The communication between the wrapper and the CM binary is performed via temporary files in a directory. The interface details are as follows.

- First the observed sky area is broken into sky bins, and an index (long integer) is assigned to each sky bin.

- Then for each SPIRE photometer detector channel, 3 files are created: one containing the actual signal time line, written as a binary sequence of 4 byte floating point numbers (It is assumed that the signal sampling is regular.), one consisting of a binary sequence of long integer numbers (4 bytes), containing the index of the sky bin, where the respective signal sample was taken, and a binary file consisting of a sequence of integer (2 bytes) numbers representing flags for the validity of the respective readout.

- A format file in ASCII describes the input format of the 3 files that were created for each detector channel.

- A chunk file is created containing entries in ASCII for each continuous signal timeline. Each entry gives the names of the 3 input files for its respective detector channel, start position and length of the signal timeline, sample frequency, highpass and lowpass frequencies etc.

- A spec file specifies the general options like number of iterations, name of the chunk file, number of bins used for the power spectrum, and the maximum number of sky bins.

- On return, CM produces a binary file that contains 4 blocks of the same length, consisting of 4 byte numbers. The blocks contain sky bin index (long integer), resulting signal (float), variance (float), and number of hits (long integer) respectively.

## 5.6 Bolocam

Bolocam is a 144 element bolometer camera in use at the CSO and elsewhere. It operates in a scanning mode not dissimilar to SPIRE. The data reduction software used for Bolocam has been adapted to allow it to reduce SPIRE scan map data for this current assessment. The Bolocam code has been used to successfully reduce data for a number of sources eg. Enoch et al., 2006. A brief description of the method based on this paper is included here. More details are available from Glenn Laurent.

### 5.6.1 Noise Removal

The sensitivity of a given observation is determined by the intrinsic sensitivity of and optical loading on the bolometers, the integration time, and the success of noise subtraction. The most important reduction step is the removal of noise, or cleaning. On scales comparable to or larger than the beam, bolocam is limited by $1/f$ noise. This noise is present in the bolometer timestreams before cleaning.

Correlated 1/f noise to first is identical for each bolometer and a template can be constructed quite simply by taking an average or median across the bolometer array at each point in time. This average cleaning method is appealingly simple, but does not deal well with multiple correlated $1/f$ noises with different correlation coefficients, or with $1/f$ noises that are correlated on spatial scales smaller than the array. In principle, correlated noise can be removed because it is correlated in time, whereas the astronomical signal is correlated in space across the array. A more sophisticated approach that addresses this issue is Principal Component Analysis (PCA) cleaning (see Laurent et al., 2005 and references therein for a discussion of PCA cleaning). In a PCA analysis the raw timestreams are projected along eigenvectors, bringing out common modes, or principal components, in the data. Patterns common to all bolometers correspond to correlated noise, so subtracting such common modes from the data is an efficient sky subtraction technique. Removing the first principal component is nearly equivalent to performing average subtraction.

Any number of components can be subtracted from the data, each removing progressively less correlated $1/f$ noise. The actual reduction in the RMS noise depends on the initial sky noise present, but typically removing 3 PCA components reduces the overall noise by $10 - 30\%$ compared to average cleaning. Although removing more components will reduce the noise further, the disadvantage of PCA cleaning is that higher components tend to remove source flux density (most of which can be recovered). Tests performed with Bolocam on both compact and extended sources indicate that removing between 1 and 5 components is most effective at eliminating stripes from $1/f$ noise while retaining source flux density and structure.

For bright and extended sources, a principal component analysis often removes a significant amount of source flux. In these cases a simple average sky subtraction is appropriate. Furthermore, much of the source signal that is removed via an average subtraction may be regained with an iterative cleaning technique (see below).

A sky template for each subscan is obtained by simply taking an average of all of the working bolometers for each time element,

$$S_i = \frac{\sum_{j=1}^{n_i} B_{\mathrm{raw},j,i}}{n_i},$$

where $S_i$ is the sky template (estimate of the correlated sky and instrument noise) for time element $i$, $B_{\mathrm{raw},j,i}$ is the signal for bolometer $j$ at time $i$, and

$n_i$ are the number of good bolometers for time element $i$. Note that $n_i$ may vary for each time element, as flagged bolometers due to cosmic rays, known sources, etc... are not included in the determination of the sky template.

The sky template is then mean subtracted to prevent the mean from skewing the correlation of the template to the individual bolometer time streams,

$$S_i' = S_i - \frac{\sum_{i=1}^{m} S_i}{m},$$

where $m$ is the number of time elements in the subscan. This mean-subtracted sky template is then correlated to each of the individual bolometer time streams to obtain the coefficient of correlated noise ($C_j$), which is the sky template corrected for the responsivity of each bolometer,

$$C_j = \frac{\sum_{i=1}^{m} S_i' B_{\text{raw},j,i}}{\sum_{i=1}^{m} S_i'}. \tag{10}$$

The cleaned bolometer time stream is then calculated by subtracting out the sky template, scaled by $C_j$,

$$B_{\text{clean},j,i} = B_{\text{raw},j,i} - C_j S_i'.$$

Finally, the mean of each time trace is subtracted to remove any remaining DC level,

$$B_{\text{clean},j,i}' = B_{\text{clean},j,i} - \frac{\sum_{i=0}^{m} B_{\text{clean},j,i}}{m}. \tag{11}$$

Note that for very bright sources (i.e. flux calibrators and pointing sources), multiple subscans for each bolometer are concatenated to ensure that the source contributes negligibly to the fit to the sky template (Equation 10) as well as preventing a negative trough around the source when performing the final mean subtraction (Equation 11).

### 5.6.2 Mapping and Calibration

To make a 2D pixel map from the bolometer timestreams, the pointing model and empirically derived pixel offsets are used to project each bolometer time sample onto an RA/Dec grid of pixel values. Timestreams are coadded using a weighted (by the inverse of the PSD) average. We bin the map at a resolution equal to 1/3 of the true instrumental resolution which gives sufficient hits per pixel for significant statistics without degrading the resolution. Given the nature of the instrument and observations, a single pixel in the map will contain data from many bolometers and possibly many scans. We refer to the coverage map as an image of the number of hits per pixel, or seconds per pixel, in the map. The coverage is dependent on pixel size, scan strategy, the number of bolometers, and the number of scans in the map.

To maximize the signal to noise of, and thus our chance of detecting, point sources, we optimally filter the map. Because the signal from a point source lies in a limited frequency band, we can use an optimal (Wiener) filter to attenuate $1/f$ noise at low frequencies, as well as high frequency noise above the signal band. Attenuating the $1/f$ noise reduces the overall RMS *per pixel* by $\sim \sqrt{3}$ (making the RMS/pixel $\sim$ RMS/beam), maximizing the probability of detection for faint point-like sources. The optimal filter $g(q)$ is given by:

$$g(q) = \frac{s^*(q)/J(q)}{\int |s(q)|^2 /J(q) d^2q} \tag{12}$$

where $q$ is the spatial wavenumber, $J(q)$ is the azimuthally averaged PSD, $s(q)$ is the Fourier transform of the beam, and $g(q)$ is normalized so that the peak brightness of point sources is preserved.

### 5.6.3 Iterative Mapping

Although they utilize different methods, both average and PCA cleaning contain a step that essentially removes the mean of each bolometer subscan. This step is necessary to eliminate noise, but when there is a bright source in a scan it biases the mean. Consequently, noise subtraction introduces negative lobes around bright sources, which are asymmetric in the scan direction. Furthermore, subscans containing sources tend to be underweighted in the coadded map because the source brightness contaminates the integrated PSD, causing a decrease in the weighting factor. Both effects tend to suppress source flux density and are mildly dependent on the brightness and structure of the source. There is an additional effect due to PCA cleaning that non-linearly removes the flux density of bright sources as more PCA components are removed. To correct for diminished source brightness and negative artifacts introduced by the above effects, we have developed an iterative mapping code that robustly restores lost flux density and structure to the map.

The iterative mapping algorithm we have implemented iteratively subtracts a source model from the real data (somewhat similar to CLEAN (, but working in the image plane). The following is a more robust method than using, for example, a source model comprised of the sum of many gaussians, because many of our sources are likely to be extended and non-gaussian. For the following, $j$ refers to bolometer number ($j = 1 - 81$), and $i$ refers to the iteration number ($i = 0 - N$, where the zeroth iteration $i = 0$ indicates raw or cleaned data before any source model has been subtracted). We begin with the raw timestream data, $t_{j,i=0}$. These data are sent through the cleaning and mapping process to produce the zeroth iteration map, $M_{i=0}$, which contains negative artifacts and is missing some fraction of the flux density of each source. Next, a cut is applied at $+N_\sigma \sigma$ to $M_{i=0}$, removing any negative pixels as well as most of the noise (pixels with values $\leq +N_\sigma$ times the RMS noise are set to zero). We now have a source model map, $M_i'$, our current best guess of the true source flux density.

From the source model $M_i'$ a model timestream $t_{j,i}'$ is generated for each bolometer and subtracted from the raw timestreams, $dt_{j,i} = t_{j,0} - t_{j,i}'$. The difference timestreams $dt_{j,i}$ contain residual source flux density that was missing from the original map. When the difference timestreams are subsequently cleaned and mapped to produce a residual map $dM_i$, there is much less contamination of the sky template by source brightness, so the negative artifacts are greatly reduced. A threshold cut at $+N_\sigma \sigma$ is again applied to $dM_i$ producing a residual source model $dM_i'$, which is added to the original source model to create a new source model for the next iteration ($M_{i+1}' = M_i' + dM_i'$). This process is iterated until there is no remaining residual source flux density in the difference timestream. After $N$ iterations, the final residual map $dM_N$, containing only noise and any source flux below the threshold cutoff, is added to the last source map to create the final map ($M_N = M_{N-1}' + dM_N$).

# 6 The Metrics

## 6.1 Point Sources (GALICS map and Test Grid

The goal of this exercise is to quantify the fidelity of any map-making code applied to a confused field (Galics simulations) and un-confused field (grid of test points). The metrics are measured against the ideal case of the input source catalogue used to create the simulator input maps. To do so, two intermediary steps are required.

- source extraction: after examination of a number of popular extraction tools such as SExtractor or APEX, we chose to use the IDL DAOPHOT tool, which has been developped for point sources.

- source cross-identification: the cross-identification between the input list and the extracted list is performed by the nearest neighbour method. The search radius is set to the HWHM of the PSW detector beam. To decrease the number of spurious cross-identifications, we used a truth list threshold (3 mJy for Galics and 0.1 mJy for the grid of test points) well below the completeness limit of the ideal noiseless map.

The main criteria for selecting the extraction tool and identification method were good performance and ease of use. The review panel should bear in mind that our goal was not to choose the absolute optimum methods of source extraction, but rather to quantify the performance of the map-making algorithms relative to each other.

### 6.1.1 Truth list vs. reconstructed source flux

Given the weighted difference $\Delta = (f_{\text{extracted}} - f_{\text{truth}})/f_{\text{truth}}$ between the reconstructed and input flux densities, we used the mean and standard deviation of $\Delta$ per bin of flux to assess the quality of the map-making algorithms.

At high flux levels the mean should tend towards zero. The standard deviation with respect to input flux increase for lower fluxes and this can be quantified and compared directly between different map-making processes.

The best map-making code is the one that has the mean closest to zero and the lowest standard deviation at any flux.

### 6.1.2 Completeness

We measured the total number of cross-identified sources and the fraction of cross-identified sources per flux bin. The map making code capable of revealing the greater number of sources and also the faintest sources should be considered the best. We note that for the Galics simulation, the number of detected sources is affected by confusion.

### 6.1.3 Number of spurious sources vs. flux

Inevitably there will be some sources detected in the output map that are not included in the input catalogue, through noise or map making artefacts. Extracted sources with no counterpart brighter than a threshold (3 mJy for Galics and 0.1 mJy for the grid of test points) are labelled as spurious sources and we measured the total number of spurious sources and the fraction of spurious sources per flux bin. This will increase with decreasing flux level in some sort of inverse of the completeness metrics. The lower the number of spurious sources detected the better the map making code.

## 6.2 Resolved Galaxies

These metrics are designed to measure the quantities that astronomers would typically measure within resolves sources of a finite width (such as nearby galaxies, supernovae, and debris disks). The metrics not only test the reliability of the map-making software in reproducing the integrated flux density of the objects in the test images, but they also test the abilities of the map-making software to reproduce the structures of the sources.

### 6.2.1 Total Flux Density Measurement

In this test, the total integrated flux density of the source (after background subtraction) is measured in both the original map and the reconstructed maps. This test determines whether the total flux density of an extended source can be reproduced, which is critically important for any photometric observation. The ratio of the flux densities is used to gage the map-making tool's effectiveness at this task.

### 6.2.2 Surface Brightness Comparison

This test compares the flux densities of the pixels in the reconstructed maps to the original maps. The comparison is made using pixels within the optical disk (or its equivalent) of each test object. Only pixels detected at the 5 sigma level or higher in the original image are used for this comparison. This test demonstrates whether the map-making software can reproduce the flux densities of both high-surface-brightness and low-surface brightness regions, especially within a target with complex structure. The measurements used to determine the quality of this comparison are the sum of the squares of the differences between the original and reconstructed map pixels and the median and standard deviation of the ratio between the original and reconstructed map pixels.

### 6.2.3 Radial Profile Comparison

This test compares the radial profile of the object in the original map to the radial profile of the object in the reconstructed map. Except for M51, the radial profile is measured up to the edge of the optical disk. In M51, the extraction is performed in a circle that is centered on the spiral galaxy NGC 5194 and that is truncated so as to exclude the dwarf galaxy NGC 5195. This test demonstrates whether the map-making software can reproduce the approximate shape of the objects and, in particular, whether the low surface brightness edges of the object can be reproduced accurately. The measurements used to determine the quality of this comparison are the median and standard deviation of the difference between the individual radial surface brightness measurements of the original and reconstructed radial profiles.

## 6.3 Galactic Cirrus

These metrics are designed to measure the flux density levels over multiple spatial scales so as to determine whether both large and small-scale structures are reproducible.

### 6.3.1 Surface Brightness Comparison

This test compares the signal (in flux density/arcsec$^2$) of the pixels in the reconstructed maps to the original maps after the maps have been rebinned using pixel scales that are a multiple of the input maps' pixel scales. The

comparison is made using pixels within the inner 20'x20' of the test map. This test demonstrates whether the map-making software can reproduce complex, large scale structures. The measurements used to determine the quality of this comparison are the sum of the squares of the differences between the original and reconstructed map pixels and the median and standard deviation of the ratio between the original and reconstructed map pixels. These measurements are made for each pixel scale.

## 6.4 Global Metrics

For each input map we also calculate two global metrics which provide general comparisons of the methods in addition to the specific tests applied to each map which are more orientated towards science goals (eg. point source selection).

### 6.4.1 The residual standard deviation

The standard deviation of the residuals has been calculated for all test images. This is a standard test for image reconstruction algorithms. To make the best use of the wide variety of test images, the standard deviation is calculated in the region of interest for the extended sources (see metrics associated with the extended sources) and in the regions of uniform coverage for the Galics and galactic field test images.

### 6.4.2 Execution time

The execution time has been measured for all test images. Because the algorithms have been tested on different hardware, the execution times have been normalized. The benchmark that we used, which computes Mandelbrot fractals, is vector and float intensive, and is reasonably well suited for normalizing the speed of non-IO limited map-making algorithms. The map-making algorithms that we used are written in C, except for the 'Fourier filtered' algorithm which is written in the slower interpreted IDL. We haven't attempted a quantitative normalization between IDL and C, but qualitatively, the conversion of the map-making algorithms to Java will increase the execution speed of the C-written algorithms but decrease that of the IDL-written algorithm.

# 7 The Results

## 7.1 Direct (or Naive) Mapmaking

This method is good at reproducing images of bright sources without introducing any biases into the data. In all maps, the ratio of the original flux levels to the flux levels in the output maps always equals 1. The key drawback to this approach is that low surface brightness regions are dominated by noise.

- **Cosmological fields** This software has difficulty reproducing images of point sources that are fainter than the 1/f noise. Consequently, the ability of this method to detect faint sources is limited.

- **Extended sources** This method works well in recreating the total flux of the extended sources. NGC 5194 and the small exponential disk are almost replicated perfectly. The fainter regions of the large exponential disk and IC 4710, however, are replicated poorly. This is demonstrated by the large dispersion in the regions with low signal in

both of these objects. However, the median ratio between the original and reconstructed pixels is always 1.

- Galactic fields This map-making routine generally produces good results, partly because of the high signal-to-noise levels in the data. Visually, the data look similar if not identical to the input data. The median ratio between reconstructed and original pixels (after the data is rebinned) is frequently close to 1.

### 7.1.1 Additional comments

- The software is generally easy to write and easy to run.

- Little computation time is used to process the data (aside from reading in the data). Typical run times are less than one minute.

- This technique can work with either single-scan maps or with cross-scanned maps.

### 7.1.2 Conclusions

This map-making method is a good, basic method for processing data that should be considered as a processing tool for bright sources (typically sources detectable with IRAS). This method is not suitable for fainter regions, where noise-removal techniques may produce superior results.

## 7.2 Direct Mapmaking with Fourier 1/f Removal

The technique works well in removing 1/f noise stripes in the images, and it can be used to reproduce the images of bright sources in relatively flat fields. However, it cannot be used to accurately reproduce low surface brightness features and it produces multiple artifacts when dealing with highly extended structures such as the galactic fields.

- **Cosmological fields** The map-making software does qualitatively and quantitatively improve the data in general. A greater number of sources are detectable in the maps compared to the nave map-making approach. However, for images with only a single scan direction, the 1/f noise is not filtered out. This could be a problem with the software identifying the 1/f noise as source emission. If the software were adjusted appropriately, the single scan direction maps would probably appear to be filtered. The technique also added a subtle background gradient to the images.

- **Extended sources.** The map-making software performs remarkably well in reproducing the images of NGC 5194 and the small exponential disk. The total flux density, the pixel-by-pixel surface brightnesses, and the radial profiles are reproduced to within a few percent. However, this map-making technique does not deal well with low surface brightness regions, partly because it cannot identify these sources as belonging to the target. Therefore, the surface brightnesses of IC 4710 and the large exponential disk in the reconstructed maps is low compared to the original maps. Note that this problem is partially (but incompletely) mitigated by having multiple scans, although it is unclear as to whether this improvement is a result of increasing the signal-to-noise in the data or having the cross-scan direction.

- **Galactic fields.** The major problems with this software are only found by visually inspecting the data. The software produces low-level stripe-like artifacts throughout the field that are the result of improper 1/f noise subtraction. In addition, the software is prone to producing stripes of unusually high or low pixels. These stripe-like artifacts contribute to relatively high standard deviations in the reconstructed/original pixel surface brightnesses when the data are rebinnied into large (>100") pixels.

### 7.2.1  Additional comments

- This map-making technique is difficult to explain and therefore may be difficult to understand. Therefore, it may be difficult to re-write the software.

- This technique infrequently produced odd streaks of bright or dark pixels at the edges of the frames.

- This technique was applied to data where it was assumed that no information was available when the telescope shifts from the end of one scan leg to the beginning of the next. If data were available during this turn-around period, it would allow for a much better Fourier analysis where a single background function can be fit to an individual bolometer's timeline for the whole observation. Such an analysis would lead to a better characterization of the noise and also mitigate most of the problems with the bright/dark streaks in the images.

### 7.2.2  Conclusions

This technique works in reproducing bright sources that are smaller than 15', although some adjustments are needed to deal with point sources. However, it cannot accurately reproduce extended low surface brightness sources, and it adds noise to high-surface brightness extended emission (as seen in the galactic fields). This software therefore may be unsuitable for extended sources in general.

## 7.3  MADMAP

All test images were processed non-interactively by using the same set of input parameters, except the inverse time-time noise correlation vector because all test image simulations do not have the same detector characteristics

- 1/f knee of 0.100 Hz (requirement) for non-Galics simulations

- 1/f knee of 0.030 Hz (goal) for the Galics simulations

In consequence, the inverse time-time noise correlation vector has been derived from the signal power spectra of

- the first 4000 readouts of NGC 5194 (which scan the background) for non-Galics simulations.

- all readouts of the first horizontal scan for the Galics simulations.

For each simulation, the PSW detectors have the same noise characteristics, and we use the same inverse time-time noise correlation vector for all detectors by averaging the detector signal power spectra. A scan TOD is obtained by concatenating the 139 detector TODs. Cross-scan and multiple scan TODs are obtained by concatenating the scan TOD. We stress

that MADmap can handle different detector noise characteristics seamlessly because an inverse time-time noise correlation vector is assigned to every chunk of the input TOD.

### 7.3.1 Discussion

Pros:

- Fast.

- Simplicity: MADmap only takes as input the inverse time-time noise correlation vector and the TOD. Work on the inverse time-time noise correlation vector would be coded in another module.

- Robust: we have not encountered difficulties in producing maps of any test image. The execution time and the map standard deviation do not vary significantly from one test image simulation to another. We note that MADmap is widely used in the CMB community.

- Java conversion: MADmap is very high quality and very well commented parallel code. Even if we do not take advantage of it, the fact that MADmap processing can be distributed has put constraints on the code architecture and has resulted in a clear workflow, which in turn would facilitate the translation of MADmap from C to Java. One of the creators of MADmap (Andrew Jaffe) is based at Imperial, so this would ease any conceptual difficulties during the coding into Java. Concerning the technical aspects, optimized Java libraries such as JMP (a sparse matrix library including preconditioned solvers) are available online and would significantly alleviate the coding effort.

- Bonus: by setting a noise correlation length of zero, MADmap produces direct ("naive") maps.

Cons:

- Needs to calculate the inverse time-time noise correlation vector. This can be calculated from any blank sky observations. It might be produced automatically from any given observation, but possible presence of bright sources in a randomly chosen OBSID means that it might be best to calculate this as a calibration product from known blank (or nearly blank) sky observations. The GTKP blank field survey programme could be used for this purpose, for example.

- Residual correlated noise across the bolometer array is not handled by MADmap, but we here assume that correlated noise has been removed by earlier stages of pipeline processing.

Potential improvements:

- Stripes around bright sources along the scan direction can be dealt with by masking high signal-to-noise pixels.

- For better results, MADmap could be used iteratively. Execution time would scale linearly with the number of iterations.

## 7.4 MOPEX

For each of the test cases, 4 PSW maps are made using the MOPEX software. Two are for the single scan observation, one with and another without high-pass filtering. Another two maps, again with and without high-pass filtering,

are for the cross-scan observation. The 20 scan simulations of Galics field was not processed because it takes too much time (see the discussion). As expected, in the maps with high-pass filtering, the striping due to the 1/f noise is greatly reduced. However, real signals in the maps of extended sources (e.g. NGC 5194) are also filtered out, as shown in the residual maps. Therefore the filtered map is useful only for point source observations.

### 7.4.1 Discussion

Pros:

- Robust: MOPEX is a well established map-making tool. It is very stable and robust.

- Versatile: Can do many things in addition to just bin and add. For example, can handle weird pixel shape, can reject outliers, can do pointing refinement, etc.

- 1/F noise: with the high-pass filtering, it can minimize the 1/f noise for point source observations.

Cons:

- Slow: It turned out that MOPEX is painfully slow. It takes more than an hour to process a single scan simulation of 1 deg$^2$. (Note: the execution time reported in the table for metrics results is not homogeneous in the sense that different cases were run on different machines.) Three factors make MOPEX so slow:

  1. work on individual frames, rather than on data cubes;
  2. the spatial re-grid is done with the real astrometry;
  3. highly modular, so it writes many intermediate products to the disk, taking a lot of I/O time.

- MOPEX is written in perl and C. With its author (Dave Makovoz) left from IPAC, it will be difficult to convert MOPEX to Java.

- It cannot deal with 1/f noise in the observations of extended sources.

## 7.5 CM

All test cases were processed automatically in the same way, with the same parameter set, using the IDL wrapper cmwrap.pro. To improve speed, the temporary directory was established on a local disk of the computer (mr-spock), where the tests were conducted, while general IO was between mr-spock and the NHSC file server nhscfs2.

After resolving a few technical issues concerning the data format used for communicating with CM, there remain two issues with potential impact on use for an automatic pipeline:

1) We found that setting the highest frequency (lowpass cutoff) that is still considered in the noise power spectrum is critical. This power spectrum is re-calculated in every iteration. If the noise drops towards higher frequencies due to a lowpass filter, the iterative process may be steered towards a false noise minimum. Setting this frequency to 5 Hz in correspondence to the existing 5 Hz lowpass filter in the SPIRE hardware seems to work. Higher cutoff frequencies have led to single detector scans going bad during iterations, or the algorithm not converging.

2) Another difficulty concerns the number of iterations. We find that iteration numbers of above 40 can lead to a condition, where the weights

per channel that can be displayed during processing, suddenly drop to zero, and no image is produced. For our tests we chose 30 iterations, which seems to be enough and doesnt lead to this condition in any of our test cases.

The resulting maps were produced quite fast and fully automatic in both, naive mode, and iterative mode. The extended cirrus map appears already quite good in naive mode, which is largely due to the large range of fluxes in this map, so that 1/f noise becomes meaningless for the overall appearance. In all cases we find that a single scan direction does not give enough constraints to CM to remove stripes. In these reconstructed maps the stripes vanish only in the region where the scans end, and the array moves to the start of the next parallel scan. Since the signal stream is not switched off during that time, the short perpendicular scans provide enough constraints to make the different scans fit together, demonstrating clearly the necessity for cross scanning observations. This effect can also be observed in all maps with scan directions crossing at a different angle than 90 deg, where parts of the scans do not overlap. We observe ringing artefacts before and after the detectors cross bright point sources. These dips below the background level appear most prominently in the single scanned maps and are somewhat alleviated in combinations of cross scanned maps.

### 7.5.1 Discussion

Pros:

- Is quite fast in both, naive and iterative mode.

- Removes 1/f noise in both, point source maps as well as structured extended source maps, provided there are scans in different directions.

- Has been demonstrated for the range of test cases to run like a pipeline without user intervention.

- Calculates noise spectrum in each iteration without making too many assumptions about the spectral shape, potentially being more robust against features in the noise spectrum.

Cons:

- The algorithm is iterative in nature, making it potentially less robust than fully deterministic algorithms.

- Currently the number of iterations is an input parameter. There is no mechanism yet to detect convergence beyond a certain threshold and stop.

- The code is written in sparsely commented pure C. Conversion into JAVA without significant loss in speed will take considerable developer effort.

### 7.6 Bolocam

Report delivered orally.

Extended sources presented severe problems.

## 8 Discussion

A range of different processing algorithms have been tested against a variety of realistic science targets and other metrics.

Summary figures comparing the metrics for each of the different methods are presented here. In each of these the colours for each method is as follows:

| | Naive map-making | CM | MADmap | Fourier Filtering | Bolocam |
|---|---|---|---|---|---|
| $\sigma$ [mJy/pix] | 0.470697 | 0.232899 | 0.279490 | 0.289732 | 0.306342 |
| Exec. time [s] | 52m20s | 20m55s | 8m47s | 50m00s | 4m05s |

Table 1: Execution time for Galics coadded 10 cross-scans

- Naive map-making : black

- CM : magenta

- MADmap : cyan

- Fourier Filtering: blue

- MOPEX : red

- MOPEX (HF) : red (dashed)

- Bolocam : green

# 9  Review Process and Discussion

## 9.1  Aims

To select mapmaking software for use in the SPG pipeline that will reduce scan map data. Ideally one method that applies to all types of target would be selected, but there is an option of selecting two methods as long as it is easy to determine which should be used. It will be beneficial if the selected method can be extended into a user tool where user interaction with the code can produce improved results. The baseline for the SPG pipeline, though, is for a interaction-free tool that can produce usable maps in a fully automatic manner.

## 9.2  The Decision Process

After studying the results of the testing process, and asking any remaining questions of the coders and testers, the panel graded each method from 1 to 10 (1 low, 10 high) in each of three areas:

- Point Sources - as tested by the GALICS and test grid fields

- Small Extended Sources - as tested by the extended galaxy fields

- Extended Flux - as tested by the cirrus test field

Other considerations, such as execution speed, coding complexity and maintainability, were also considered.

After this grading process several of the codes were eliminated from further consideration. The remaining methods were then discussed further with the quantitative results of the tests being examined in detail, as well as further analysis of the other considerations.

## 9.3  Results

The initial scoring system produced the following results:

- MOPEX was eliminated as it is slow and not as good as other methods for any of the sets of test data, be they point source, extended source, or cirrus field
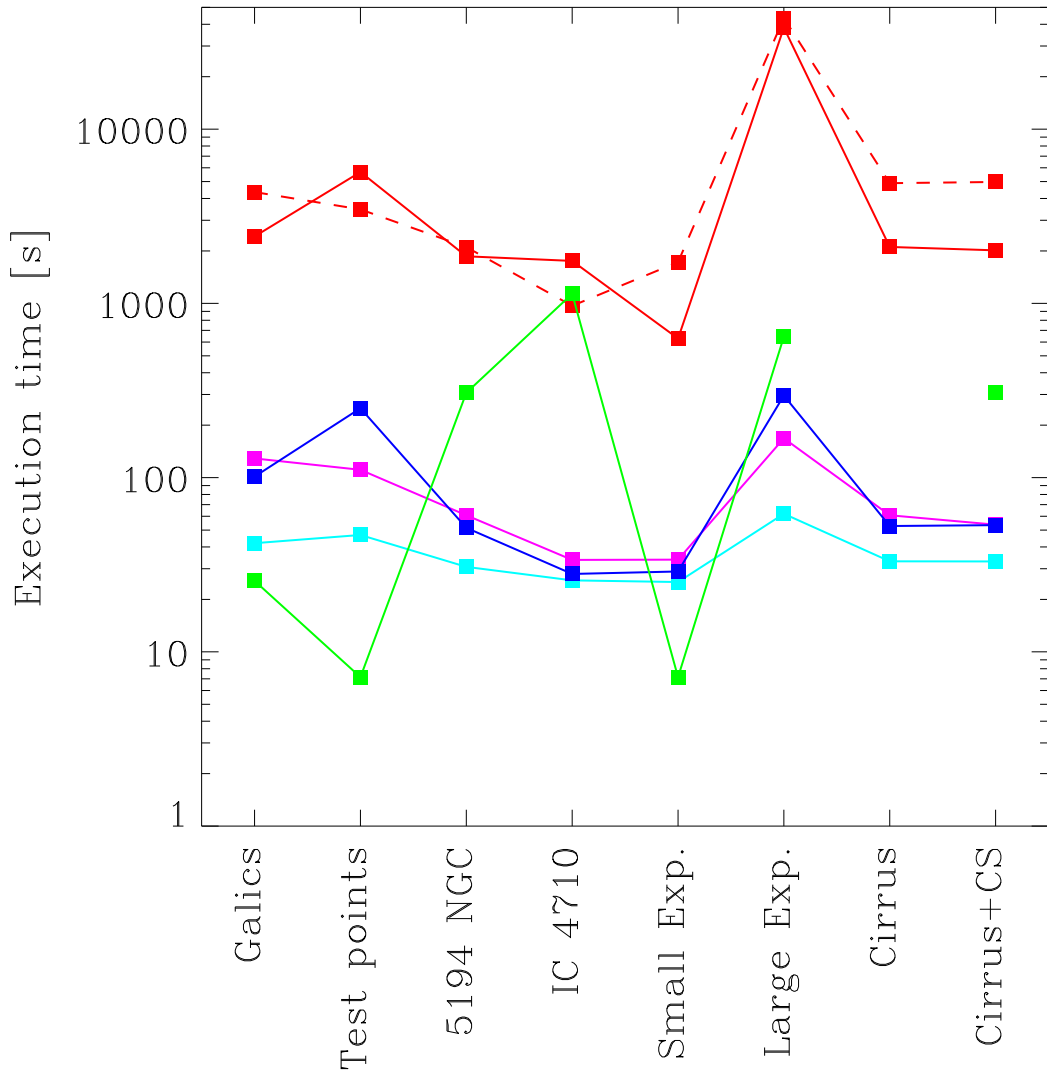
Figure 7: Execution time for Cross Scan
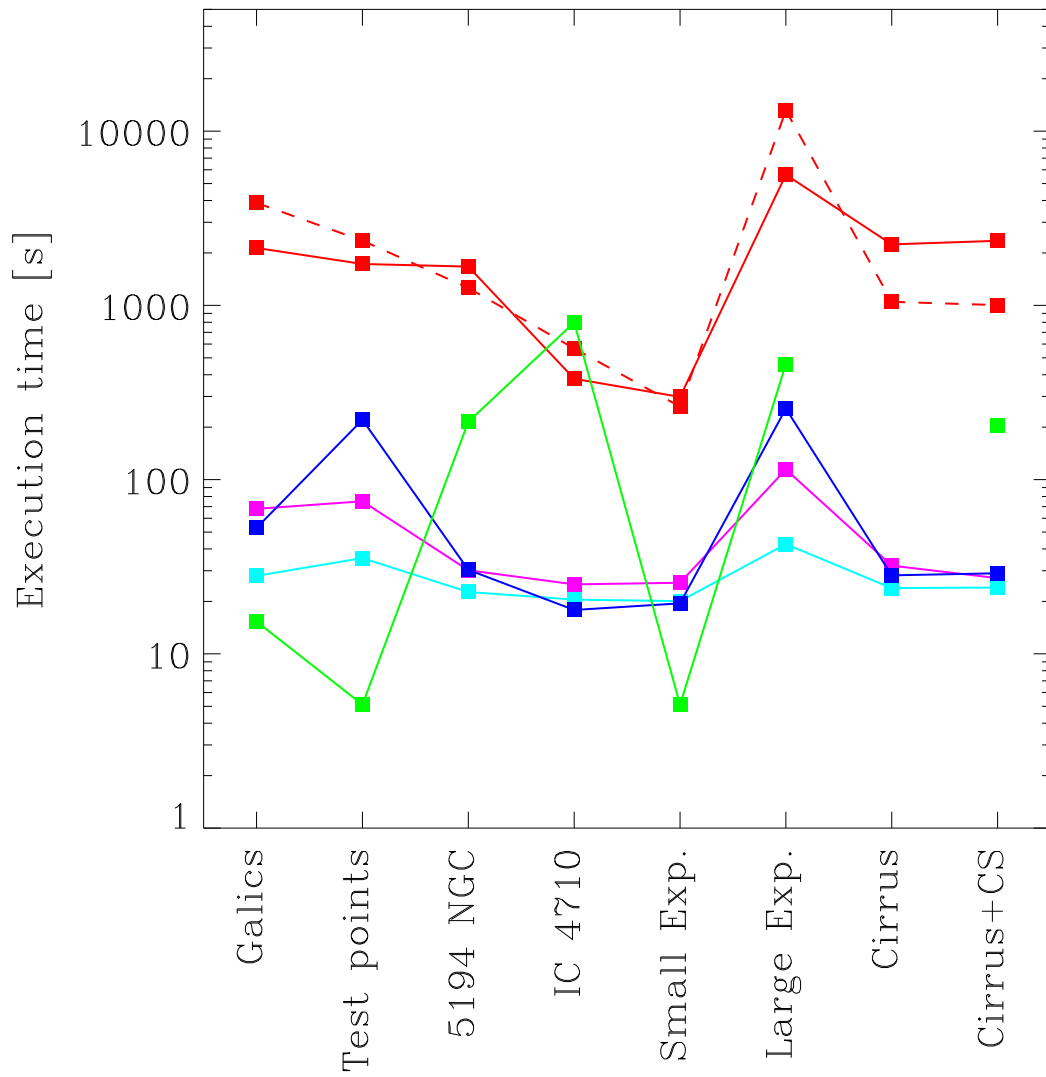
Figure 8: Execution time for single scan
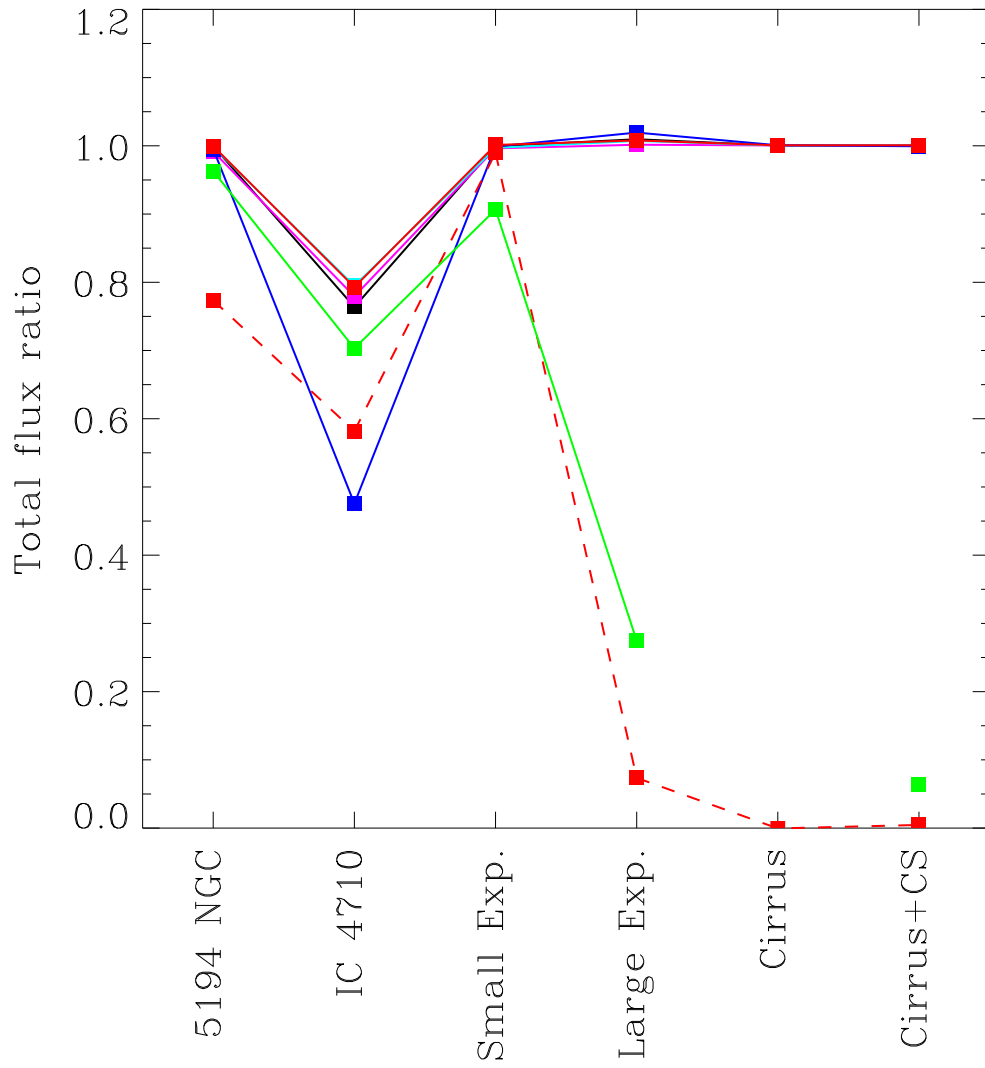
Figure 9: Ratio for cross scan
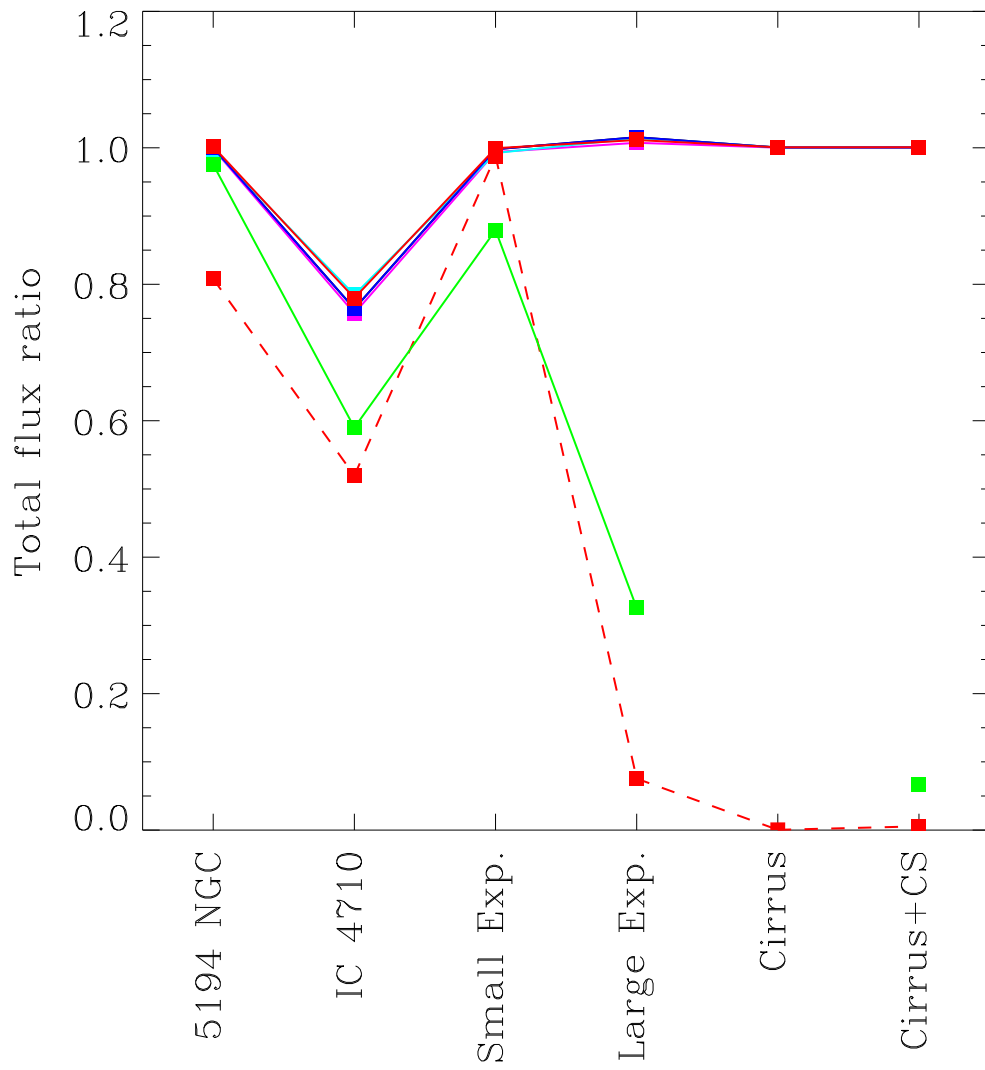
Figure 10: Ratio for single scan
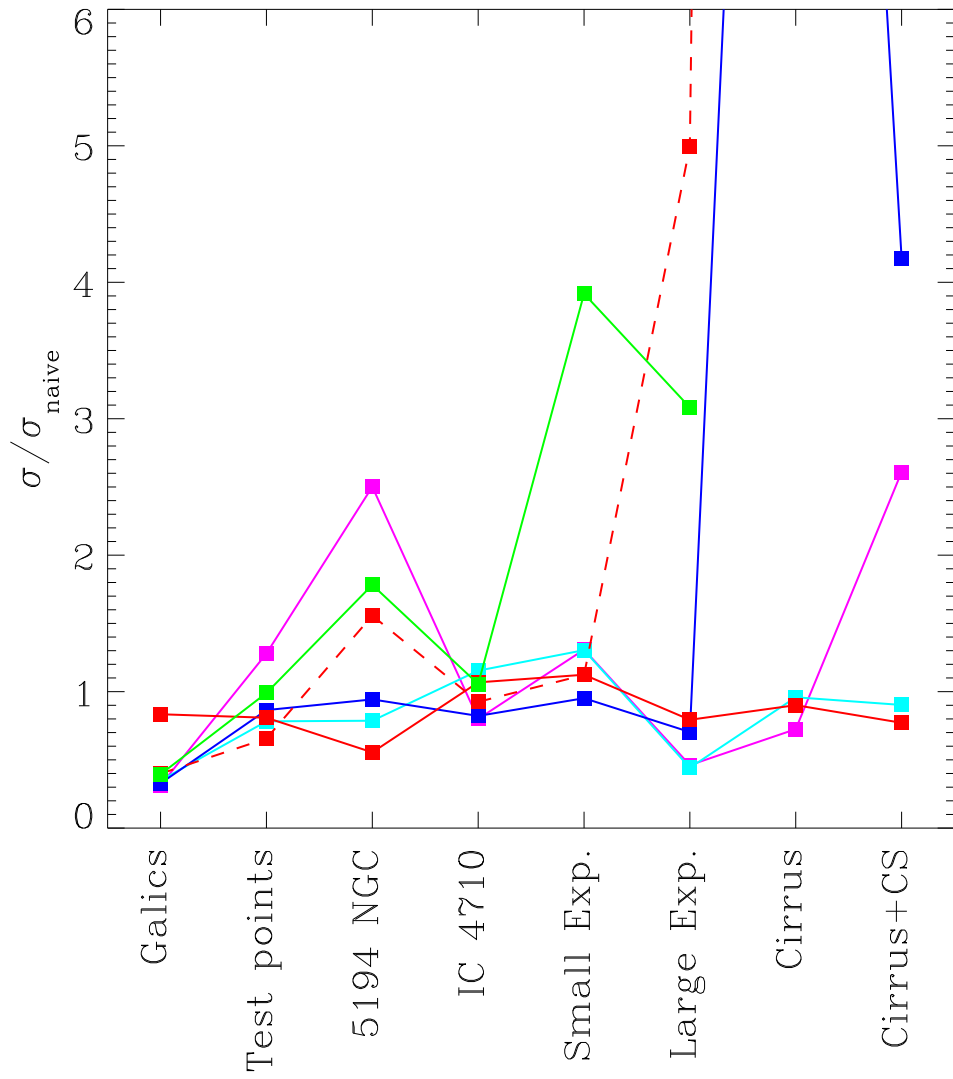
Figure 11: Std Dev for cross scan
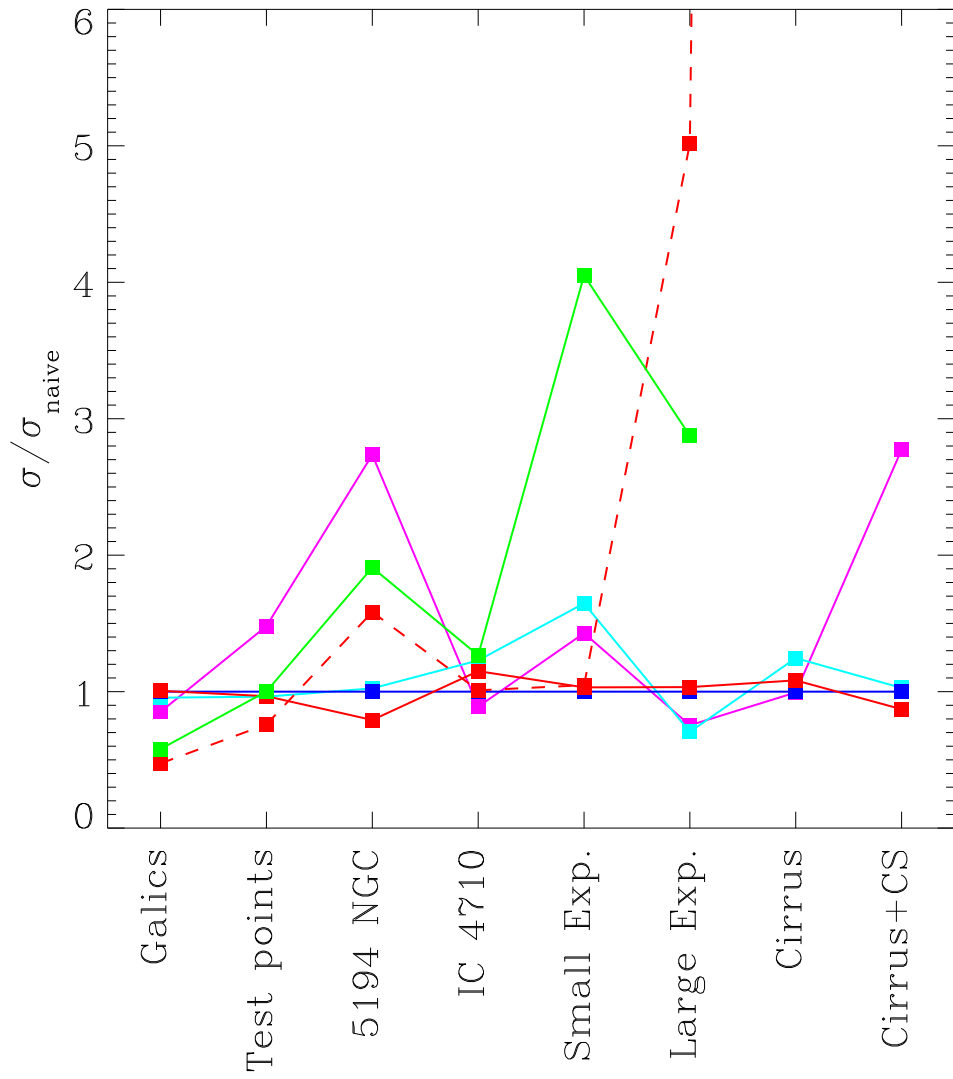
Figure 12: Std Dev for single scan

- Bolocam was eliminated because it is optimised for point sources and ground-based obsevations - it does very well for point sources but is inherently unsuited to extended structure. However its point source performance is not significantly better than other routines

- Fourier 1/f Removal was eliminated as it had problems with extended sources, and did not provide any real benefits for point sources over naive mapmaking

More detailed analysis of the test results for the remaining methods, and further discussion of other issues related to development or running these codes, then produced the following decisions.

- Nave mapping does surprisingly well overall, and is noted as a very useful thing to do as an instructive/dioagnostic stage in any scheme. Eliminated per se as it is produced as an intermediate product by MadMap

- MadMap and CM are the two most powerful and versatile coded.

- Madmap was finally chosen in preference to CM for the following reasons:

    - It performs better than CM on extended sources
    - It is more robust
    - It is competitive with all other methods for both cases with just a single iteration
    - It produces a naive map as a matter of course before the iteration stage begins
    - It is capable of improved performance with two or more iterations. This could be incorporated as part of the pipeline without allowing convergence to become a problem (eg. apply 2 iterations to all maps), and would be an easy extension to a user-controlable function in a user tool for mapmaking
    - The need to have a good estimate of the noise covariance matrix should pose no problem. It can be derived if needed as a calibration product from other science observations or, in many cases, from the data itself

## 10    Conclusions

MADMap was selected as the mapmaking method for SPIRE scanmap data. The current simplified version, using only a single iteration, was found to be superior or comparable to all other codes in our tests. The code is stable and reliable, is well documented and supported, and there are clear routes by which it can be improved as both a pipeline element (by going to 2 iterations) and as a user tool (by allowing variable numbers of iterations and selection of different covariance matrices.

Pierre Chanial will now go ahead with implementing MADMap in Java as a module for the SPIRE data reduction pipeline.

## 11    References

Enoch et al., 2006, Bolocam Survey for 1.1mm Dust Continuum Emission in the c2d Legacy Clouds 1. Perseus, ApJ, 638, 293, 2006

Guatier, T., Boulanger, F., A calculation of cirrus noise due to infrared cirrus, The Astronomical Journal, vol. 103, number 4, 1992

Hatton, S., et al., GALICS I. A hybrid N-body /semi-analytic model of hierarchical galaxgy formation, MNRAS 343, 75, 2003

Hogbom, J. A. 1974, A&AS, 15, 417

Laurent, G., et al. 2005, ApJ, 623, 742

Motte, F., Andre, P., Ward-Thompson, D., Bontemps, S., A SCUBA survey of the NGC 2068/2071 protoclusters, A&A, 372L 41M 2001

Schwarz, U. J. 1978, A&A, 65, 345

Sibthorpe, B., Griffin, M., SPIRE Photometer Simulator V1.01BS, 2006

Waskett, T., Sibthorpe, B., Scan-map scanning angles V3.0, 2006

# 12 Appendices

Results from individual tests are presented here.

Table 2: Galics Simulation – Direct (Naive) Mapping
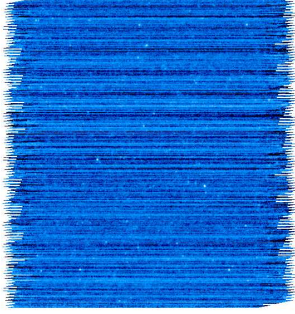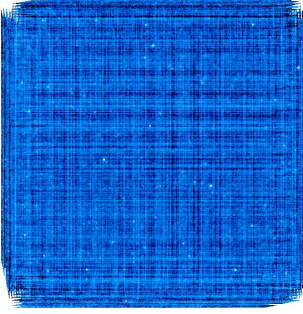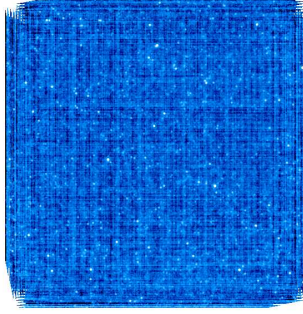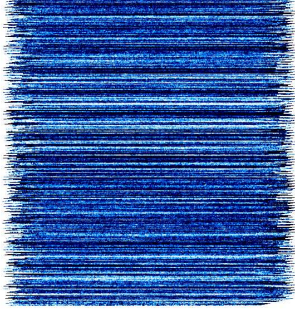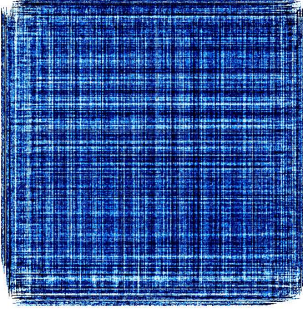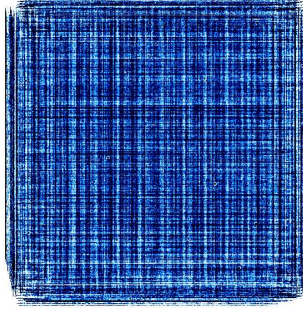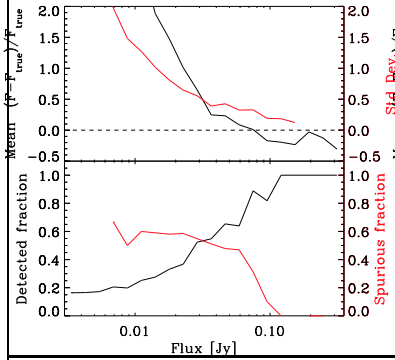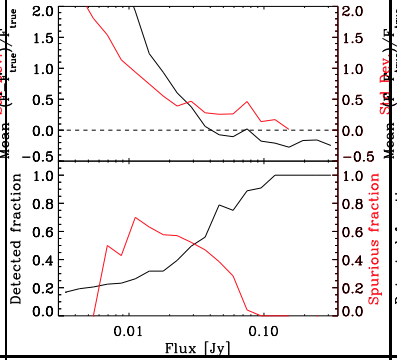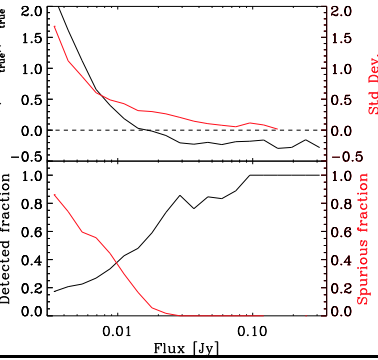
| Single scan | Cross scan | 10 cross scans |
|---|---|---|
| 6″ Reconstructed maps (log scale) | | |
|  |  |  |
| Residuals (histogram-equalized) | | |
|  |  |  |
|  |  |  |
| $\sigma$ [mJy/pixel]  2.1634 | 1.4943 | 0.4707 |
| $N_{\text{crossid.}}$  2704 | 2986 | 3697 |
| $N_{\text{spurious}}$  2800 | 3134 | 1836 |
| Execution time  16.3s | 34.9s | 52m20s |

Table 3: Grid of Point Sources – Direct (Naive) Mapping
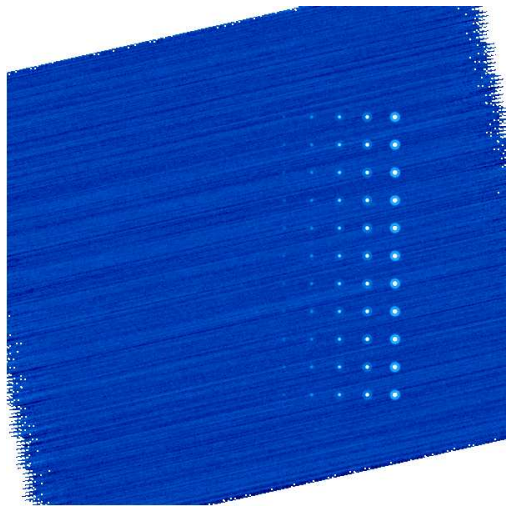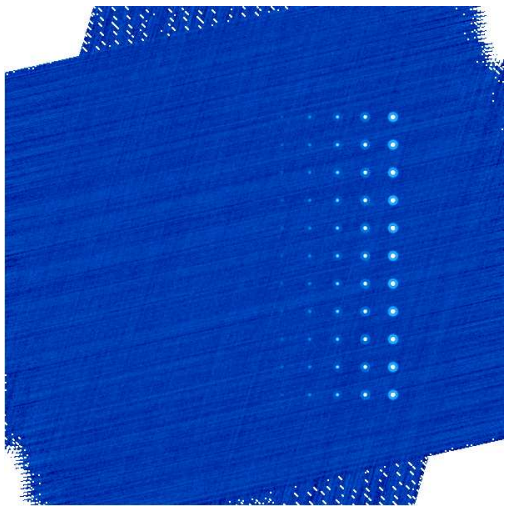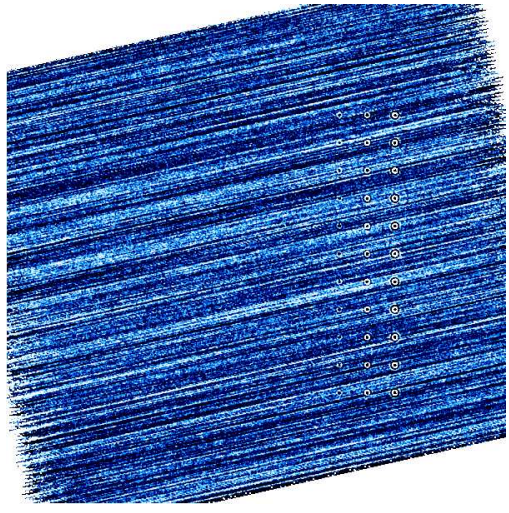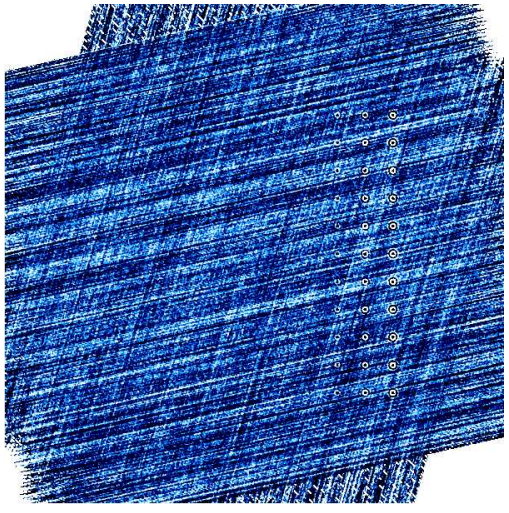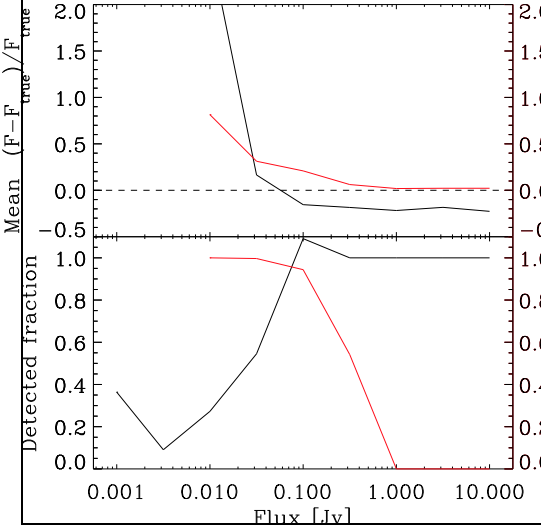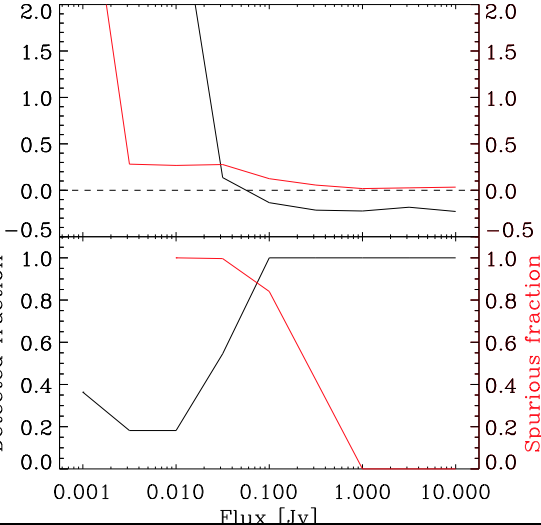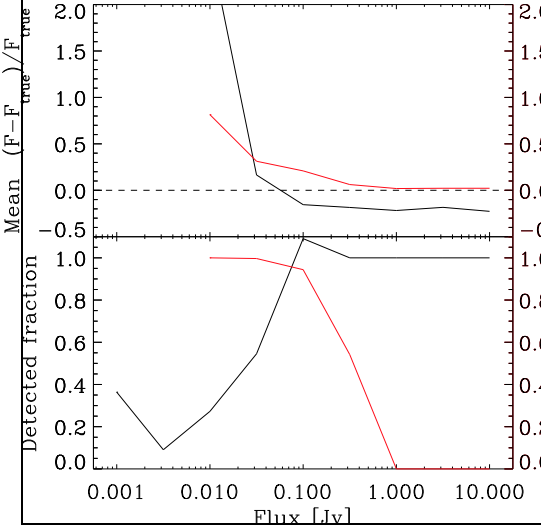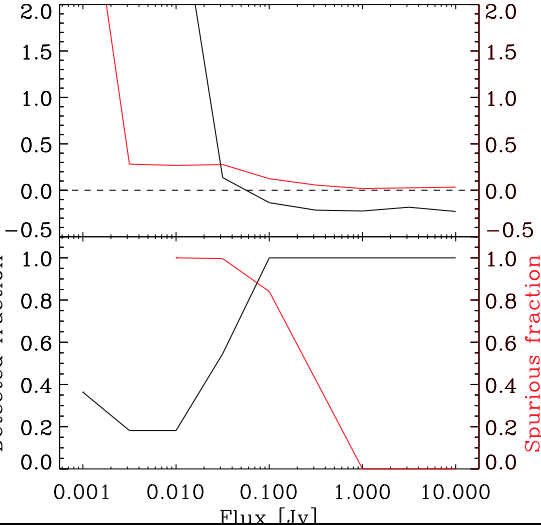
| Single scan | Cross scan |
|---|---|
| 6″ Reconstructed maps (log scale) | |



| Residuals (histogram-equalized) | |





| $\sigma$ [mJy/pixel] | 2.7953 | 2.6039 |
|---|---|---|
| $N_{crossid.}$ | 73 | 74 |
| $N_{spurious}$ | 5510 | 5834 |
| Execution time | 23.3s | 38.2s |

Table 4: NGC 5194 – Direct (Naive) Mapping
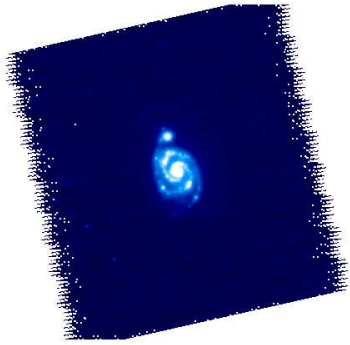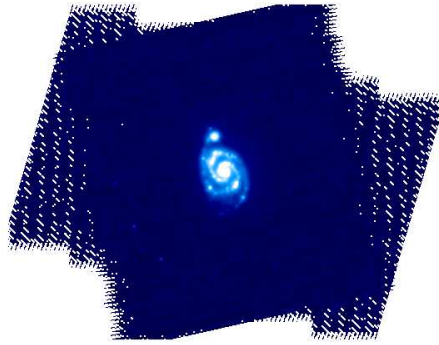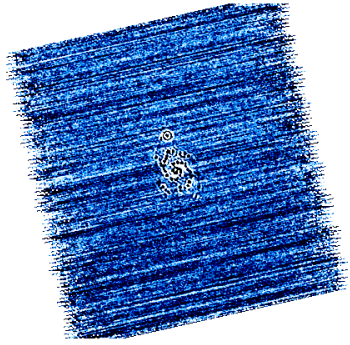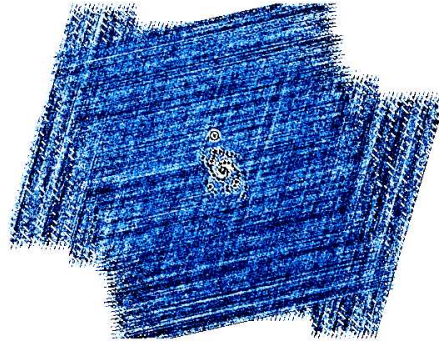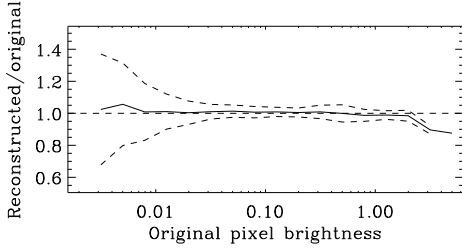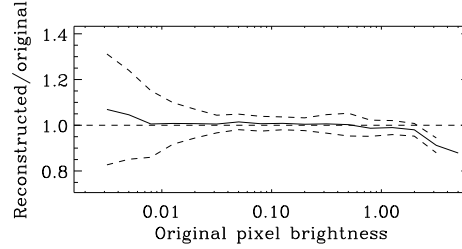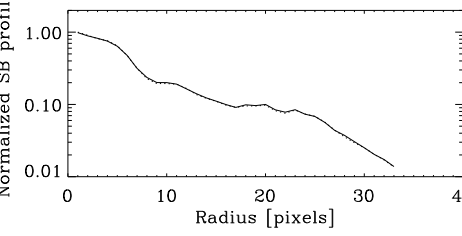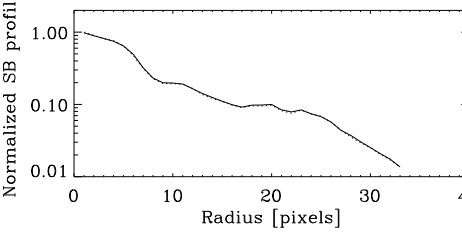
| Single scan | Cross scan |
|---|---|
| 6″ Reconstructed maps (log scale) | |



| Residuals (histogram-equalized) | |
|---|---|





| $\sigma$ [mJy/pixel] | 14.0972 | 13.3147 |
|---|---|---|
| Total flux ratio | 0.9998 | 0.9997 |
| Mean profile ratio | 1.0104 | 1.0139 |
| Std. Dev. profile ratio | 0.0186 | 0.0179 |
| Execution time | 11.1s | 19.4s |

Table 5: IC 4710 – Direct (Naive) Mapping
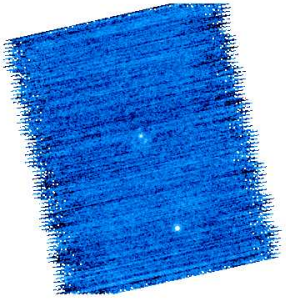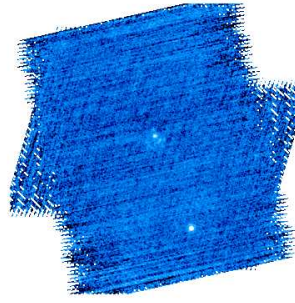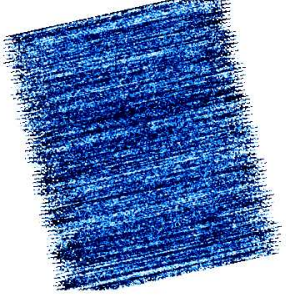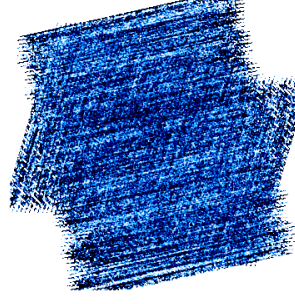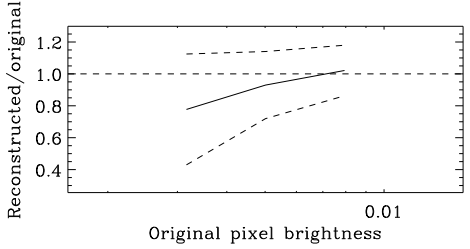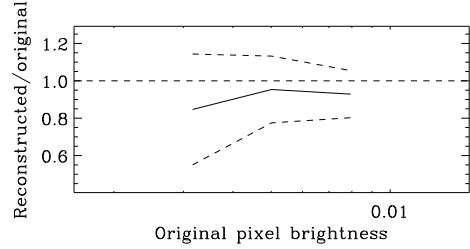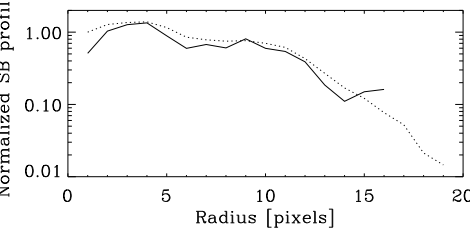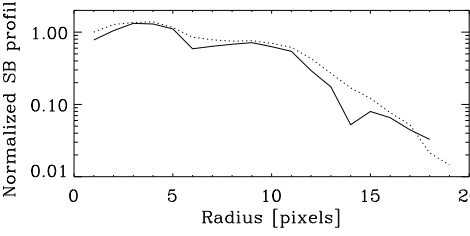
| Single scan | Cross scan |
|:---:|:---:|
| 6″ Reconstructed maps (log scale) | |
|  |  |
| Residuals (histogram-equalized) | |
|  |  |
|  |  |

| | Single scan | Cross scan |
|:---|:---:|:---:|
| $\sigma$ [mJy/pixel] | 1.0761 | 0.9319 |
| Total flux ratio | 0.7641 | 0.7638 |
| Mean profile ratio | 0.3553 | 0.7749 |
| Std. Dev. profile ratio | 1.4257 | 0.3691 |
| Execution time | 9.2s | 15.1s |

Table 6: Small Exponential Disk – Direct (Naive) Mapping
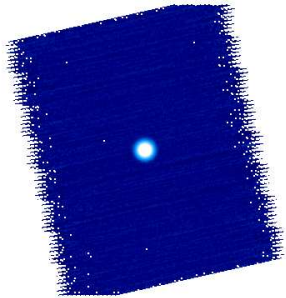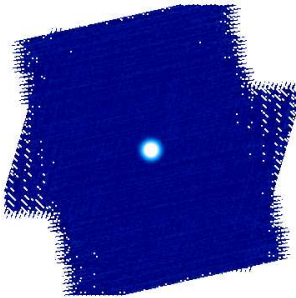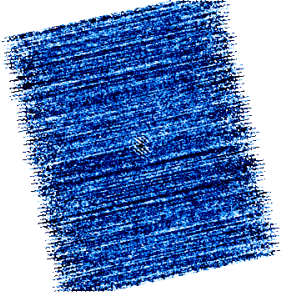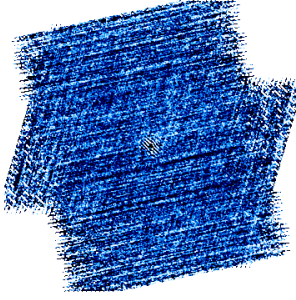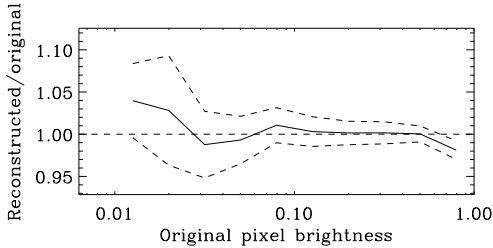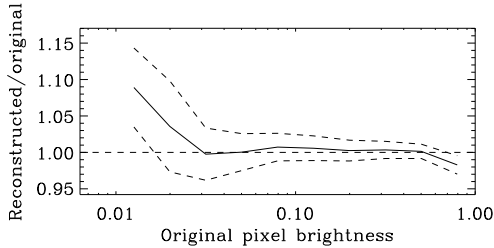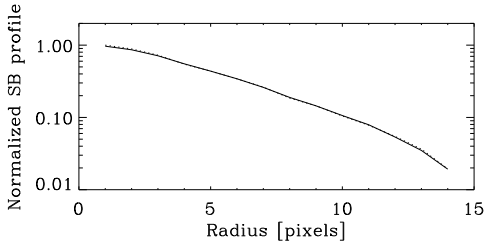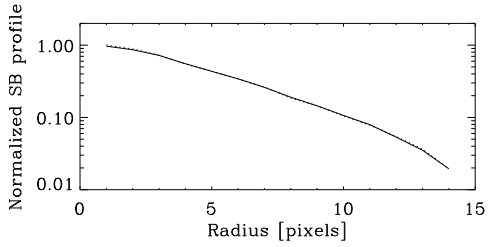
| Single scan | Cross scan |
|---|---|
| 6″ Reconstructed maps (log scale) | |



| Residuals (histogram-equalized) | |
|---|---|



| $\sigma$ [mJy/pixel] | 4.1423 | 3.9915 |
|---|---|---|
| Total flux ratio | 0.9980 | 0.9994 |
| Mean profile ratio | 0.9934 | 0.9962 |
| Std. Dev. profile ratio | 0.0192 | 0.0199 |
| Execution time | 9.3s | 16.6s |

Table 7: Large Exponential Disk – Direct (Naive) Mapping
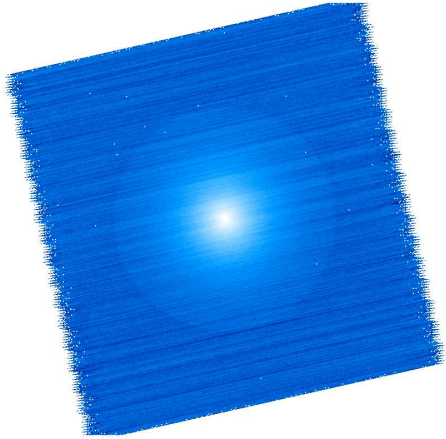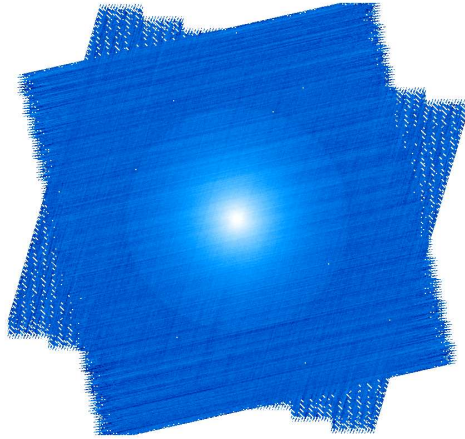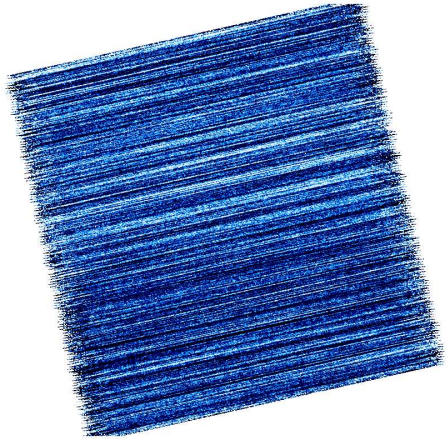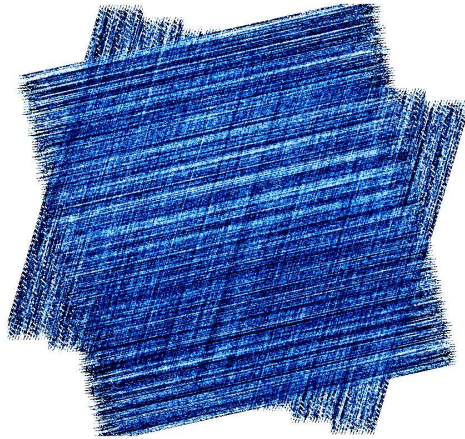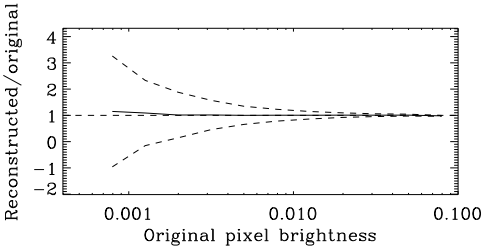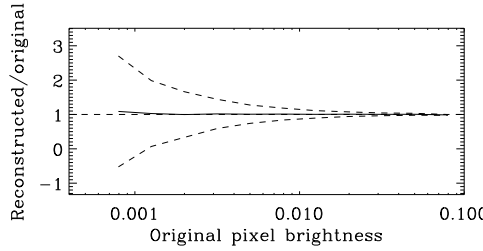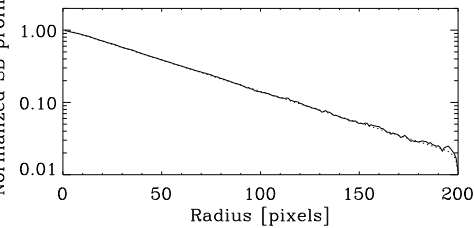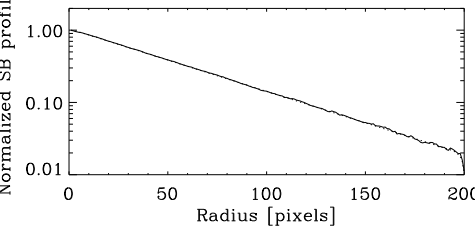
| Single scan | Cross scan |
|---|---|
| 6″ Reconstructed maps (log scale) | |



| Residuals (histogram-equalized) | |
|---|---|





| $\sigma$ [mJy/pixel] | 1.7027 | 1.3082 |
|---|---|---|
| Total flux ratio | 1.0155 | 1.0097 |
| Mean profile ratio | 1.0134 | 1.0082 |
| Std. Dev. profile ratio | 0.0339 | 0.0204 |
| Execution time | 33.1s | 56.6s |

Table 8: Cirrus – Direct (Naive) Mapping
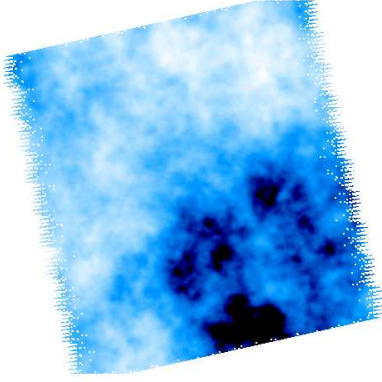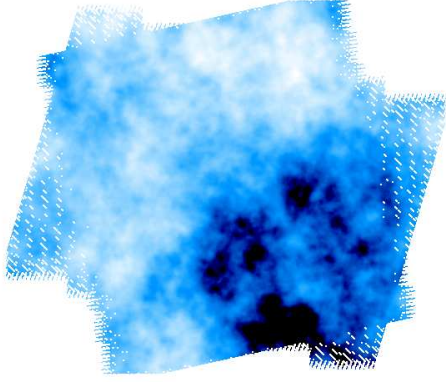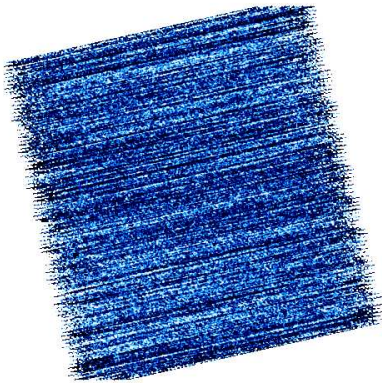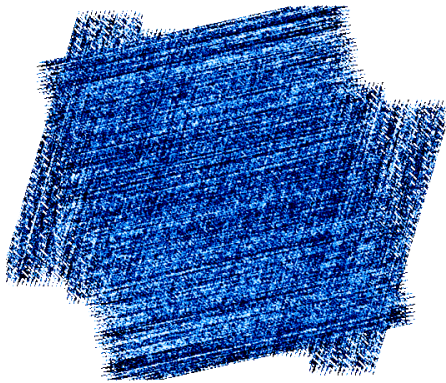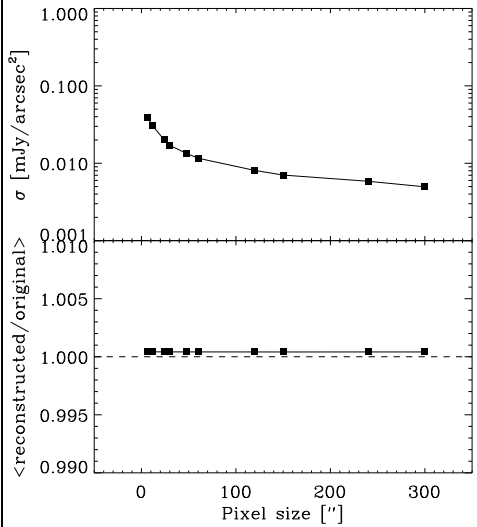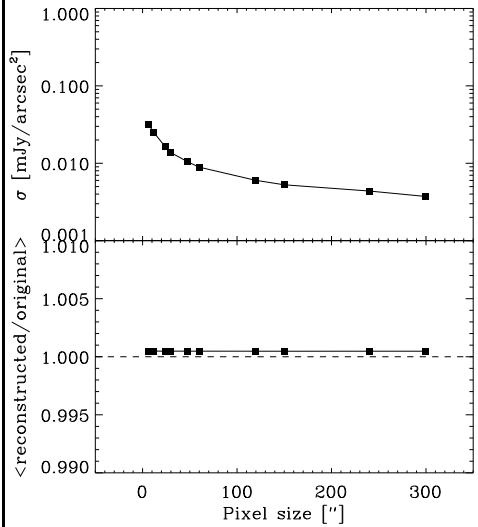
| Single scan | Cross scan |
|---|---|
| 6″ Reconstructed maps (log scale) | |



| Residuals (histogram-equalized) | |
|---|---|





| | Single scan | Cross scan |
|---|---|---|
| $\sigma$ [mJy/pixel] | 1.4034 | 1.1576 |
| <reconstructed/original> | 1.0004 | 1.0005 |
| Execution time | 12.3s | 21.6s |

Table 9: Cirrus with Compact Sources – Direct (Naive) Mapping
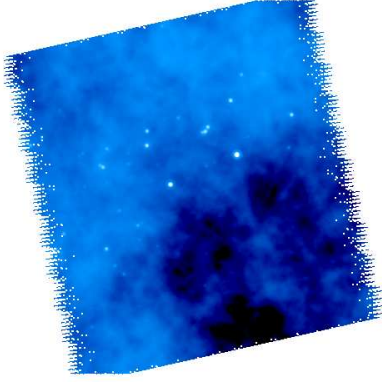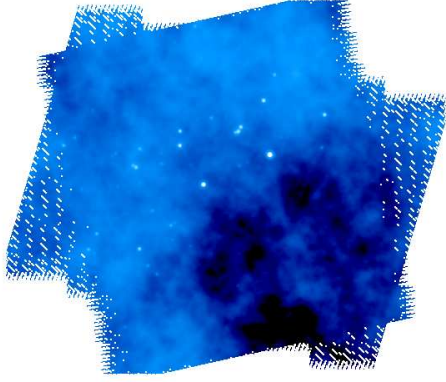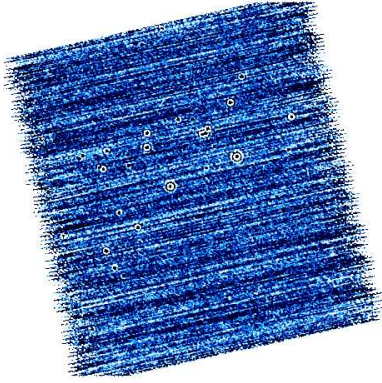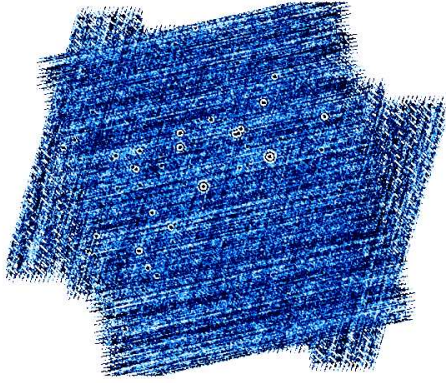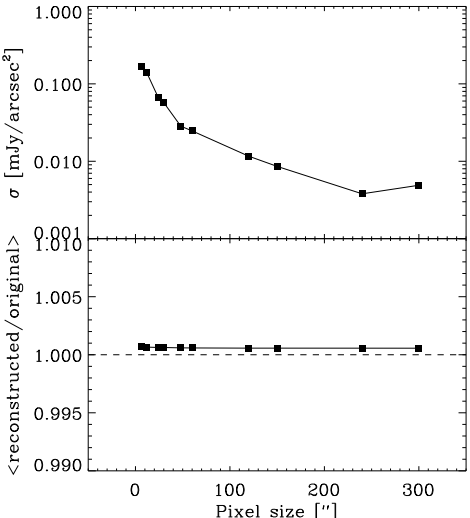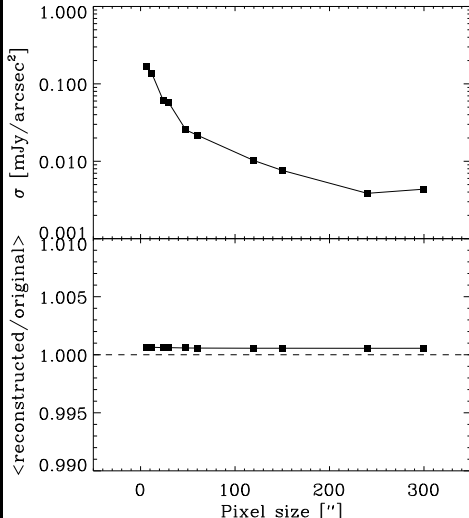
| Single scan | Cross scan |
|---|---|
| 6″ Reconstructed maps (log scale) | |



| Residuals (histogram-equalized) | |
|---|---|





| $\sigma$ [mJy/pixel] | 6.0890 | 5.9649 |
|---|---|---|
| <reconstructed/original> | 1.0007 | 1.0007 |
| Execution time | 12.5s | 24.5s |

41

Table 10: Galics Simulation – CM
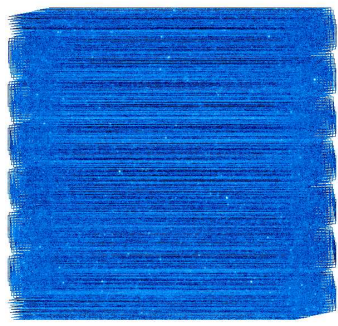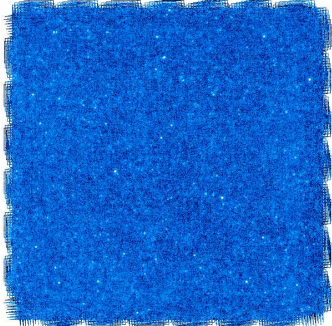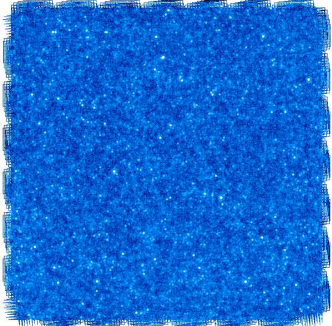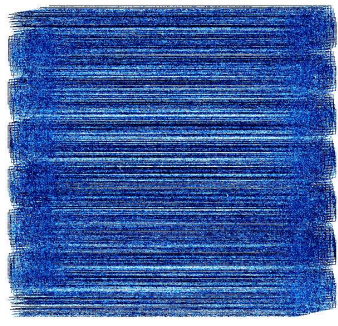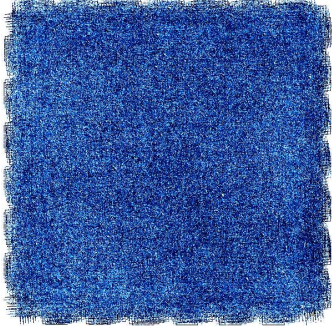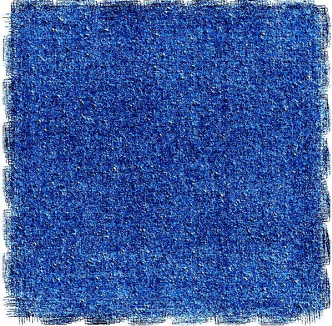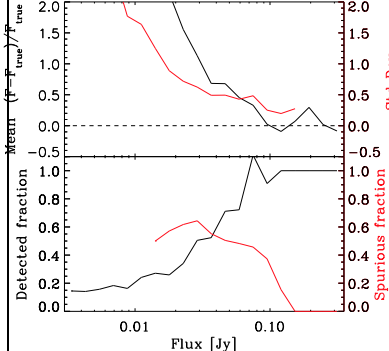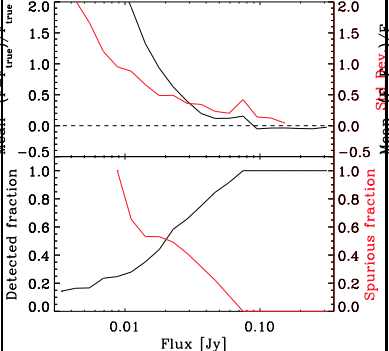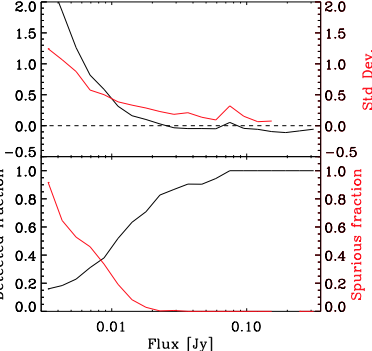
| Single scan | Cross scan | 10 cross scans |
|---|---|---|
| 6″ Reconstructed maps (log scale) | | |
|  |  |  |
| Residuals (histogram-equalized) | | |
|  |  |  |
|  |  |  |
| $\sigma$ [mJy/pixel] 2.6011 | 1.1410 | 0.3975 |
| $N_{\text{crossid.}}$ 2423 | 2908 | 3930 |
| $N_{\text{spurious}}$ 2476 | 1898 | 863 |
| Execution time 1m08s | 2m08s | 20m55s |

Table 11: Grid of Point Sources – CM
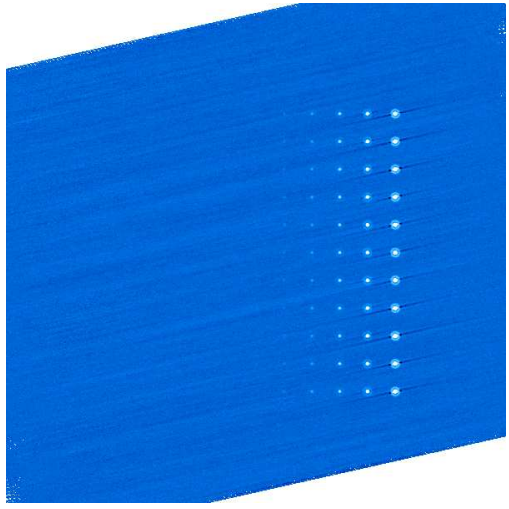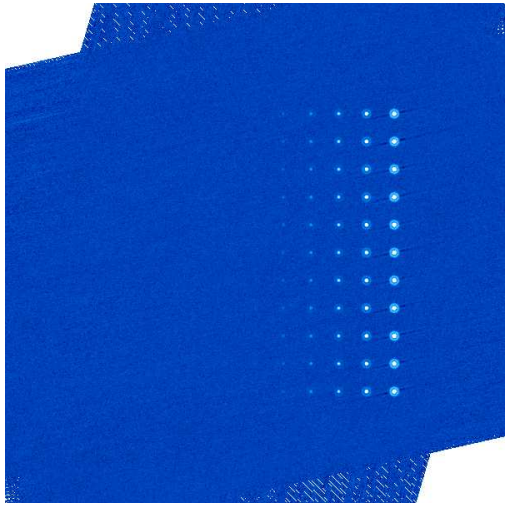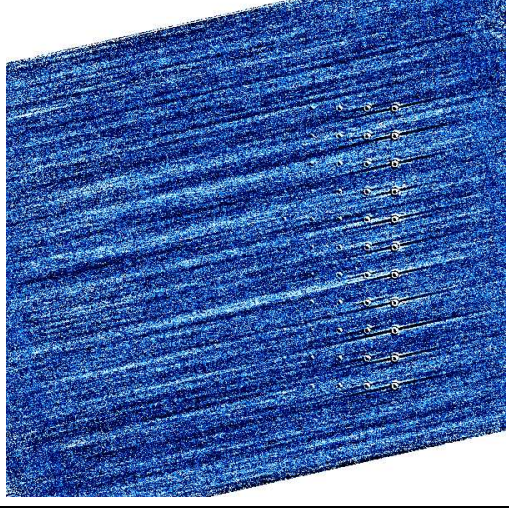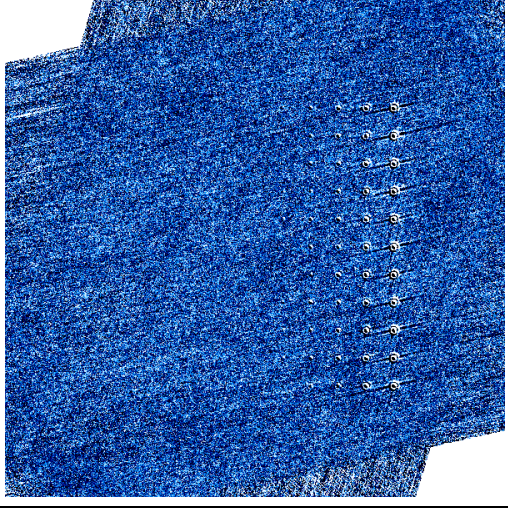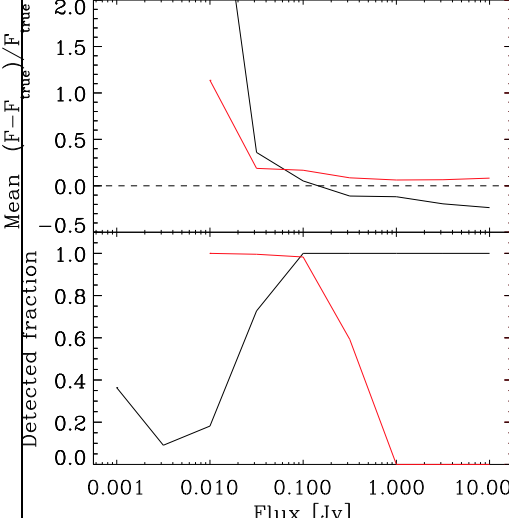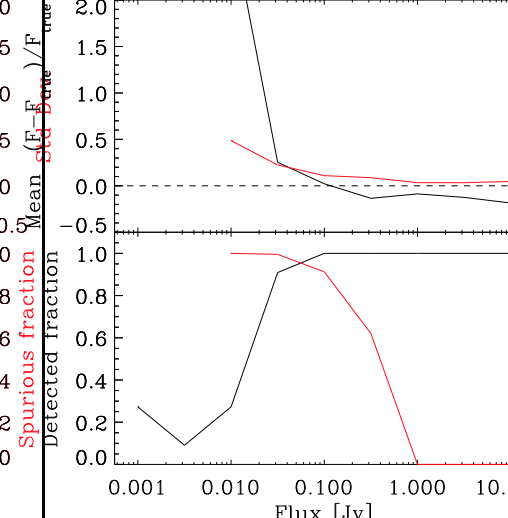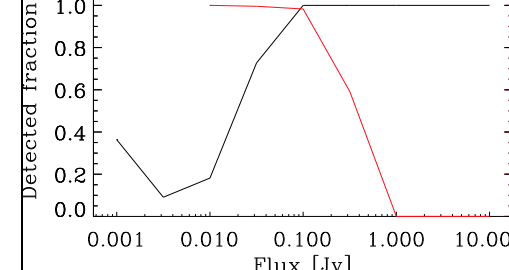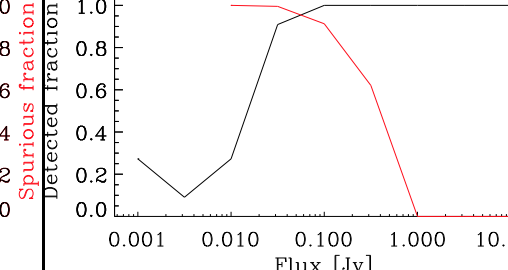
| Single scan | Cross scan |
|---|---|
| 6″ Reconstructed maps (log scale) | |



| Residuals (histogram-equalized) | |
|---|---|





| $\sigma$ [mJy/pixel] | 5.5992 | 5.1958 |
|---|---|---|
| $N_{crossid.}$ | 73 | 76 |
| $N_{spurious}$ | 4621 | 4622 |
| Execution time | 1m15s | 1m50s |

Table 12: NGC 5194 – CM
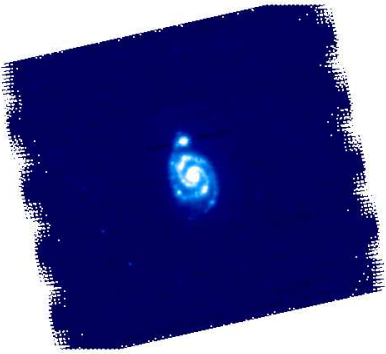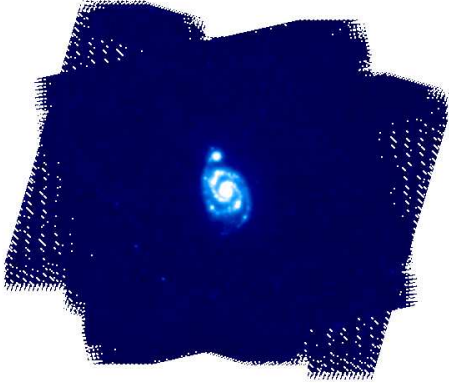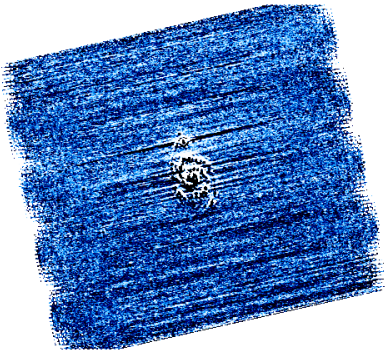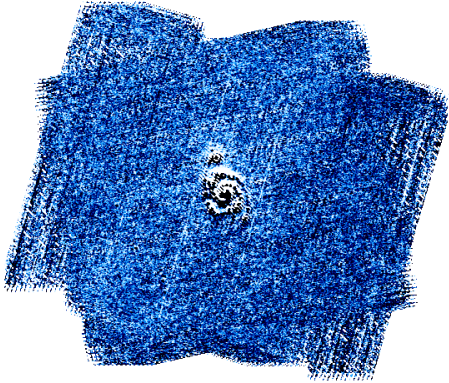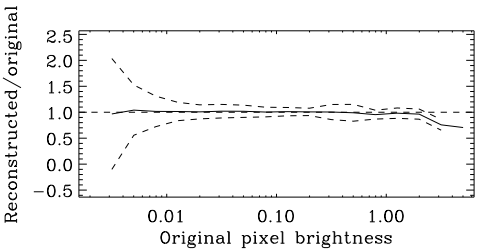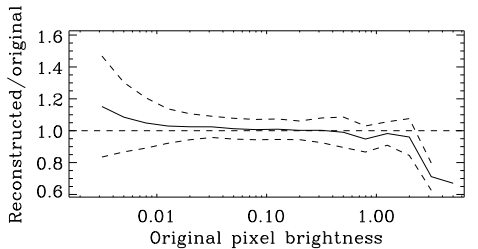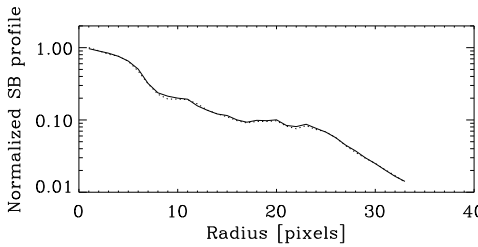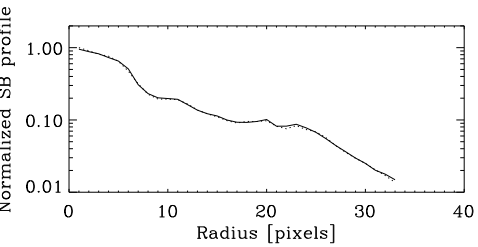
| Single scan | Cross scan |
|---|---|
| 6″ Reconstructed maps (log scale) | |



| Residuals (histogram-equalized) | |
|---|---|





| $\sigma$ [mJy/pixel] | 39.1766 | 36.7005 |
|---|---|---|
| Total flux ratio | 0.9985 | 0.9916 |
| Mean profile ratio | 1.0186 | 1.0119 |
| Std. Dev. profile ratio | 0.0314 | 0.0344 |
| Execution time | 30.2s | 1m00s |

Table 13: IC 4710 – CM
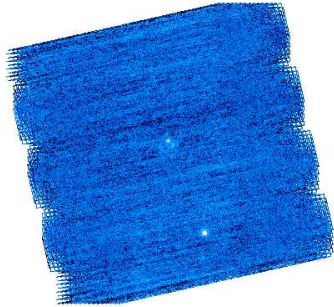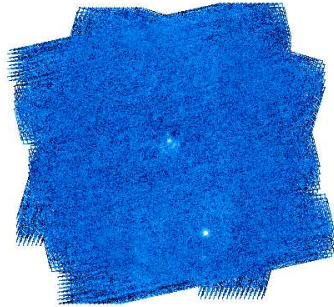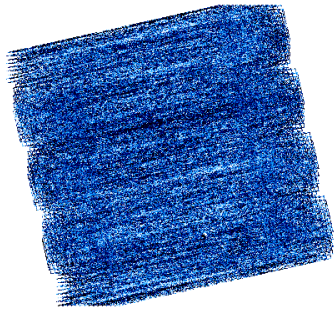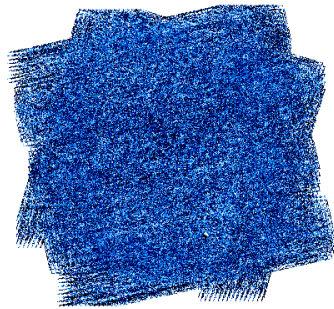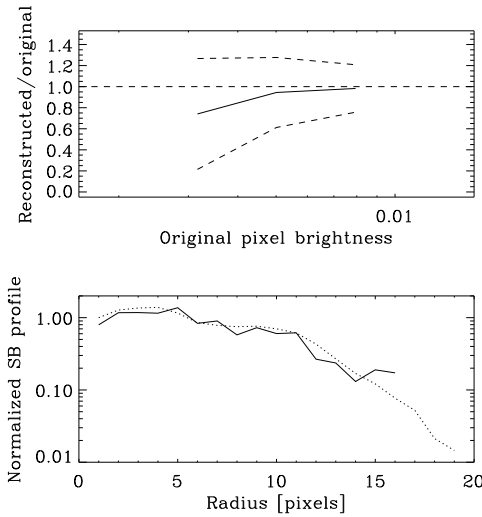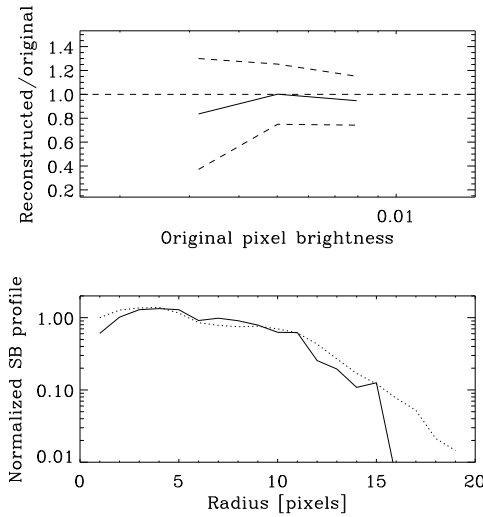
| Single scan | Cross scan |
|---|---|
| 6″ Reconstructed maps (log scale) | |



| Residuals (histogram-equalized) | |
|---|---|





| $\sigma$ [mJy/pixel] | 1.6607 | 1.4618 |
|---|---|---|
| Total flux ratio | 0.7524 | 0.7710 |
| Mean profile ratio | 0.7309 | 0.5981 |
| Std. Dev. profile ratio | 0.9411 | 0.7556 |
| Execution time | 25.0s | 33.7s |

Table 14: Small Exponential Disk – CM
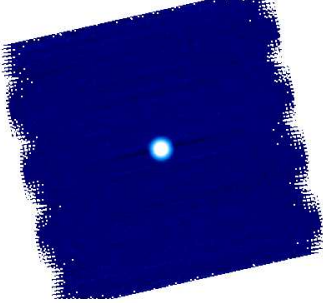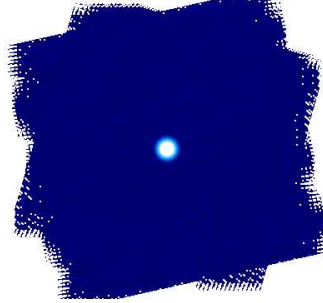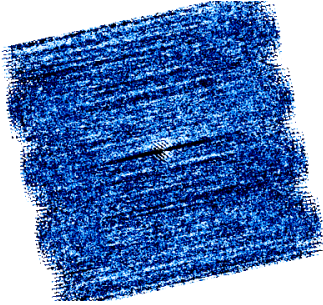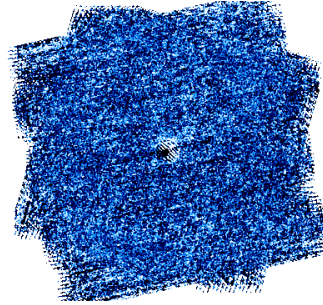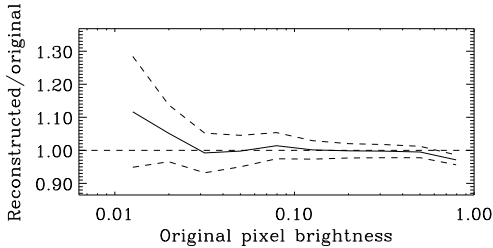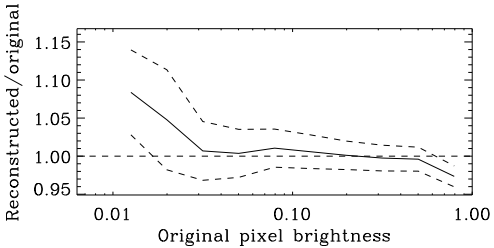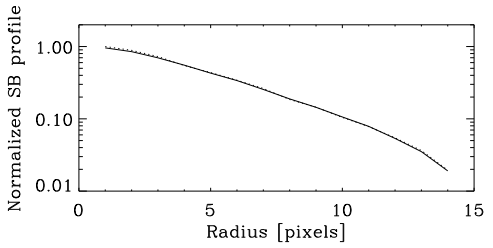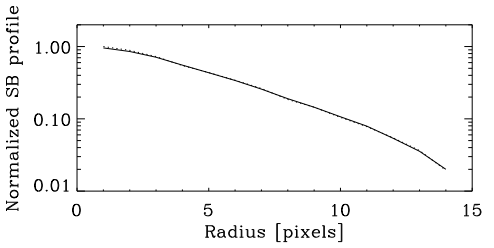
| Single scan | Cross scan |
|---|---|
| 6″ Reconstructed maps (log scale) | |



| Residuals (histogram-equalized) | |
|---|---|





| $\sigma$   [mJy/pixel] | 6.1572 | 5.6375 |
|---|---|---|
| Total flux ratio | 0.9938 | 0.9964 |
| Mean profile ratio | 0.9853 | 0.9954 |
| Std. Dev. profile ratio | 0.0218 | 0.0232 |
| Execution time | 25.6s | 33.8s |

Table 15: Large Exponential Disk – CM
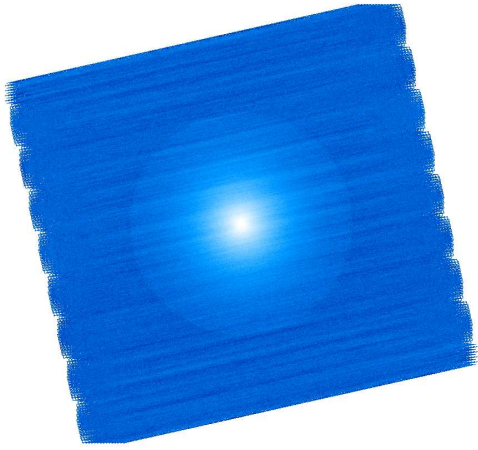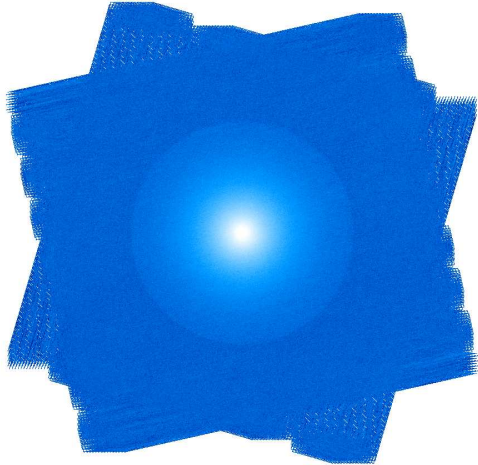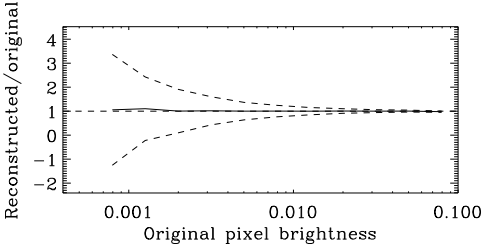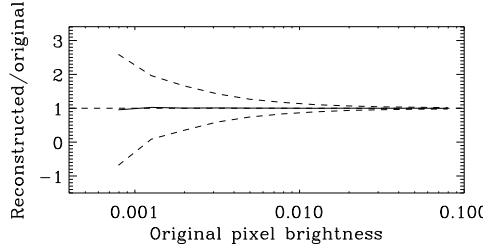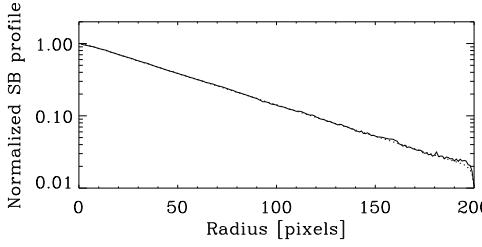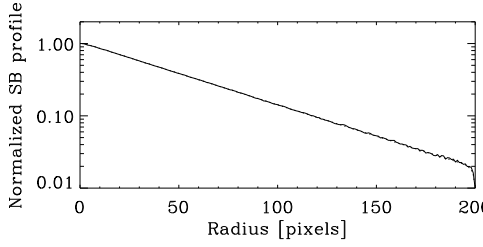
| Single scan | Cross scan |
|---|---|
| 6″ Reconstructed maps (log scale) | |



| Residuals (histogram-equalized) | |
|---|---|





| $\sigma$  [mJy/pixel] | 1.8160 | 1.2887 |
|---|---|---|
| Total flux ratio | 1.0074 | 1.0019 |
| Mean profile ratio | 1.0099 | 1.0037 |
| Std. Dev. profile ratio | 0.0337 | 0.0158 |
| Execution time | 1m54s | 2m48s |

Table 16: Cirrus – CM
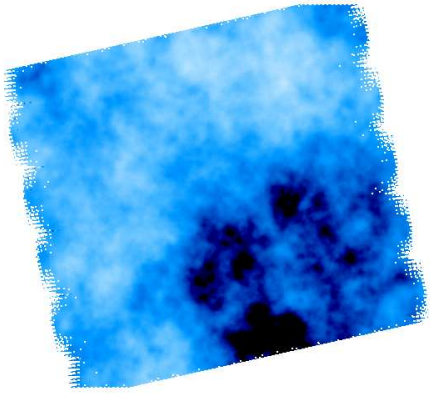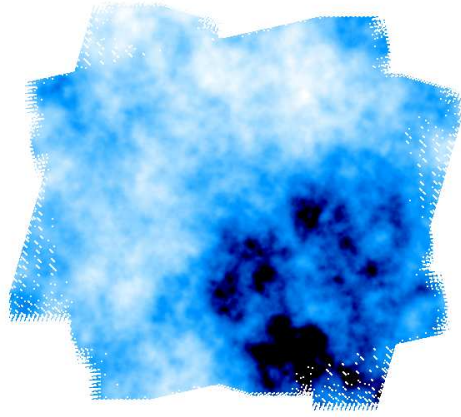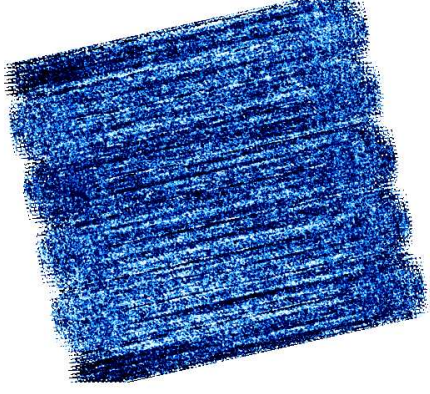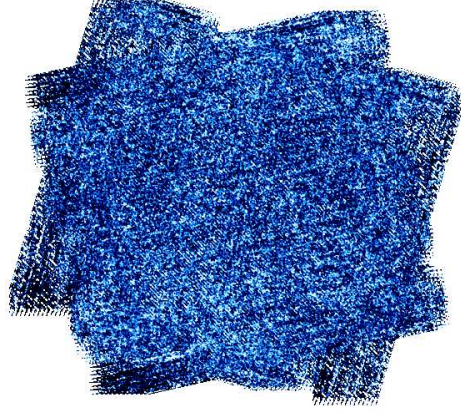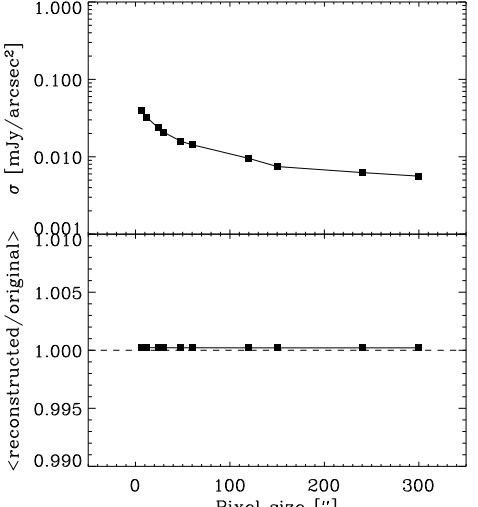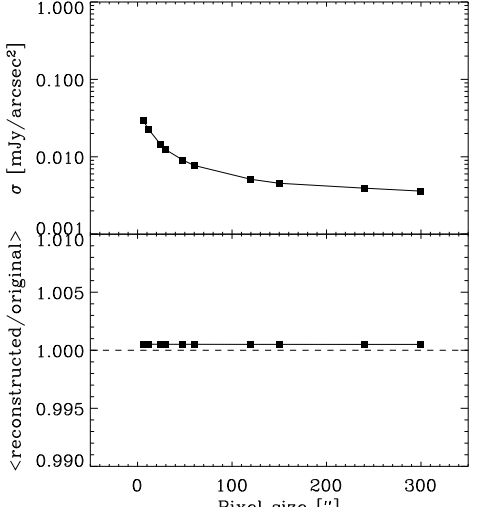
| Single scan | Cross scan |
|---|---|
| 6″ Reconstructed maps (log scale) | |



| Residuals (histogram-equalized) | |





| | Single scan | Cross scan |
|---|---|---|
| $\sigma$  [mJy/pixel] | 1.4334 | 1.0508 |
| <reconstructed/original> | 1.0002 | 1.0005 |
| Execution time | 32.1s | 1m00s |

Table 17: Cirrus with Compact Sources – CM
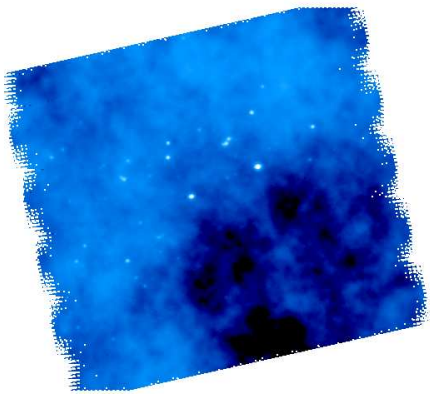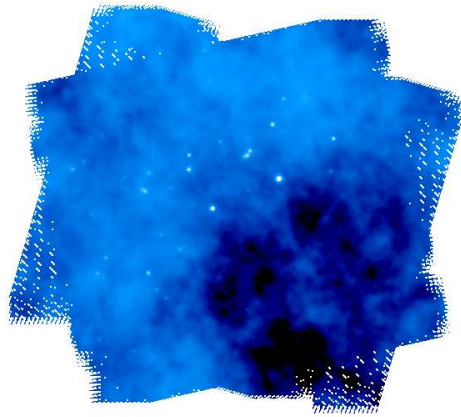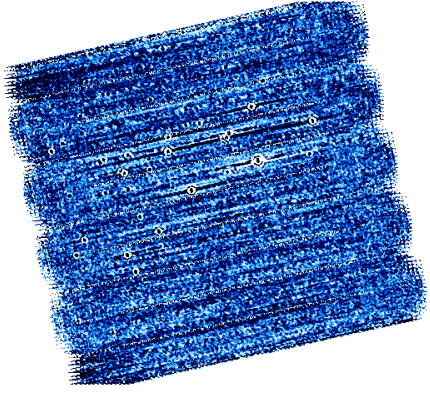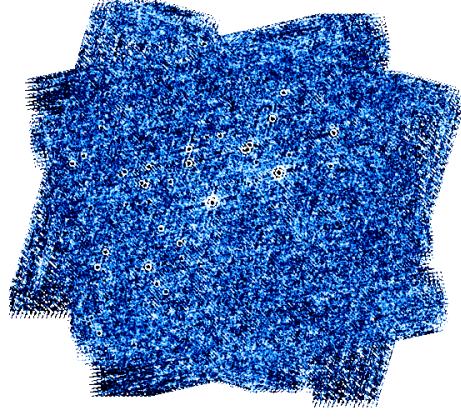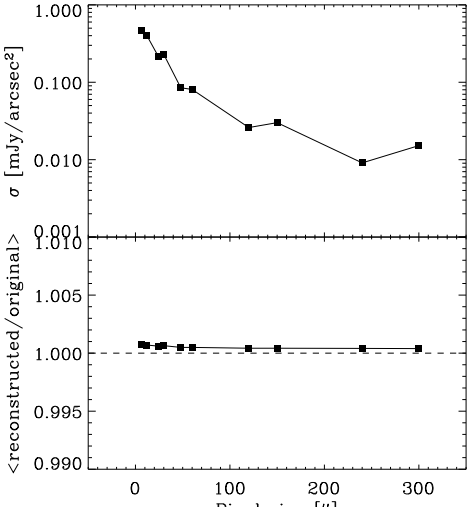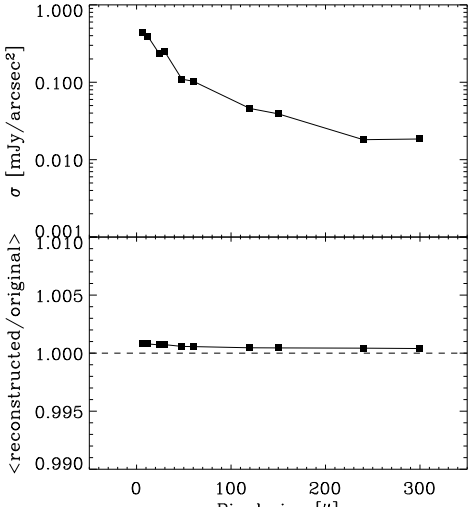
| Single scan | Cross scan |
|:---:|:---:|
| 6″ Reconstructed maps (log scale) | |



| Residuals (histogram-equalized) | |
|:---:|:---:|





| $\sigma$ [mJy/pixel] | 16.8784 | 15.8804 |
|:---|:---:|:---:|
| <reconstructed/original> | 1.0007 | 1.0008 |
| Execution time | 27.2s | 53.7s |

Table 18: Galics Simulation – MADmap (Ncorr=200)
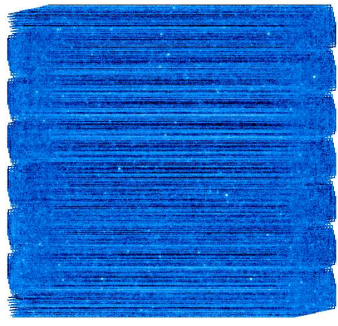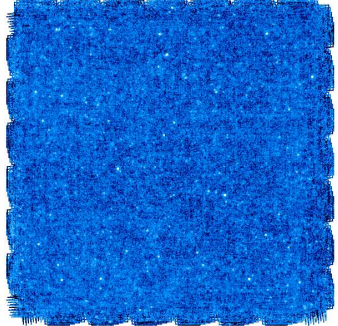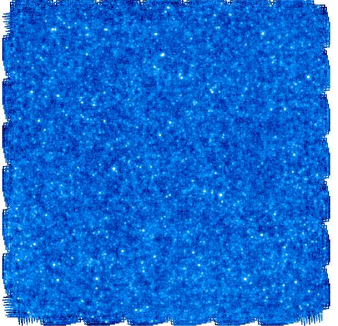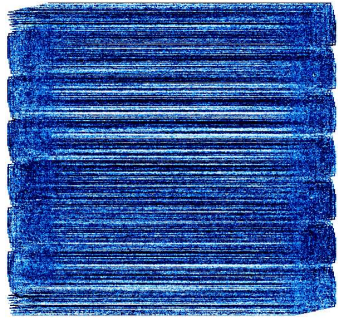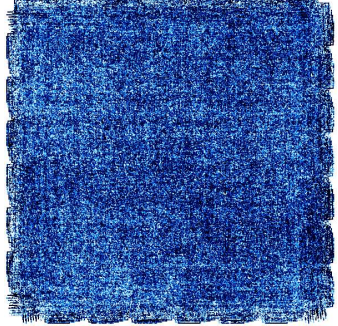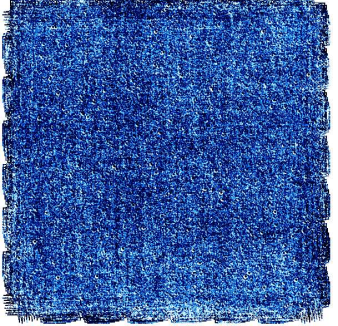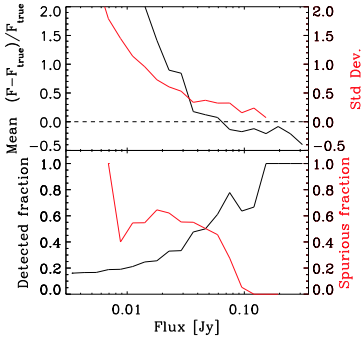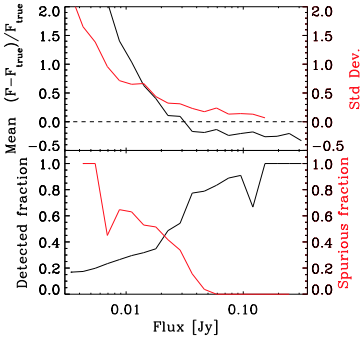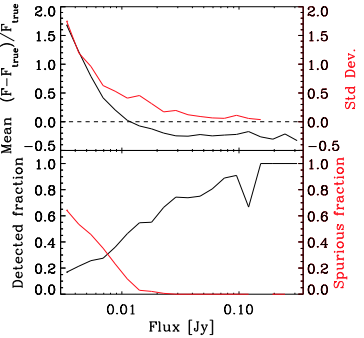
| Single scan | Cross scan | 10 cross scans |
|---|---|---|
| 6″ Reconstructed maps (log scale) | | |
|  |  |  |
| Residuals (histogram-equalized) | | |
|  |  |  |
|  |  |  |
| $\sigma$ [mJy/pixel]  2.0679 | 0.7560 | 0.2795 |
| $N_{crossid.}$  2529 | 3048 | 3826 |
| $N_{spurious}$  2912 | 2507 | 1200 |
| Execution time  28.1s | 42.0s | 8m47s |

50

Table 19: Grid of Point Sources – MADmap (Ncorr=200)
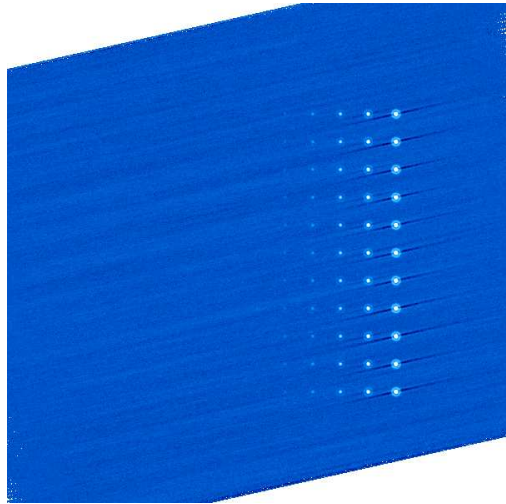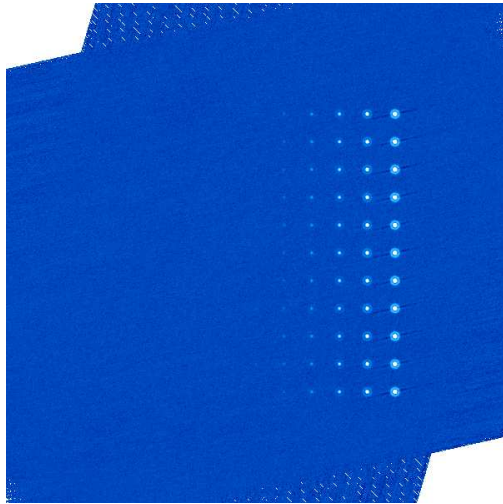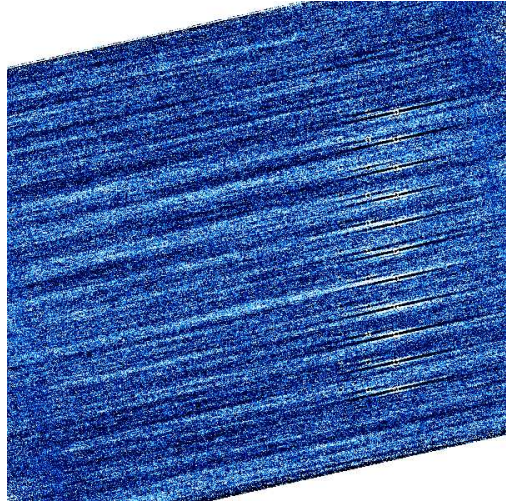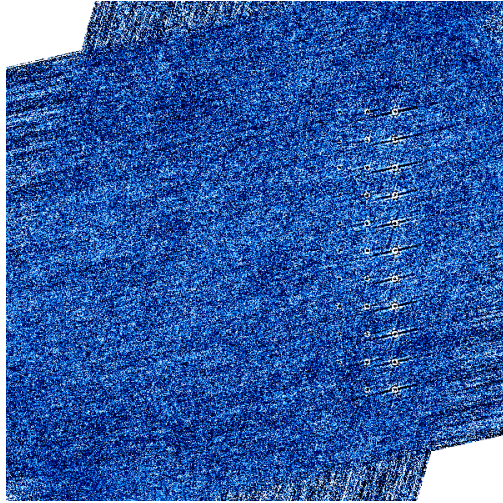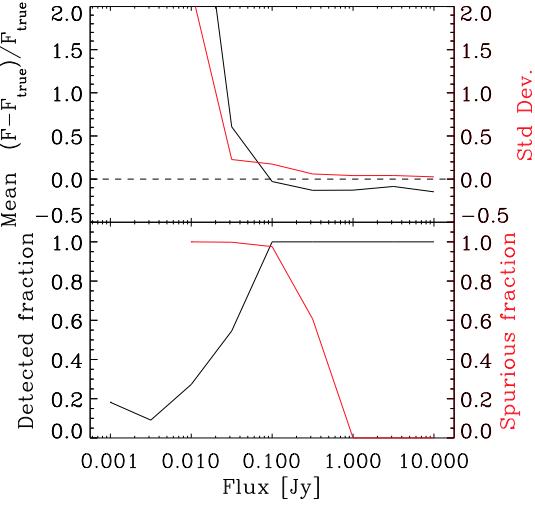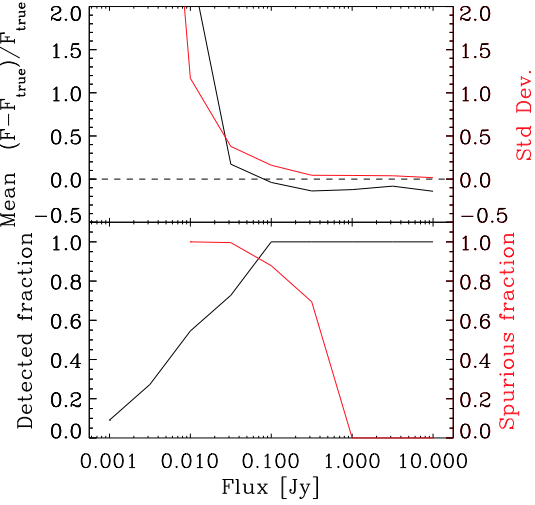
| Single scan | Cross scan |
|:---:|:---:|
| 6″ Reconstructed maps (log scale) | |
|  |  |
| Residuals (histogram-equalized) | |
|  |  |
|  |  |
| $\sigma$ [mJy/pixel]  2.6925 | 2.1873 |
| $N_{crossid.}$  67 | 74 |
| $N_{spurious}$  4575 | 4597 |
| Execution time  35.4s | 46.9s |

Table 20: NGC 5194 – MADmap (Ncorr=200)
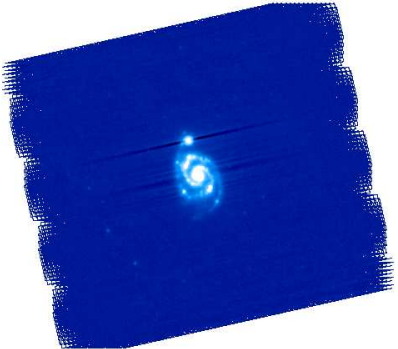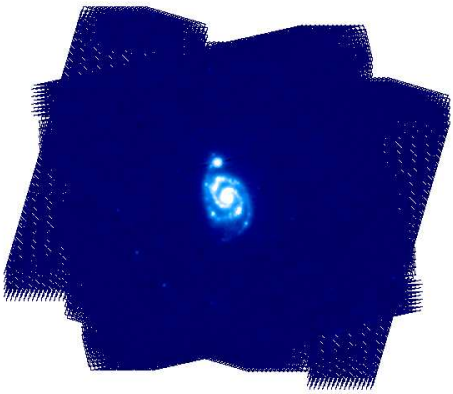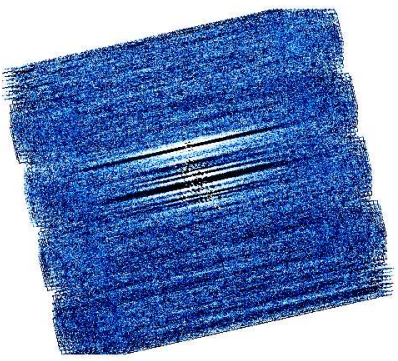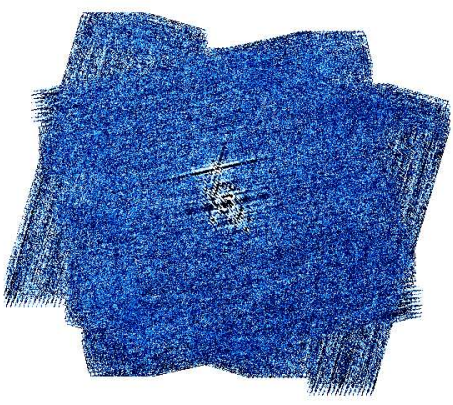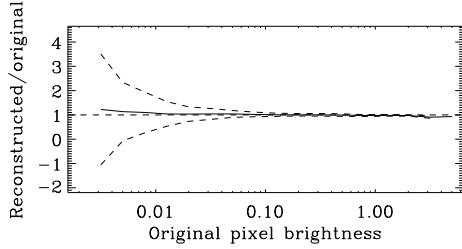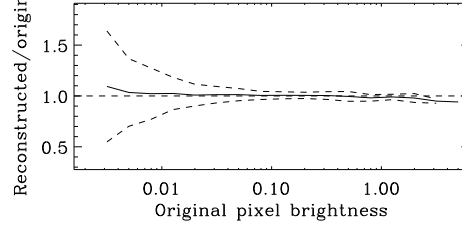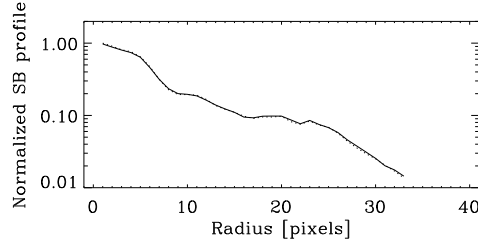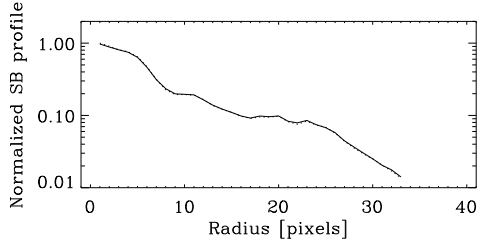
| Single scan | Cross scan |
|---|---|
| 6″ Reconstructed maps (log scale) | |



| Residuals (histogram-equalized) | |
|---|---|





| $\sigma$   [mJy/pixel] | 14.4322 | 11.0900 |
|---|---|---|
| Total flux ratio | 0.9980 | 0.9983 |
| Mean profile ratio | 1.0101 | 1.0078 |
| Std. Dev. profile ratio | 0.0273 | 0.0183 |
| Execution time | 22.6s | 30.7s |

Table 21: IC 4710 – MADmap (Ncorr=200)
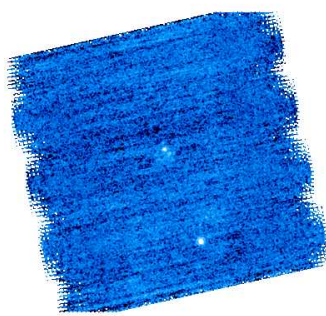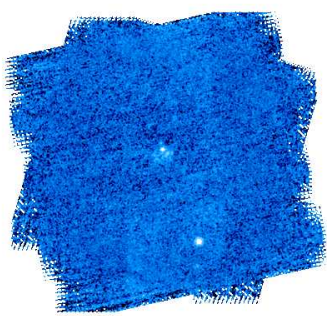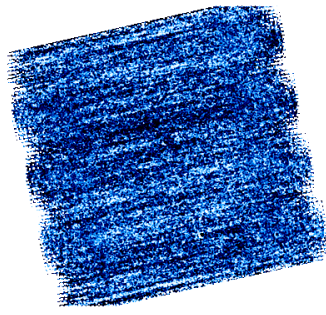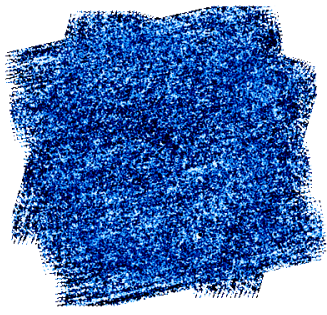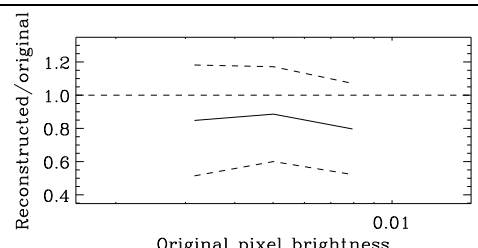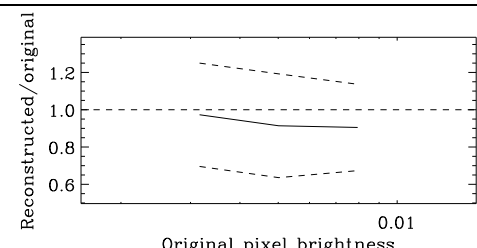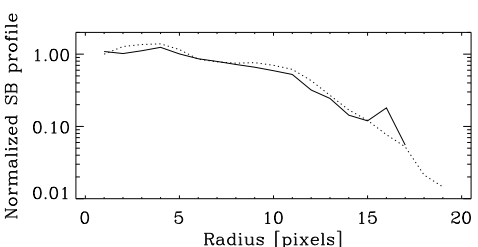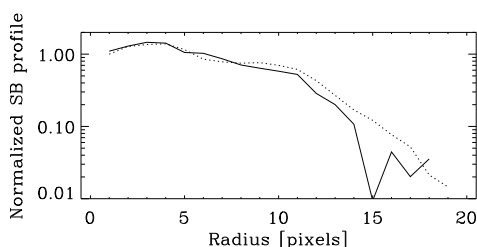
| Single scan | Cross scan |
|:---:|:---:|
| 6″ Reconstructed maps (log scale) | |



| Residuals (histogram-equalized) | |
|:---:|:---:|





| $\sigma$ [mJy/pixel] | 1.3221 | 1.2412 |
|:---|:---:|:---:|
| Total flux ratio | 0.7845 | 0.7948 |
| Mean profile ratio | 0.8812 | 0.5842 |
| Std. Dev. profile ratio | 0.4800 | 1.2855 |
| Execution time | 20.5s | 25.7s |

Table 22: Small Exponential Disk – MADmap (Ncorr=200)
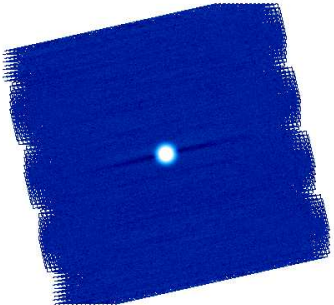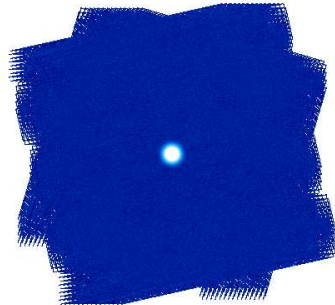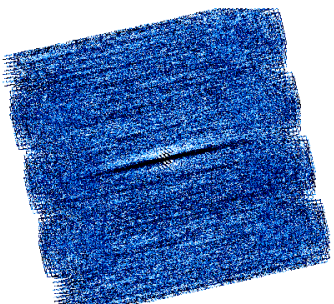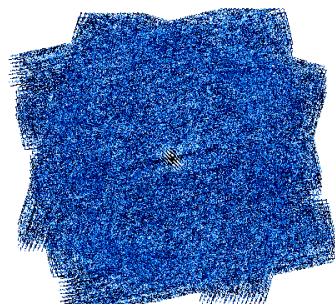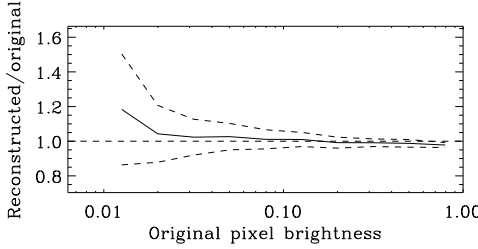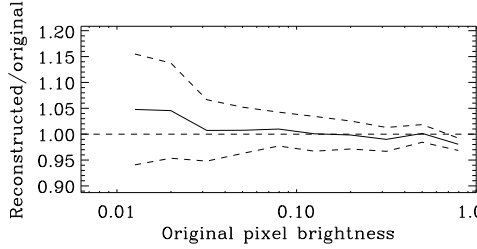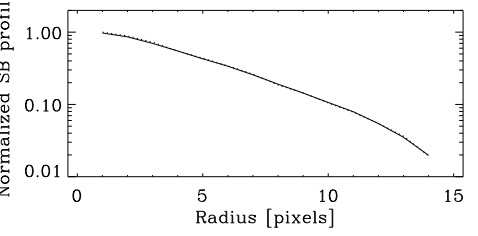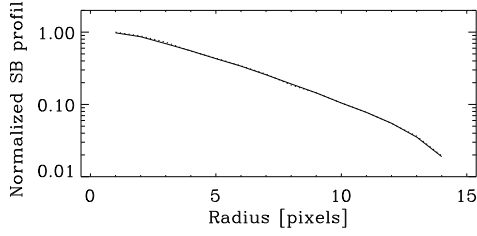
| Single scan | Cross scan |
|---|---|
| 6″ Reconstructed maps (log scale) | |



| Residuals (histogram-equalized) | |
|---|---|



| $\sigma$   [mJy/pixel] | 6.8222 | 5.4015 |
|---|---|---|
| Total flux ratio | 0.9924 | 0.9970 |
| Mean profile ratio | 0.9920 | 0.9898 |
| Std. Dev. profile ratio | 0.0222 | 0.0207 |
| Execution time | 20.1s | 25.2s |

Table 23: Large Exponential Disk – MADmap (Ncorr=200)
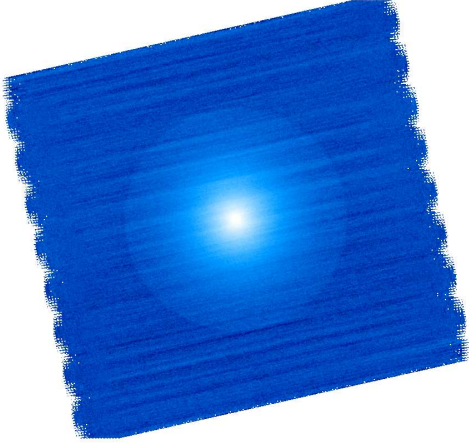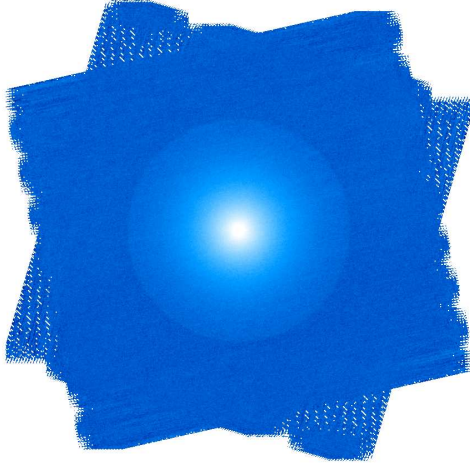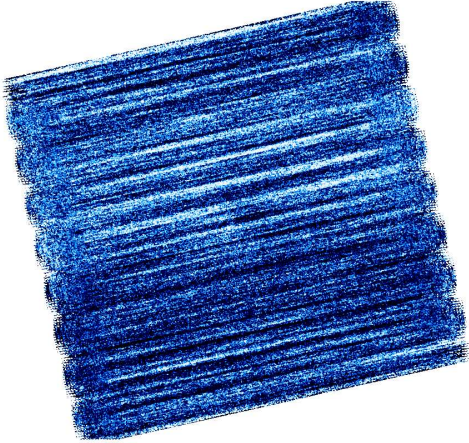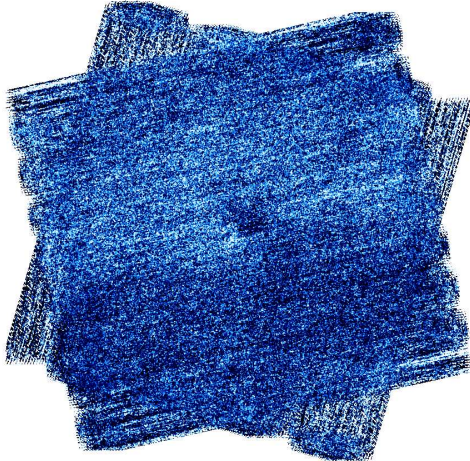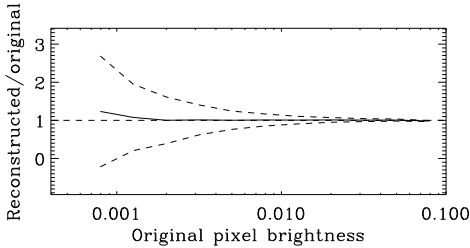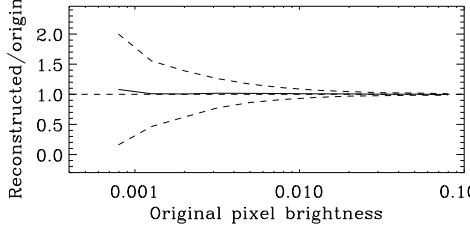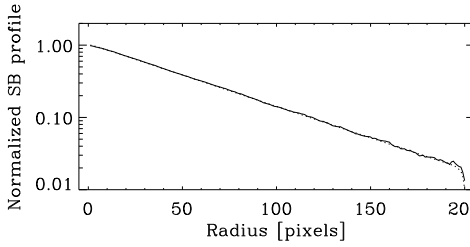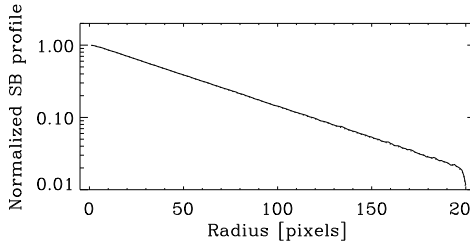
| Single scan | Cross scan |
|---|---|
| 6″ Reconstructed maps (log scale) | |



| Residuals (histogram-equalized) | |
|---|---|





| $\sigma$ [mJy/pixel] | 1.2005 | 0.7526 |
|---|---|---|
| Total flux ratio | 1.0141 | 1.0072 |
| Mean profile ratio | 1.0120 | 1.0090 |
| Std. Dev. profile ratio | 0.0341 | 0.0145 |
| Execution time | 42.6s | 1m02s |

Table 24: Cirrus – MADmap (Ncorr=200)
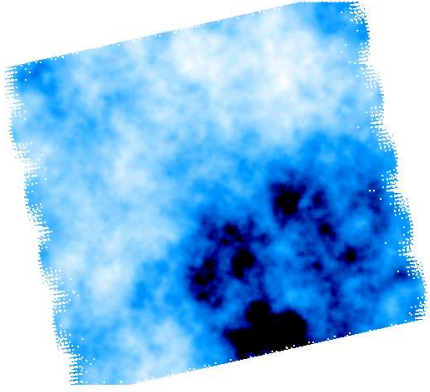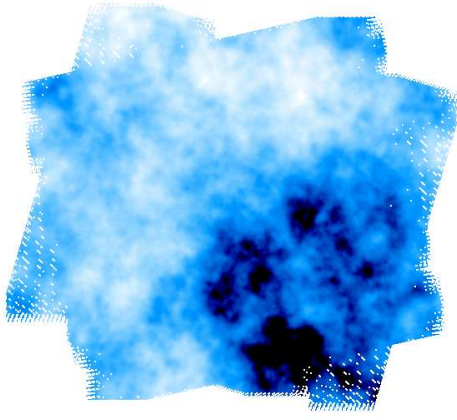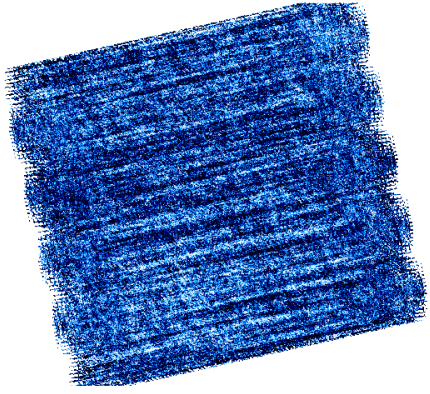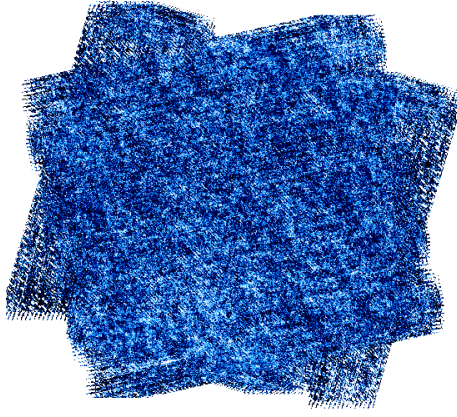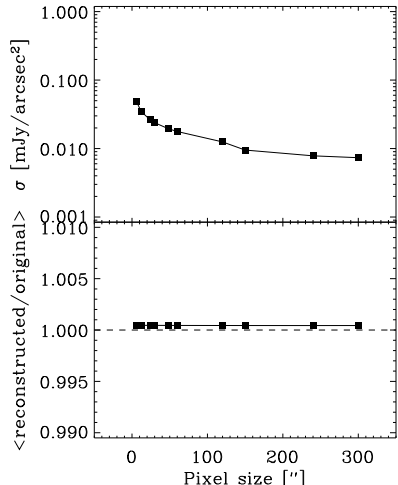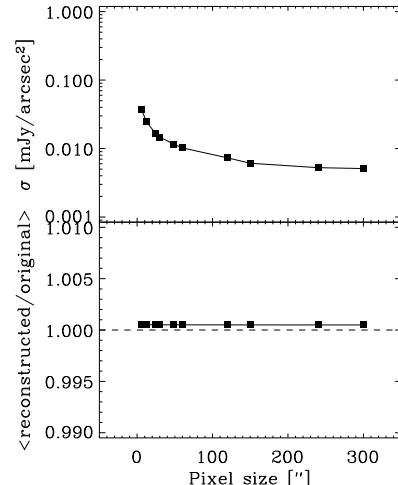
| Single scan | Cross scan |
|---|---|
| 6″ Reconstructed maps (log scale) | |
|  |  |
| Residuals (histogram-equalized) | |
|  |  |
|  |  |

| | Single scan | Cross scan |
|---|---|---|
| $\sigma$ [mJy/pixel] | 1.7485 | 1.3456 |
| <reconstructed/original> | 1.0005 | 1.0005 |
| Execution time | 23.8s | 33.1s |

Table 25: Cirrus with Compact Sources – MADmap (Ncorr=200)
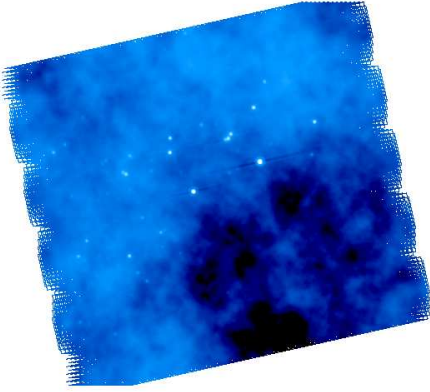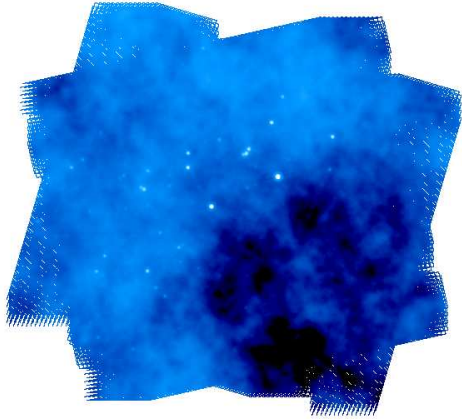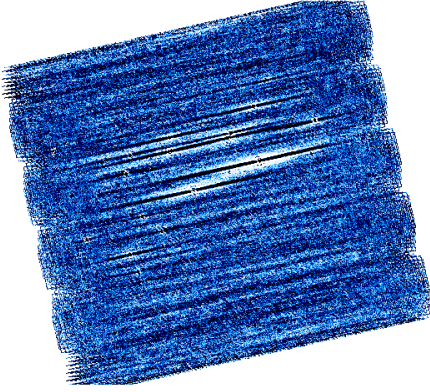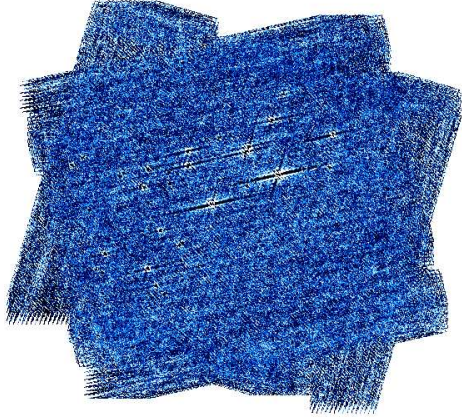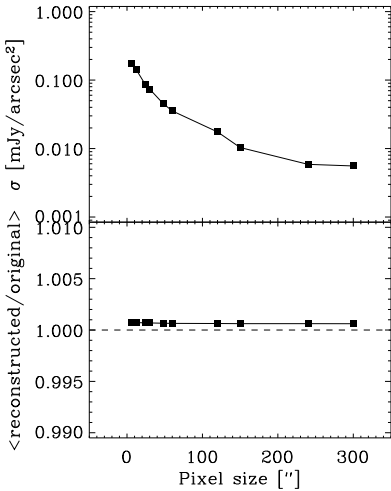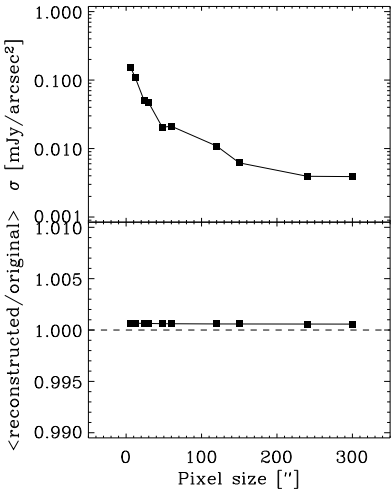
| Single scan | Cross scan |
|---|---|
| 6″ Reconstructed maps (log scale) | |
|  |  |
| Residuals (histogram-equalized) | |
|  |  |
|  |  |

| | Single scan | Cross scan |
|---|---|---|
| $\sigma$ [mJy/pixel] | 6.2538 | 5.4937 |
| <reconstructed/original> | 1.0007 | 1.0007 |
| Execution time | 24.0s | 33.0s |

Table 26: Galics Simulation – Filtered Mapping

| Single scan | Cross scan | 10 cross scans |
|:---:|:---:|:---:|
| 6″ Reconstructed maps (log scale) | | |
|  |  |  |
| Residuals (histogram-equalized) | | |
|  |  |  |
|  |  |  |
| $\sigma$ [mJy/pixel]  2.1634 | 0.7089 | 0.2897 |
| $N_{\text{crossid.}}$  2704 | 3361 | 4134 |
| $N_{\text{spurious}}$  2800 | 2401 | 1085 |
| Execution time  52.8s | 1m41s | 50m00s |
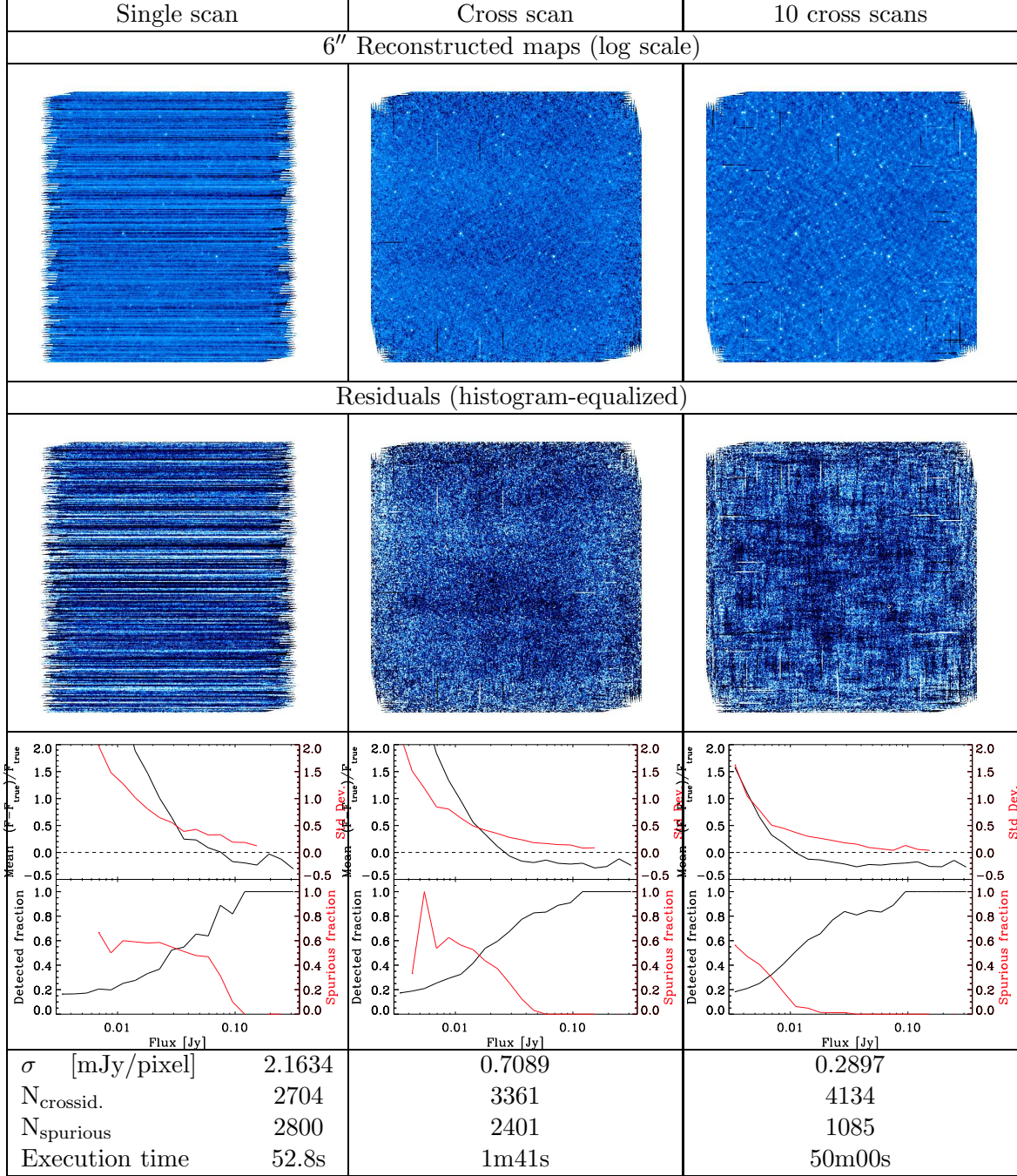
Table 27: Grid of Point Sources – Filtered Mapping

| Single scan | Cross scan |
|---|---|
| 6″ Reconstructed maps (log scale) | |



| Residuals (histogram-equalized) | |
|---|---|





| $\sigma$ [mJy/pixel] | 2.7953 | 2.4170 |
|---|---|---|
| $N_{crossid.}$ | 73 | 80 |
| $N_{spurious}$ | 5510 | 5712 |
| Execution time | 3m40s | 4m10s |
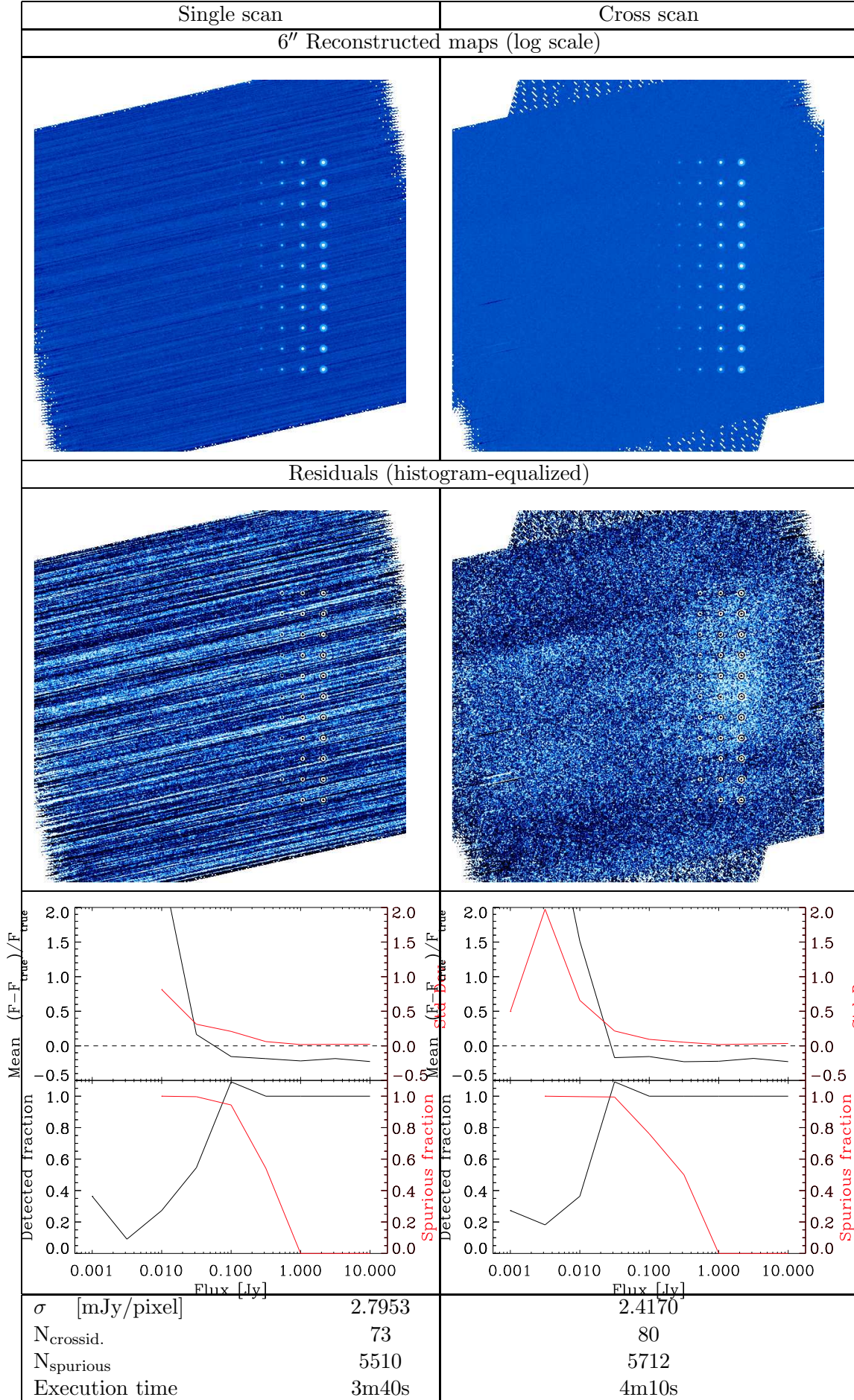
Table 28: NGC 5194 – Filtered Mapping
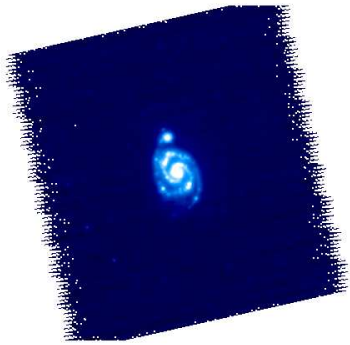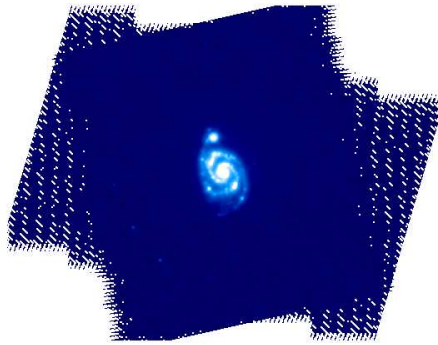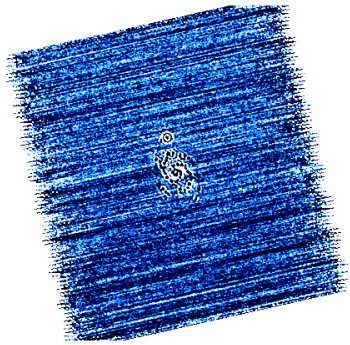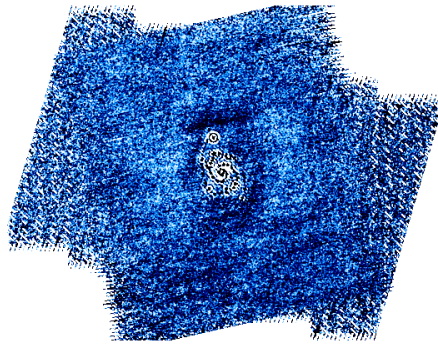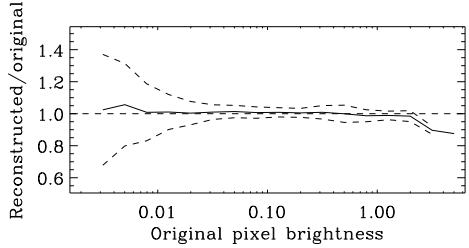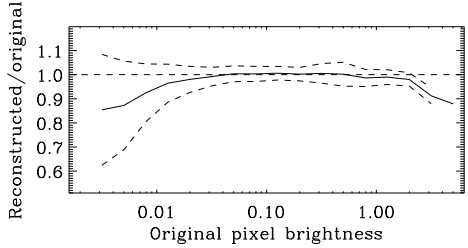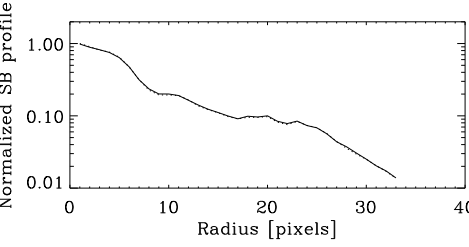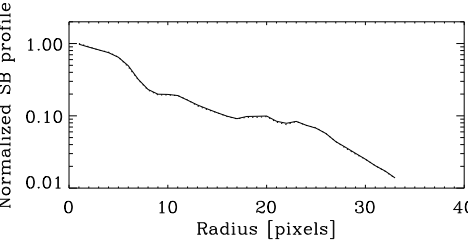
| Single scan | Cross scan |
|---|---|
| 6″ Reconstructed maps (log scale) | |



| Residuals (histogram-equalized) | |
|---|---|





| $\sigma$ [mJy/pixel] | 14.0972 | 13.2926 |
|---|---|---|
| Total flux ratio | 0.9998 | 0.9953 |
| Mean profile ratio | 1.0104 | 1.0109 |
| Std. Dev. profile ratio | 0.0186 | 0.0172 |
| Execution time | 30.3s | 51.5s |

Table 29: IC 4710 – Filtered Mapping
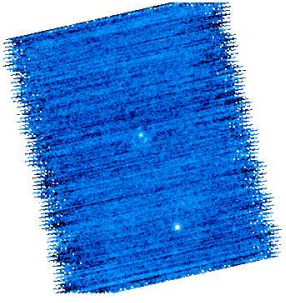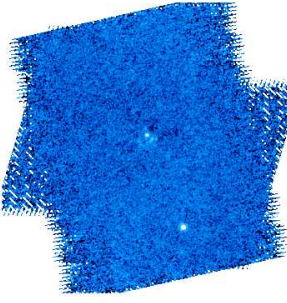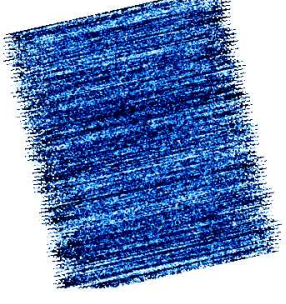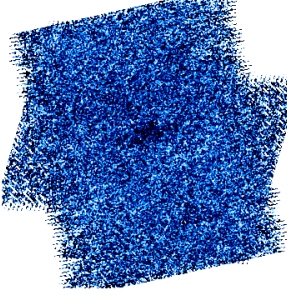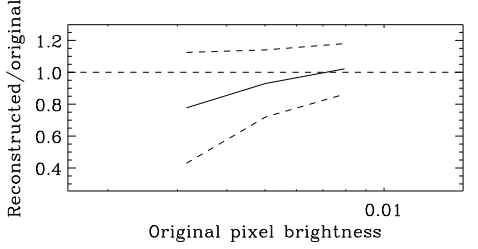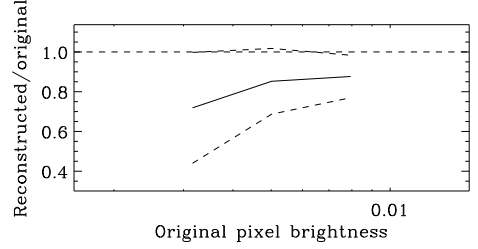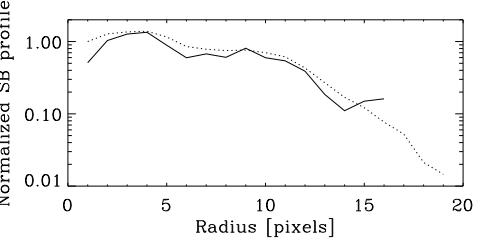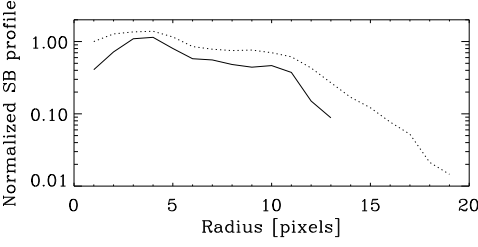
| Single scan | Cross scan |
|---|---|
| 6″ Reconstructed maps (log scale) | |
| | |
| Residuals (histogram-equalized) | |
| | |

| $\sigma$   [mJy/pixel] | 1.0761 | 0.8843 |
|---|---|---|
| Total flux ratio | 0.7641 | 0.4756 |
| Mean profile ratio | 0.3553 | 0.0020 |
| Std. Dev. profile ratio | 1.4257 | 1.0351 |
| Execution time | 17.9s | 28.0s |

Table 30: Small Exponential Disk – Filtered Mapping
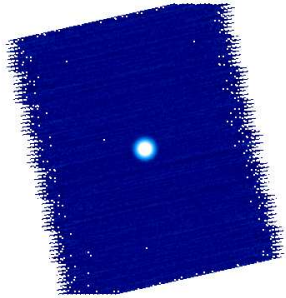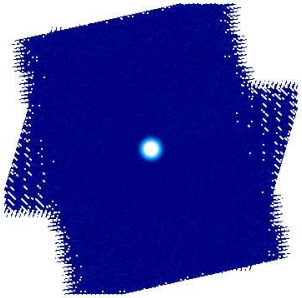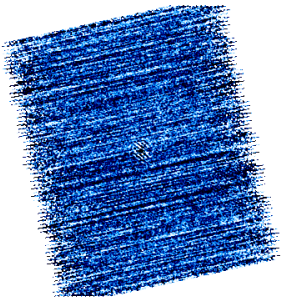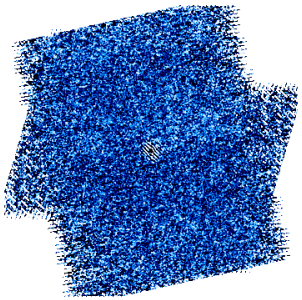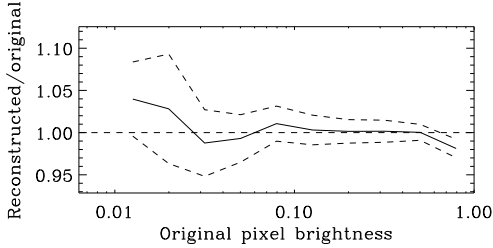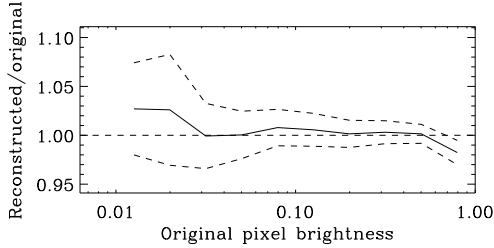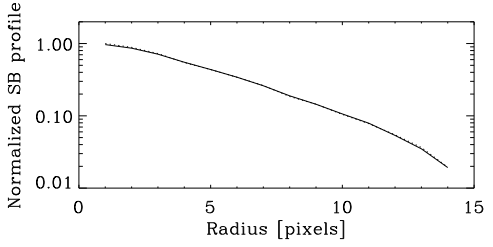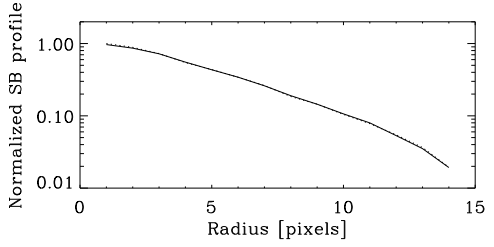
| Single scan | Cross scan |
|---|---|
| 6″ Reconstructed maps (log scale) | |



| Residuals (histogram-equalized) | |
|---|---|





| | Single scan | Cross scan |
|---|---|---|
| $\sigma$ [mJy/pixel] | 4.1423 | 3.9425 |
| Total flux ratio | 0.9980 | 0.9990 |
| Mean profile ratio | 0.9934 | 0.9952 |
| Std. Dev. profile ratio | 0.0192 | 0.0199 |
| Execution time | 19.5s | 28.9s |

Table 31: Large Exponential Disk – Filtered Mapping
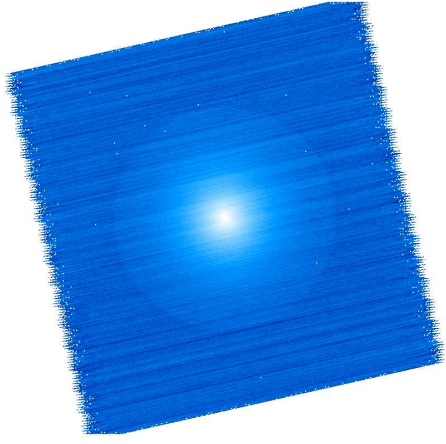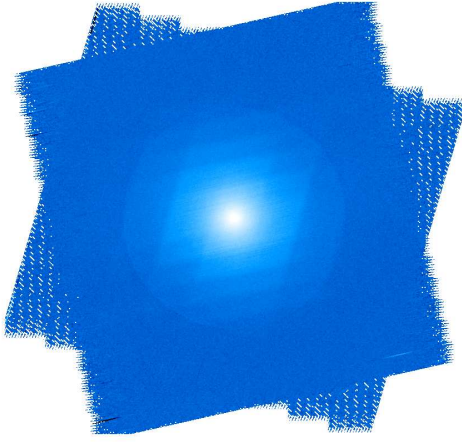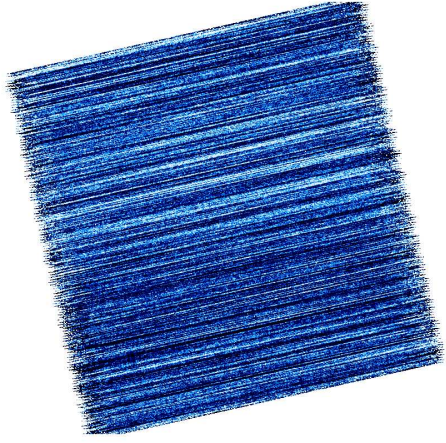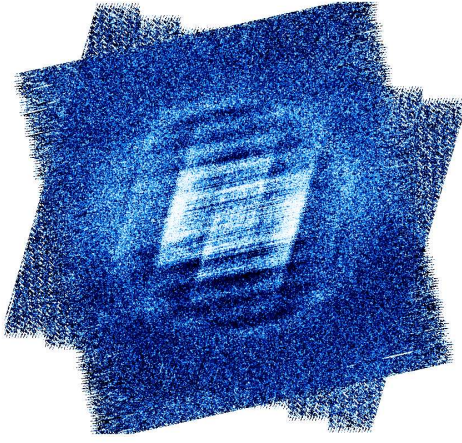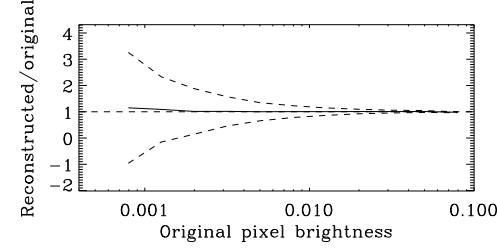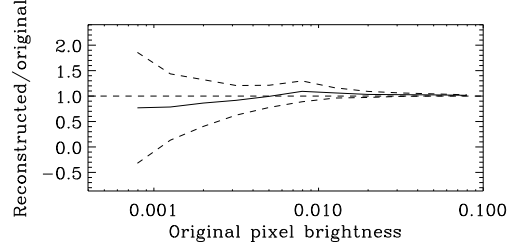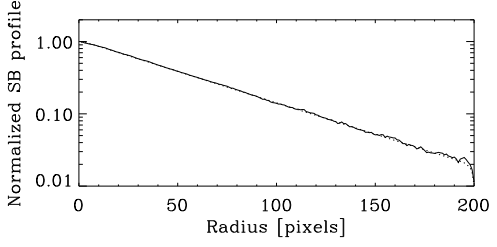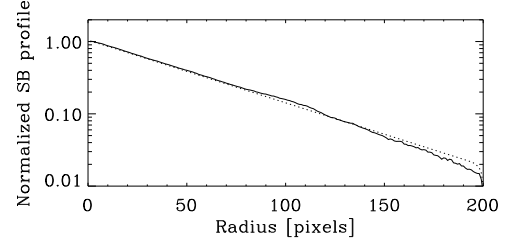
| Single scan | Cross scan |
|---|---|
| 6″ Reconstructed maps (log scale) | |



| Residuals (histogram-equalized) | |
|---|---|



| $\sigma$ [mJy/pixel] | 1.7027 | 1.1988 |
|---|---|---|
| Total flux ratio | 1.0155 | 1.0194 |
| Mean profile ratio | 1.0134 | 0.9891 |
| Std. Dev. profile ratio | 0.0339 | 0.0876 |
| Execution time | 4m15s | 4m56s |

63

Table 32: Cirrus – Filtered Mapping
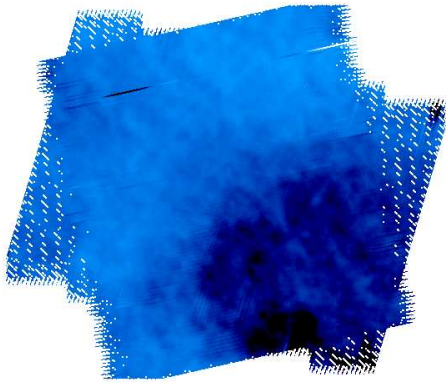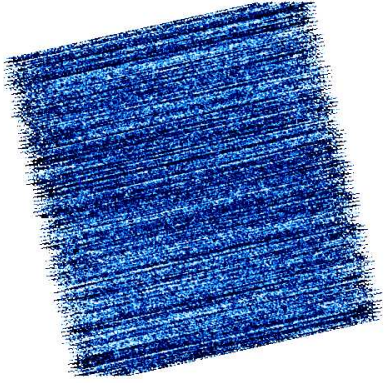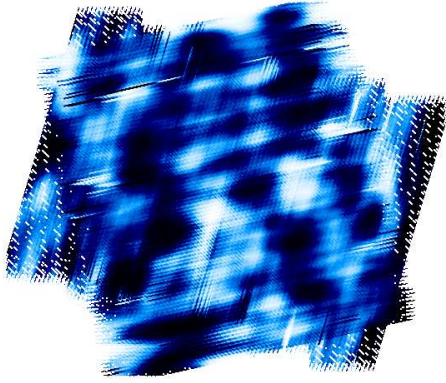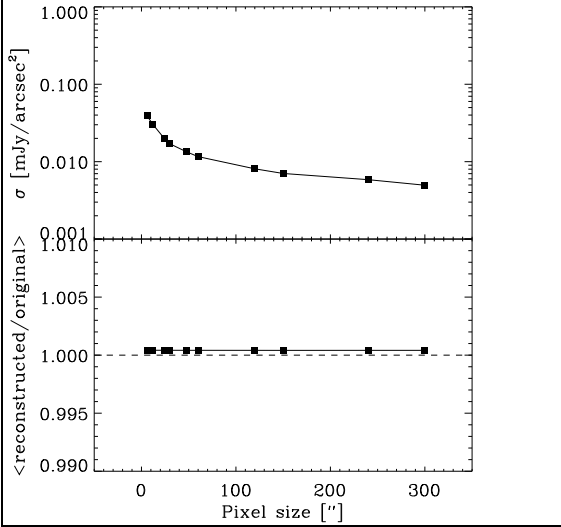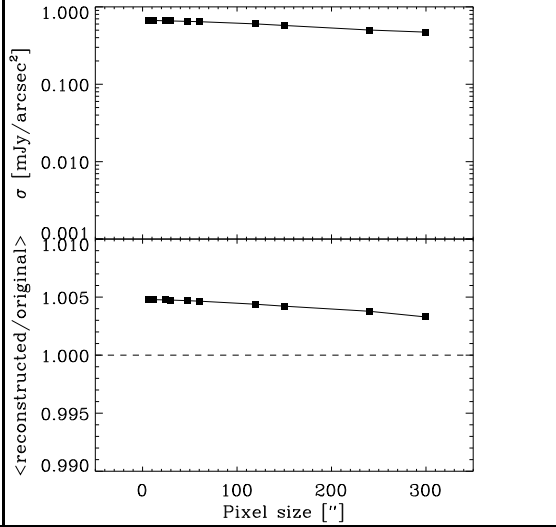
| Single scan | Cross scan |
|---|---|
| 6″ Reconstructed maps (log scale) | |
|  |  |
| Residuals (histogram-equalized) | |
|  |  |
|  |  |

| | Single scan | Cross scan |
|---|---|---|
| $\sigma$ [mJy/pixel] | 1.4034 | 24.2505 |
| <reconstructed/original> | 1.0004 | 1.0048 |
| Execution time | 28.2s | 52.7s |

64

Table 33: Cirrus with Compact Sources – Filtered Mapping
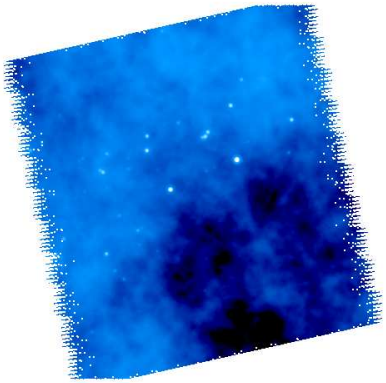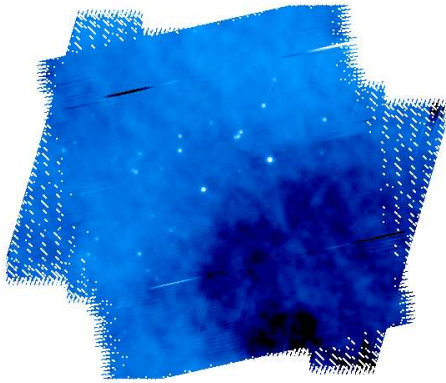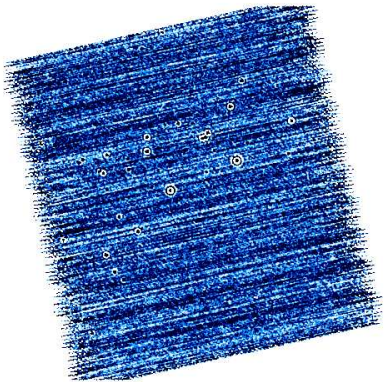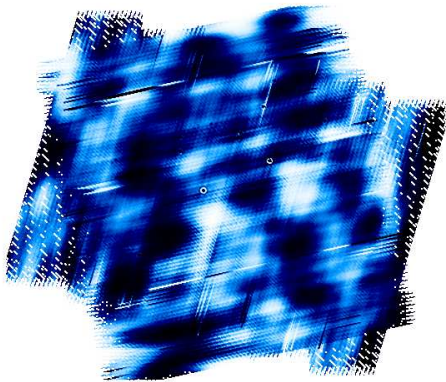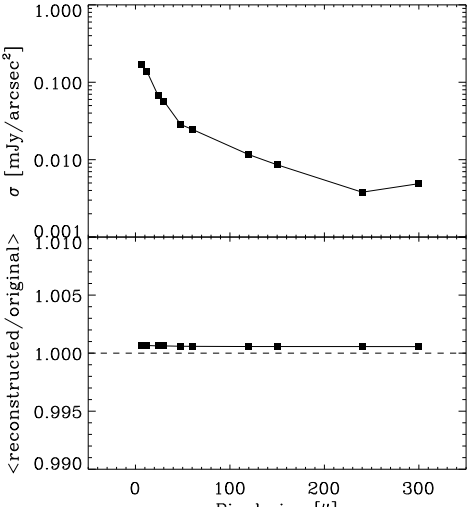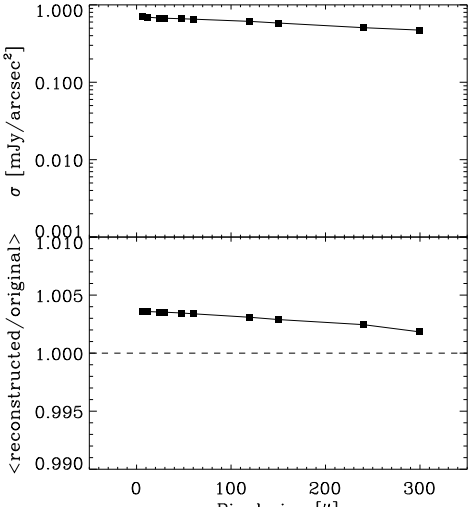
| Single scan | Cross scan |
|---|---|
| 6″ Reconstructed maps (log scale) | |



| Residuals (histogram-equalized) | |
|---|---|





| $\sigma$ [mJy/pixel] | 6.0890 | 25.4287 |
|---|---|---|
| <reconstructed/original> | 1.0007 | 1.0036 |
| Execution time | 29.0s | 53.4s |

Table 34: Galics Simulation – MOPEX NO Filter

| Single scan | Cross scan | 10 cross scans |
|---|---|---|
| 6″ Reconstructed maps (log scale) | | |
|  |  | |
| Residuals (histogram-equalized) | | |
|  |  | |
|  |  |  |
| $\sigma$ [mJy/pixel] 2.1767 | 1.8048 | N/A |
| $N_{crossid.}$ 2870 | 3118 | N/A |
| $N_{spurious}$ 2953 | 3249 | N/A |
| Execution time 35m36s | 40m22s | N/A |

Table 35: Grid of Point Sources – MOPEX NO Filter

| Single scan | Cross scan |
|---|---|
| 6″ Reconstructed maps (log scale) | |



| Residuals (histogram-equalized) | |
|---|---|





| $\sigma$   [mJy/pixel] | 2.7010 | 2.2611 |
|---|---|---|
| $N_{\text{crossid.}}$ | 72 | 70 |
| $N_{\text{spurious}}$ | 5152 | 5268 |
| Execution time | 28m48s | 1h34m36s |
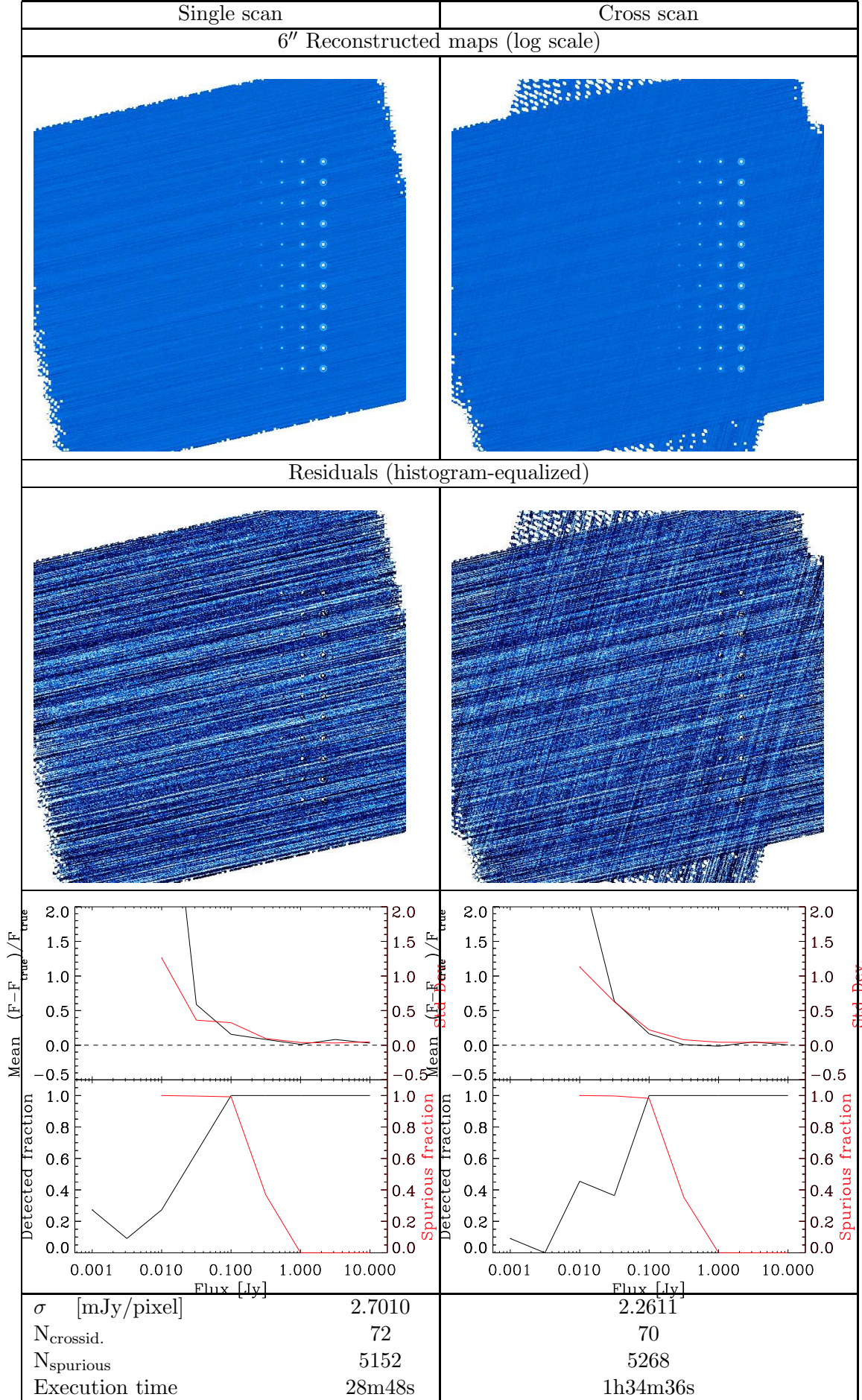
Table 36: NGC 5194 – MOPEX NO Filter
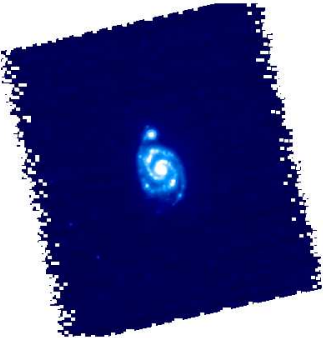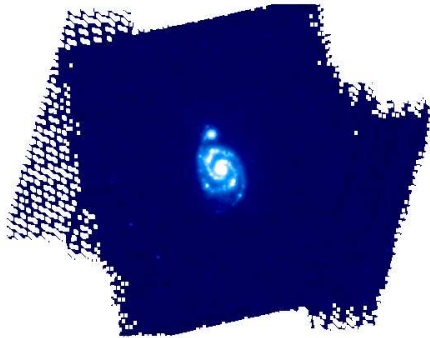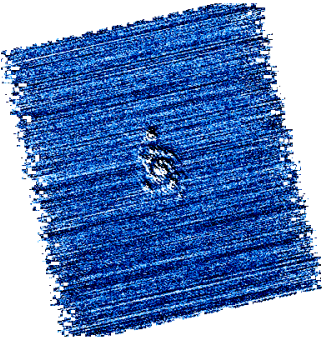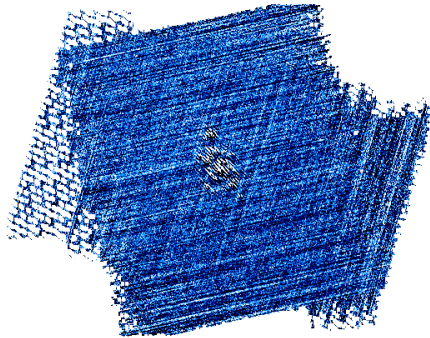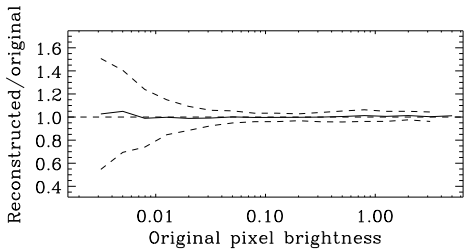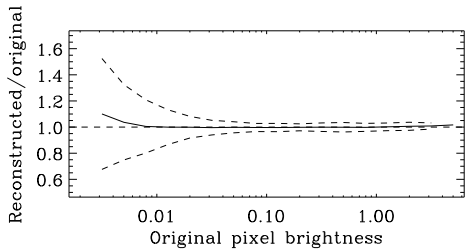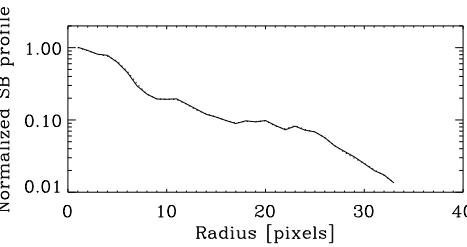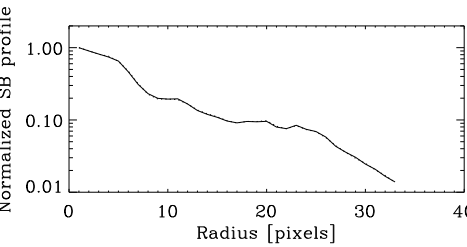
| Single scan | Cross scan |
|:---:|:---:|
| 6″ Reconstructed maps (log scale) | |



| Residuals (histogram-equalized) | |
|:---:|:---:|





| $\sigma$ [mJy/pixel] | 11.1666 | 7.8256 |
|:---|:---:|:---:|
| Total flux ratio | 1.0017 | 0.9996 |
| Mean profile ratio | 0.9986 | 0.9985 |
| Std. Dev. profile ratio | 0.0230 | 0.0167 |
| Execution time | 27m50s | 31m02s |

68

Table 37: IC 4710 – MOPEX NO Filter
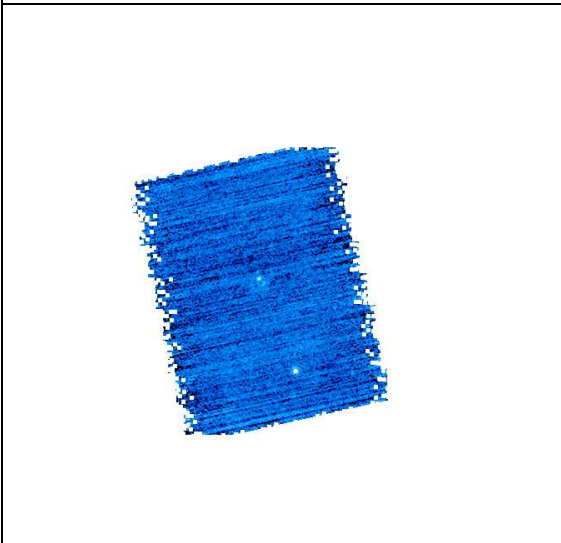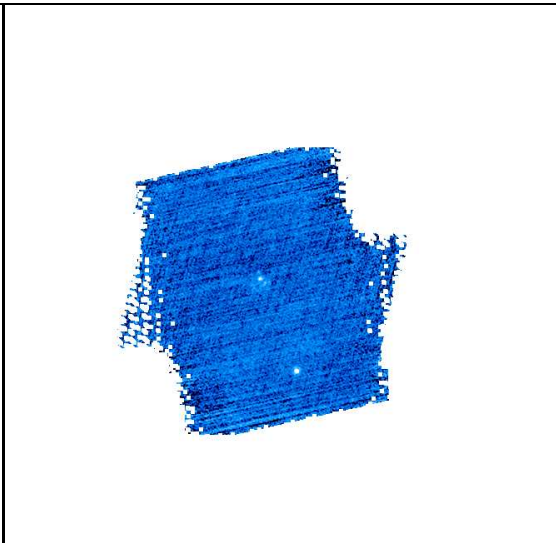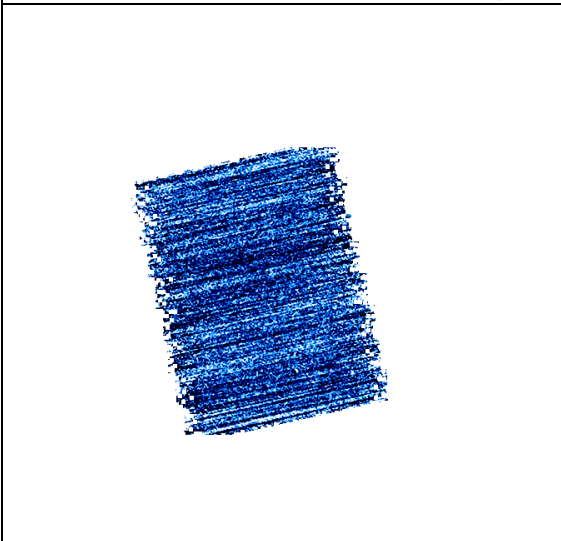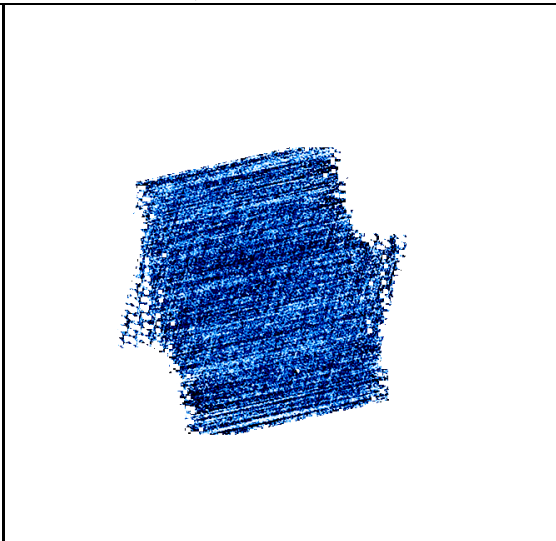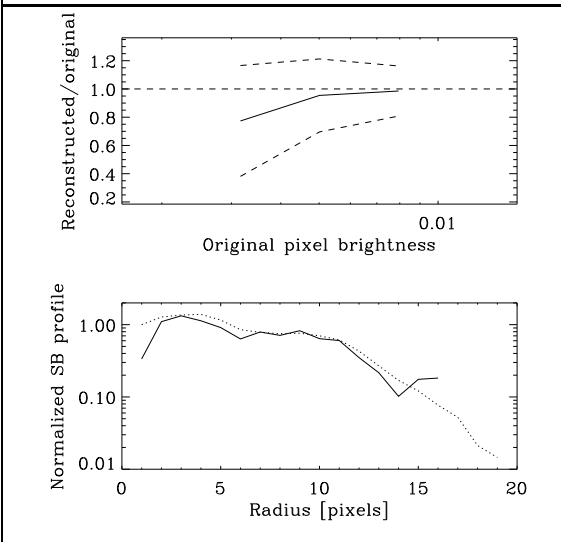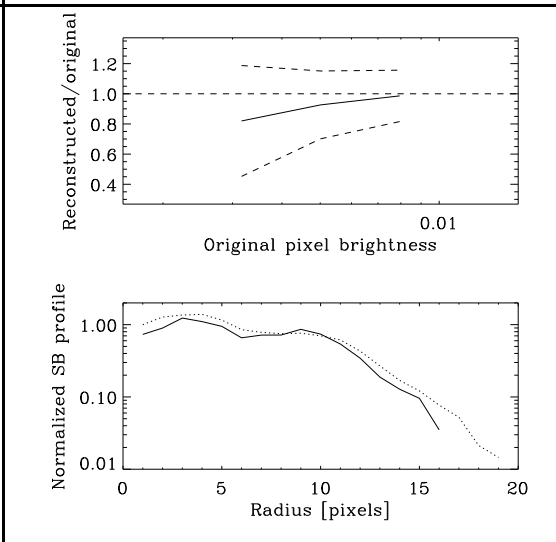
| Single scan | Cross scan |
|---|---|
| 6″ Reconstructed maps (log scale) | |



| Residuals (histogram-equalized) | |
|---|---|





| | Single scan | Cross scan |
|---|---|---|
| $\sigma$  [mJy/pixel] | 1.2374 | 1.1491 |
| Total flux ratio | 0.7798 | 0.7929 |
| Mean profile ratio | 0.4483 | 0.4550 |
| Std. Dev. profile ratio | 1.3408 | 1.2372 |
| Execution time | 6m19s | 29m12s |

Table 38: Small Exponential Disk – MOPEX NO Filter
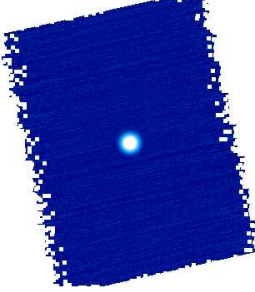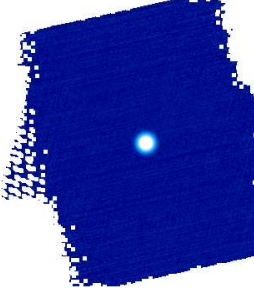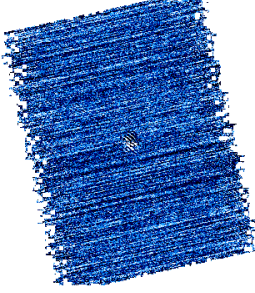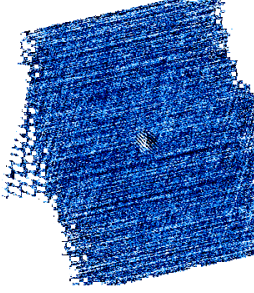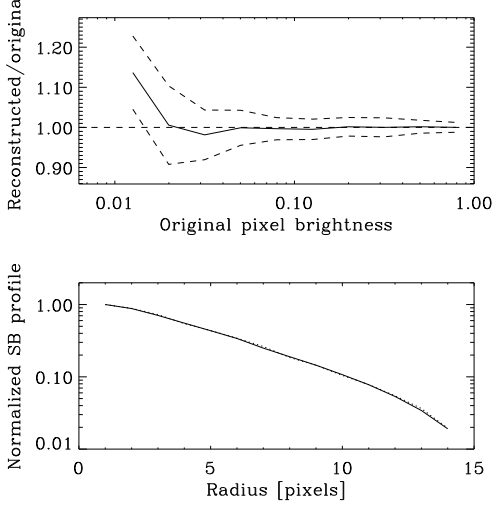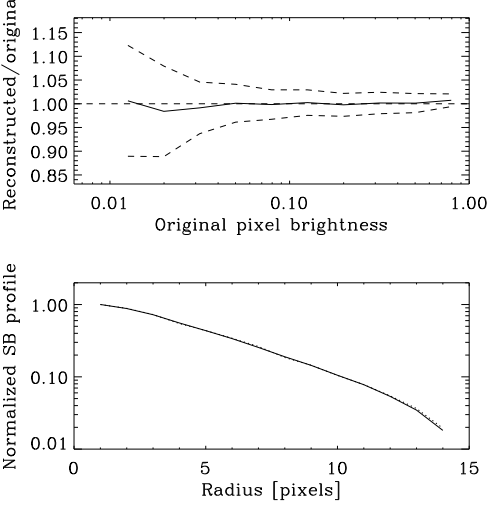
| Single scan | Cross scan |
|---|---|
| 6″ Reconstructed maps (log scale) | |



| Residuals (histogram-equalized) | |
|---|---|





| $\sigma$ [mJy/pixel] | 4.2714 | 4.6546 |
|---|---|---|
| Total flux ratio | 0.9994 | 1.0013 |
| Mean profile ratio | 0.9906 | 0.9896 |
| Std. Dev. profile ratio | 0.0248 | 0.0245 |
| Execution time | 4m58s | 10m28s |

Table 39: Large Exponential Disk – MOPEX NO Filter
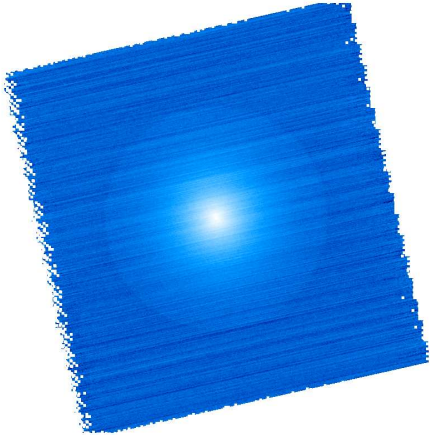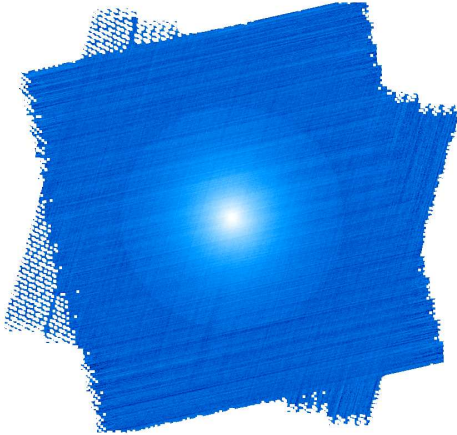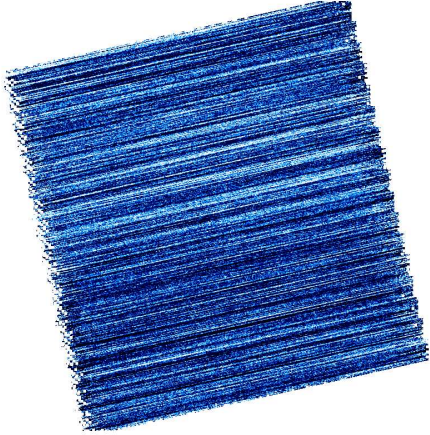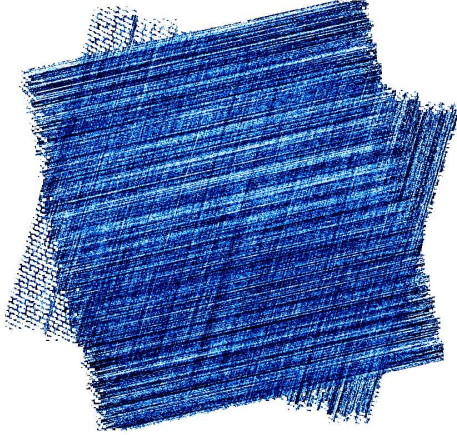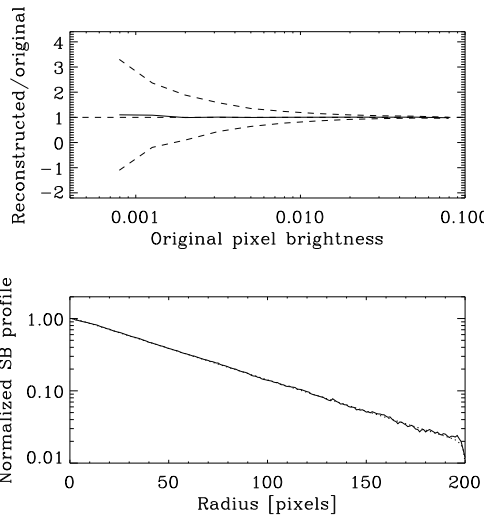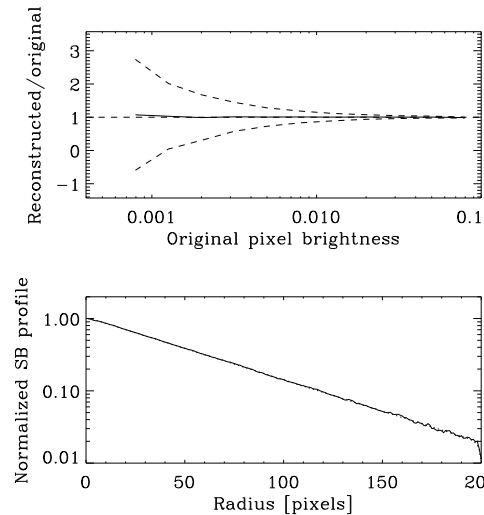
| Single scan | Cross scan |
|---|---|
| 6″ Reconstructed maps (log scale) | |



| Residuals (histogram-equalized) | |
|---|---|





| $\sigma$ [mJy/pixel] | 1.7594 | 1.3512 |
|---|---|---|
| Total flux ratio | 1.0114 | 1.0078 |
| Mean profile ratio | 1.0074 | 1.0062 |
| Std. Dev. profile ratio | 0.0341 | 0.0235 |
| Execution time | 1h33m43s | 10h36m53s |

71

Table 40: Cirrus – MOPEX NO Filter
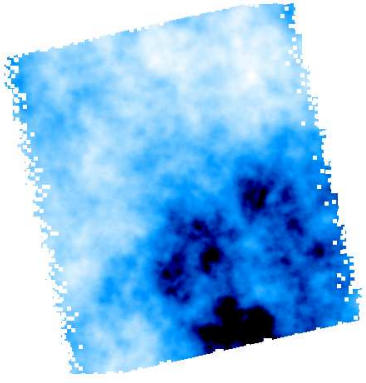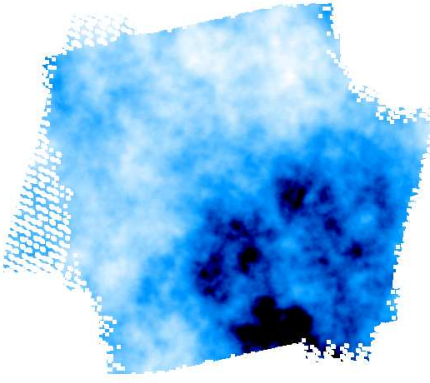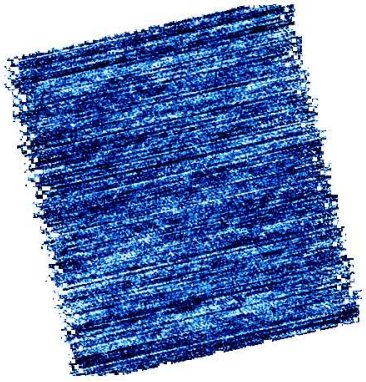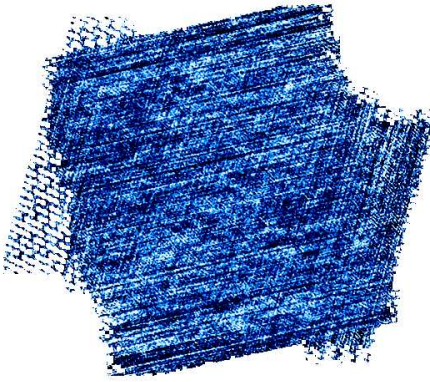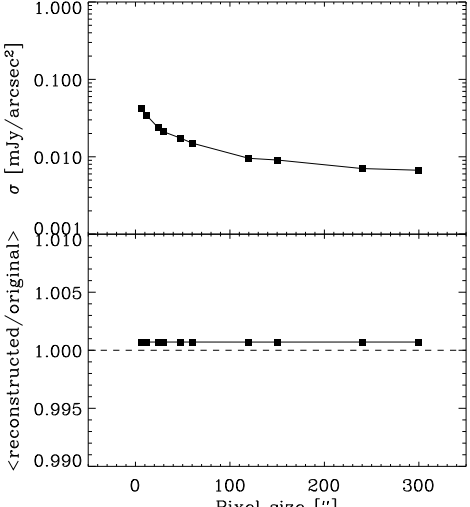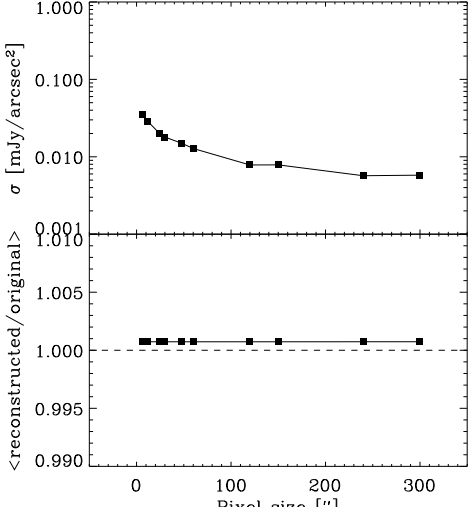
| Single scan | Cross scan |
|---|---|
| 6″ Reconstructed maps (log scale) | |



| Residuals (histogram-equalized) | |
|---|---|





| $\sigma$ [mJy/pixel] | 1.5196 | 1.2644 |
|---|---|---|
| <reconstructed/original> | 1.0007 | 1.0007 |
| Execution time | 37m18s | 35m08s |

Table 41: Cirrus with Compact Sources – MOPEX NO Filter
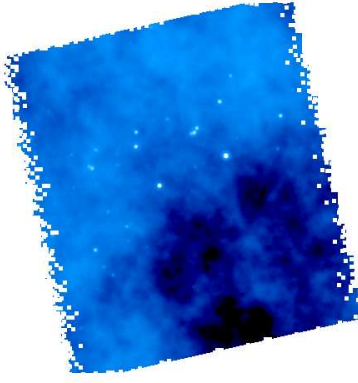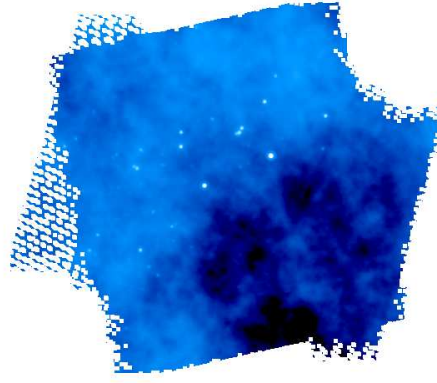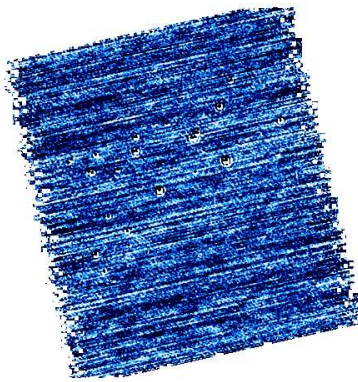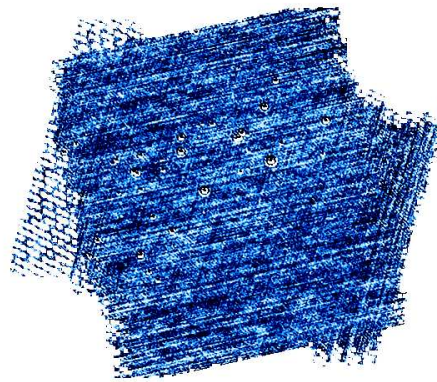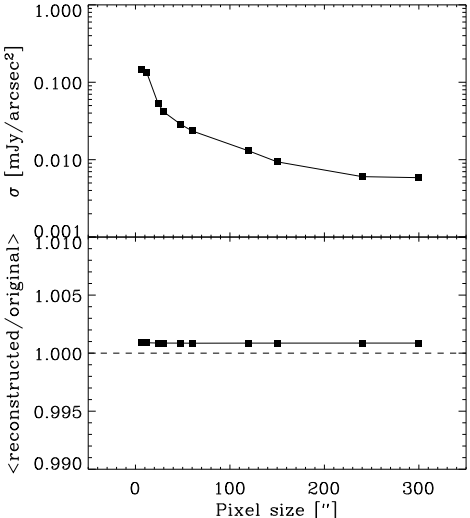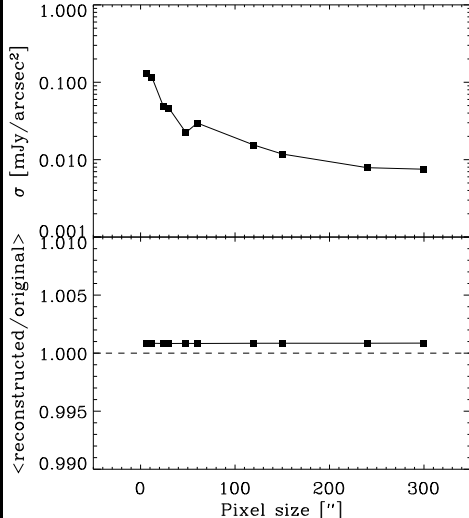
| Single scan | Cross scan |
|---|---|
| 6″ Reconstructed maps (log scale) | |
|  |  |
| Residuals (histogram-equalized) | |
|  |  |
|  |  |
| $\sigma$  [mJy/pixel]  5.3043 | 4.6977 |
| <reconstructed/original>  1.0009 | 1.0009 |
| Execution time  39m07s | 33m35s |

Table 42: Galics Simulation – MOPEX with High Pass Filter
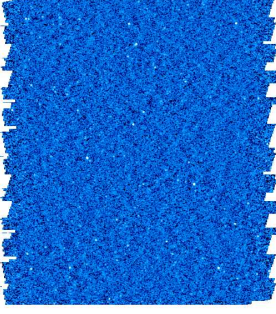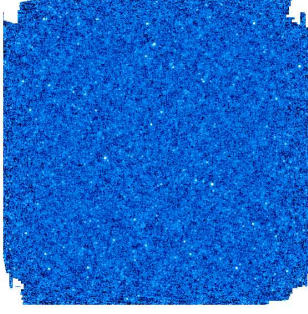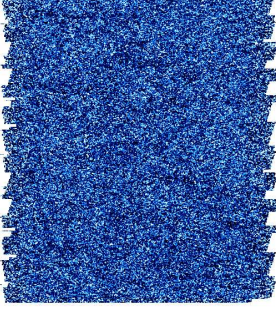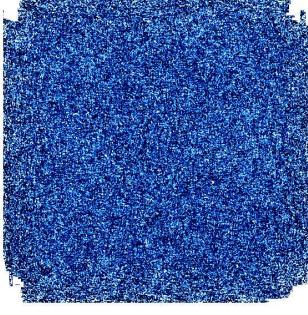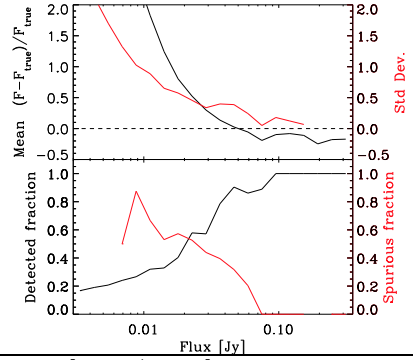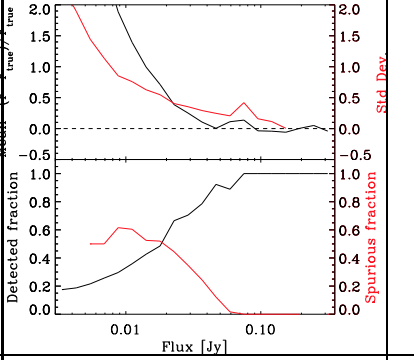
| Single scan | Cross scan | 10 cross scans |
|---|---|---|
| 6″ Reconstructed maps (log scale) | | |
|  |  | |
| Residuals (histogram-equalized) | | |
|  |  | |
|  |  | |
| $\sigma$ [mJy/pixel] 1.0245 | 0.8629 | N/A |
| $N_{crossid.}$ 3198 | 3431 | N/A |
| $N_{spurious}$ 2643 | 2344 | N/A |
| Execution time 1h04m35s | 1h12m33s | N/A |

74

Table 43: Grid of Point Sources – MOPEX with High Pass Filter

| Single scan | Cross scan |
|---|---|
| 6″ Reconstructed maps (log scale) | |



| Residuals (histogram-equalized) | |
|---|---|





| $\sigma$ [mJy/pixel] | 2.1236 | 1.8347 |
|---|---|---|
| $N_{crossid.}$ | 81 | 80 |
| $N_{spurious}$ | 5095 | 5007 |
| Execution time | 39m12s | 57m42s |
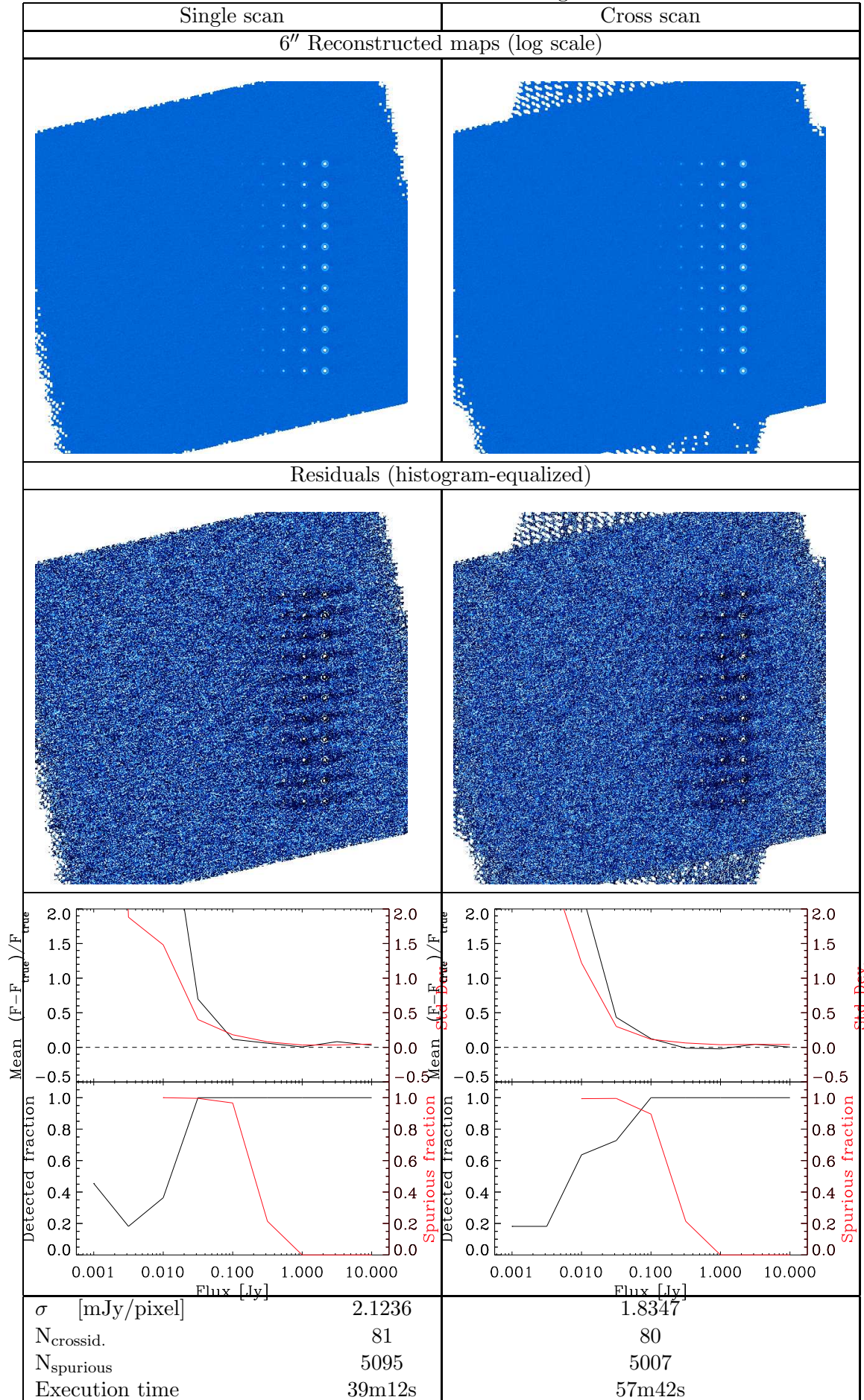
Table 44: NGC 5194 – MOPEX with High Pass Filter
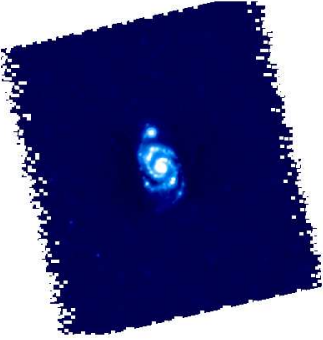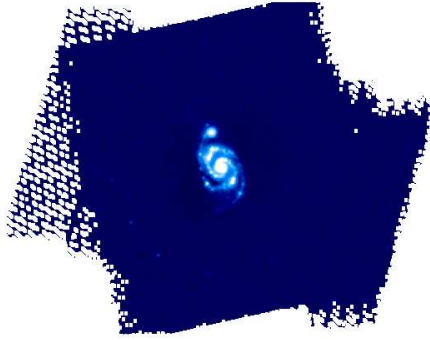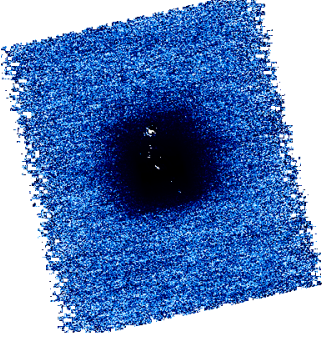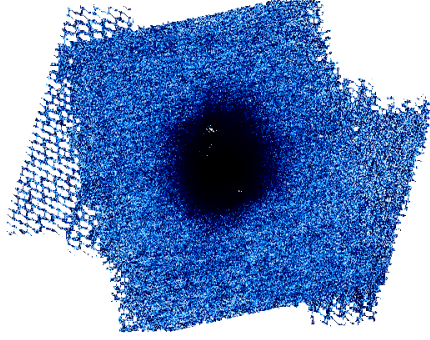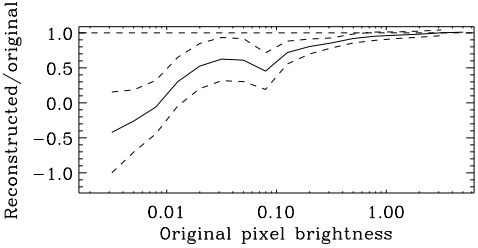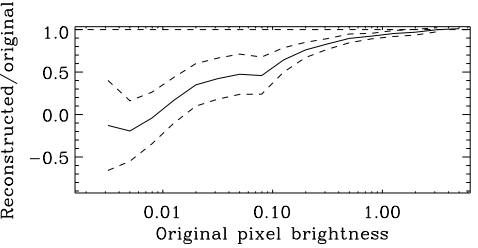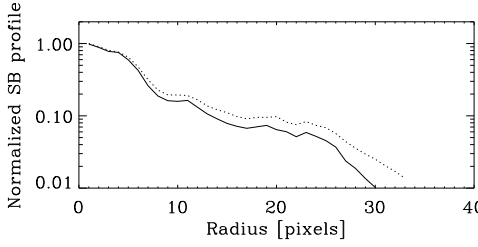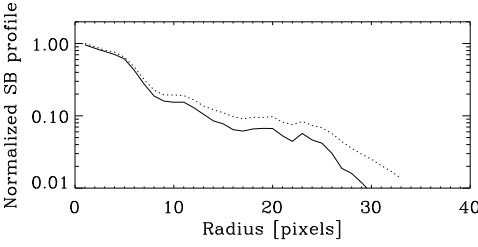
| Single scan | Cross scan |
|:---:|:---:|
| 6″ Reconstructed maps (log scale) | |



| Residuals (histogram-equalized) | |
|:---:|:---:|





| $\sigma$ [mJy/pixel] | 22.3169 | 21.9536 |
|:---|:---:|:---:|
| Total flux ratio | 0.8079 | 0.7735 |
| Mean profile ratio | 0.7050 | 0.6686 |
| Std. Dev. profile ratio | 0.2126 | 0.2216 |
| Execution time | 21m00s | 35m04s |

76

Table 45: IC 4710 – MOPEX with High Pass Filter
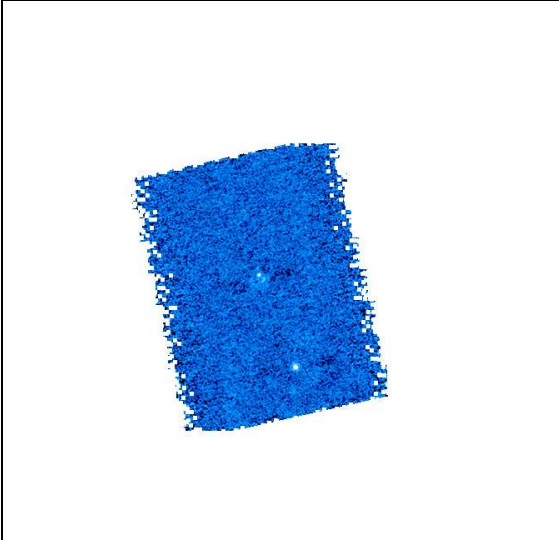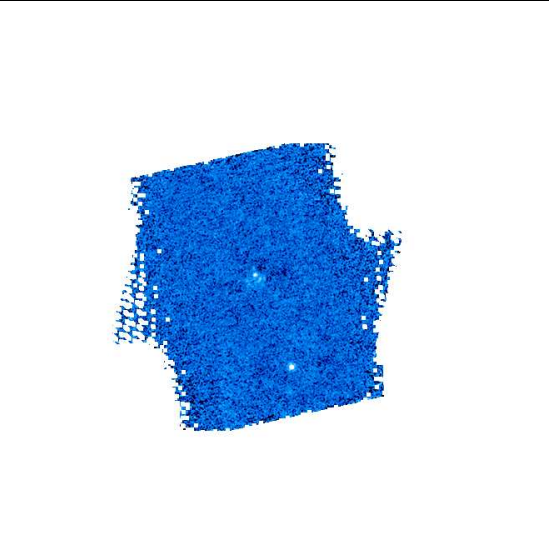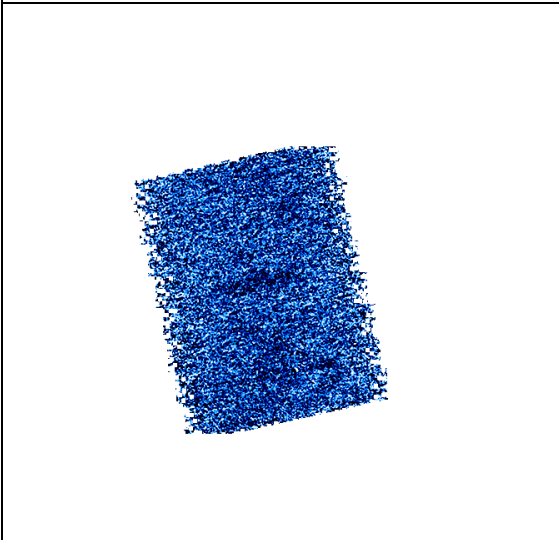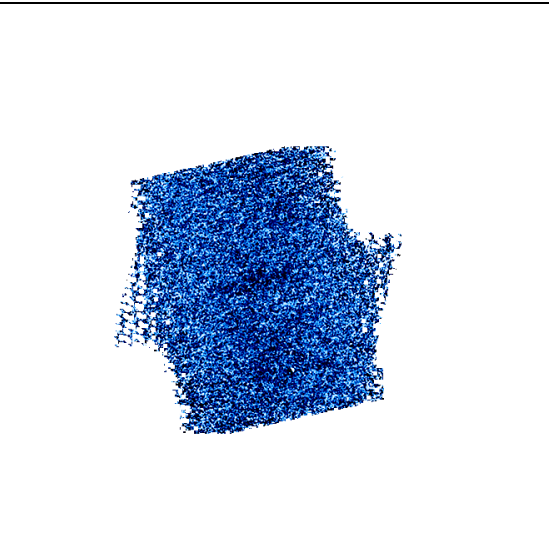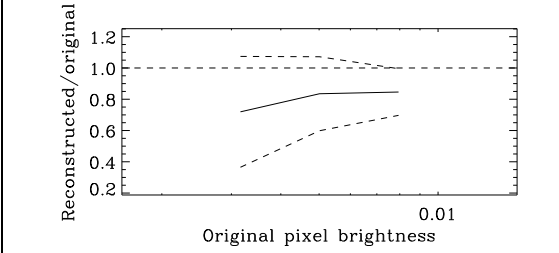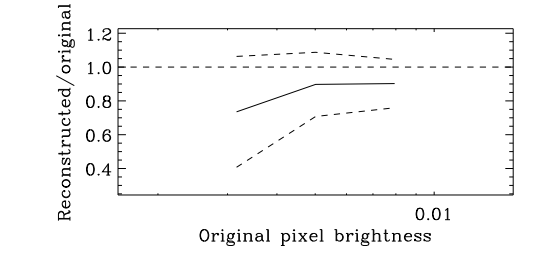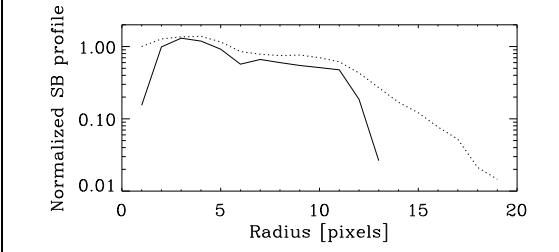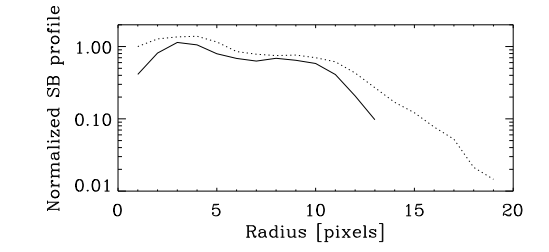
| Single scan | Cross scan |
|---|---|
| 6″ Reconstructed maps (log scale) | |



| Residuals (histogram-equalized) | |
|---|---|



| | Single scan | Cross scan |
|---|---|---|
| $\sigma$  [mJy/pixel] | 1.0866 | 0.9950 |
| Total flux ratio | 0.5195 | 0.5819 |
| Mean profile ratio | -0.1825 | 0.2067 |
| Std. Dev. profile ratio | 1.7070 | 0.8427 |
| Execution time | 9m26s | 16m08s |

Table 46: Small Exponential Disk – MOPEX with High Pass Filter
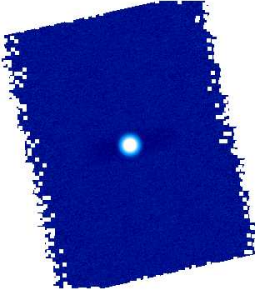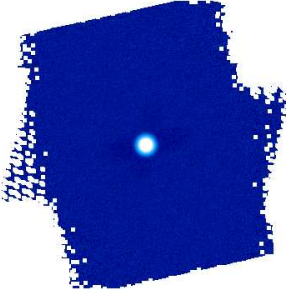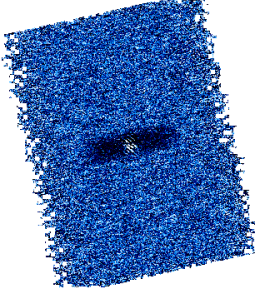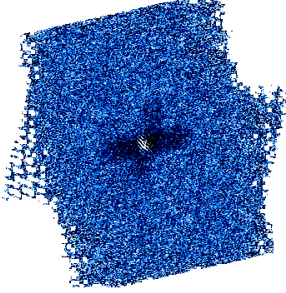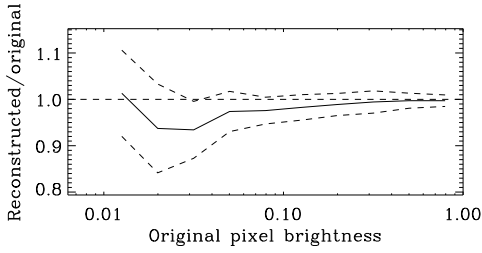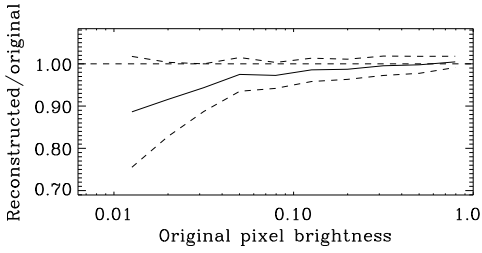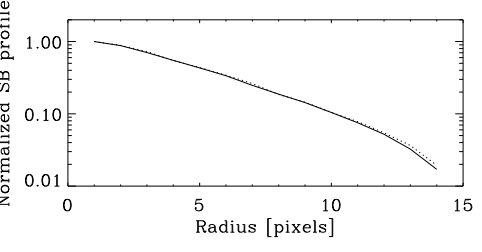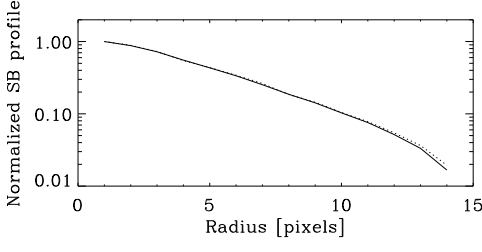
| Single scan | Cross scan |
|:---:|:---:|
| 6″ Reconstructed maps (log scale) | |



| Residuals (histogram-equalized) | |
|:---:|:---:|





| $\sigma$ [mJy/pixel] | 4.3389 | 4.6492 |
|:---|:---:|:---:|
| Total flux ratio | 0.9880 | 0.9898 |
| Mean profile ratio | 0.9690 | 0.9710 |
| Std. Dev. profile ratio | 0.0411 | 0.0415 |
| Execution time | 4m22s | 28m45s |

Table 47: Large Exponential Disk – MOPEX with High Pass Filter
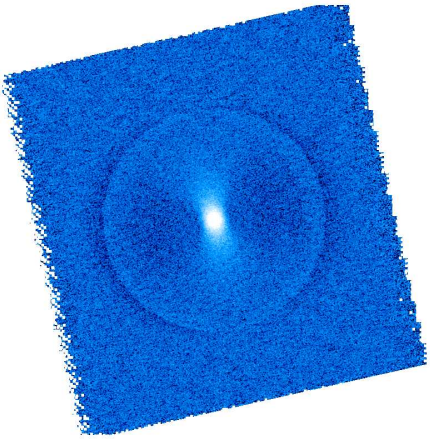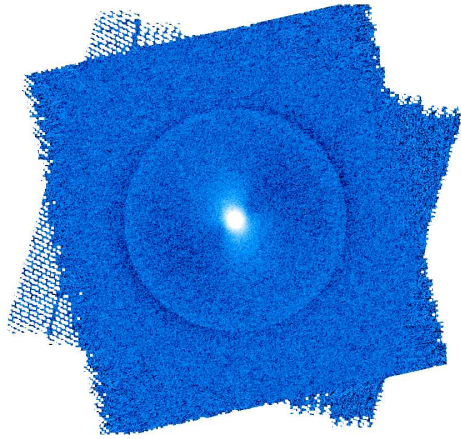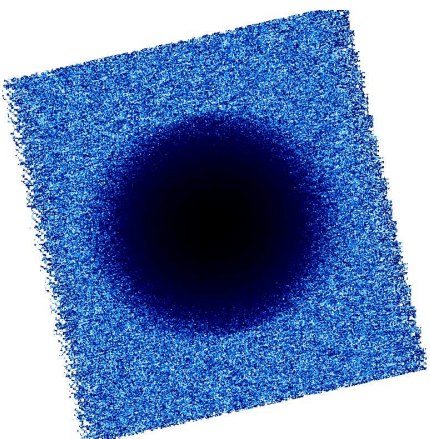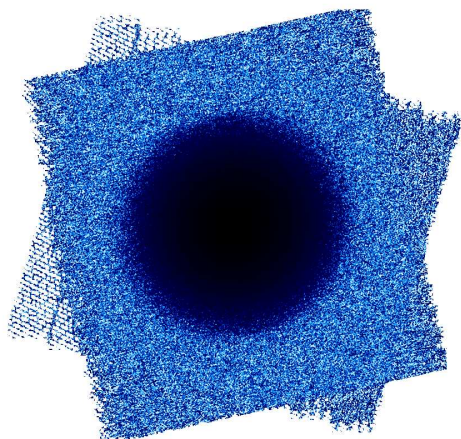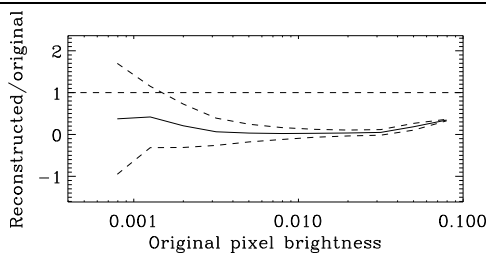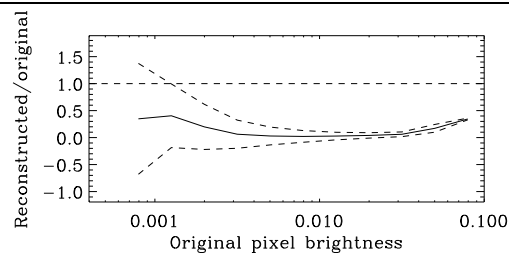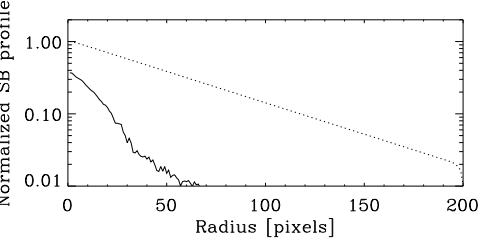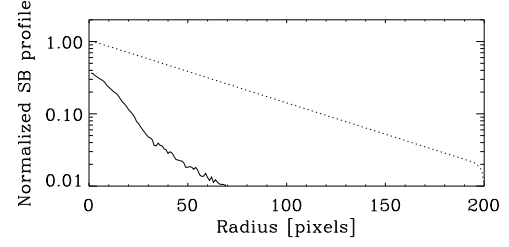
| Single scan | Cross scan |
|:---:|:---:|
| 6″ Reconstructed maps (log scale) | |



| Residuals (histogram-equalized) | |
|:---:|:---:|





| | Single scan | Cross scan |
|:---|:---:|:---:|
| $\sigma$ [mJy/pixel] | 8.5428 | 8.5051 |
| Total flux ratio | 0.0754 | 0.0736 |
| Mean profile ratio | 0.1070 | 0.1067 |
| Std. Dev. profile ratio | 0.1180 | 0.1147 |
| Execution time | 3h39m29s | 12h03m15s |

Table 48: Cirrus – MOPEX with High Pass Filter
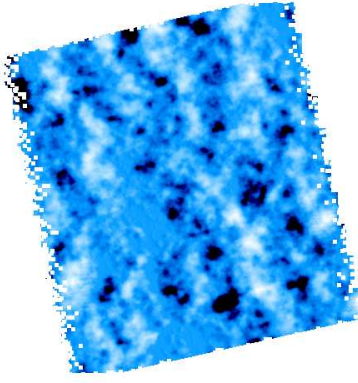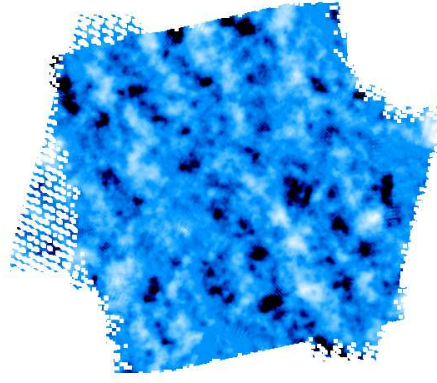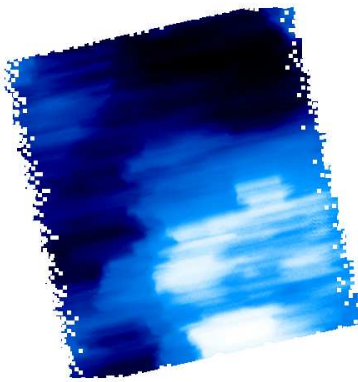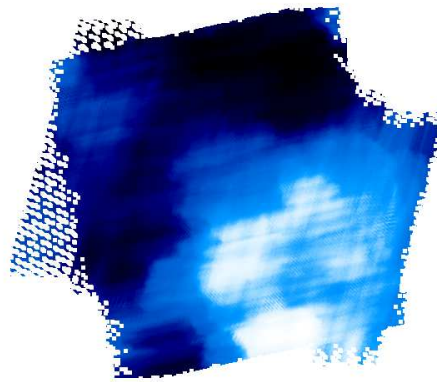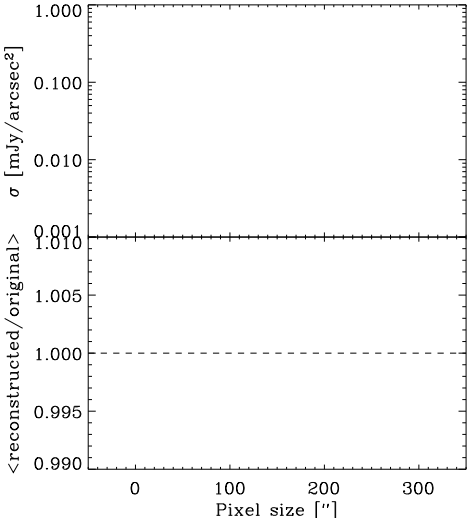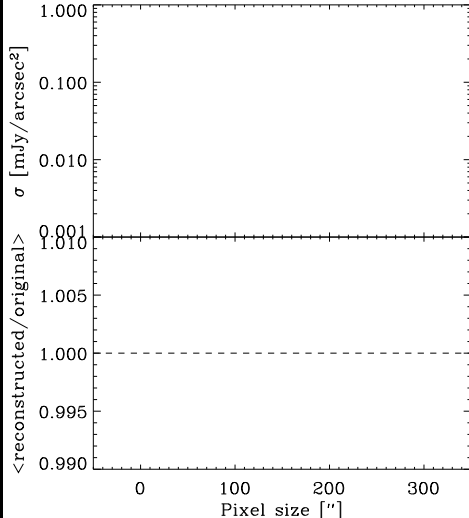
| Single scan | Cross scan |
|---|---|
| 6″ Reconstructed maps (log scale) | |



| Residuals (histogram-equalized) | |
|---|---|





| $\sigma$   [mJy/pixel] | 92.8671 | 92.5398 |
|---|---|---|
| <reconstructed/original> | -0.0020 | -0.0028 |
| Execution time | 17m28s | 1h21m34s |

Table 49: Cirrus with Compact Sources – MOPEX with High Pass Filter
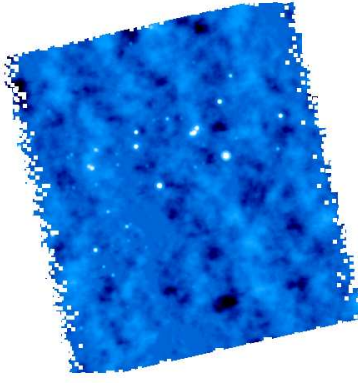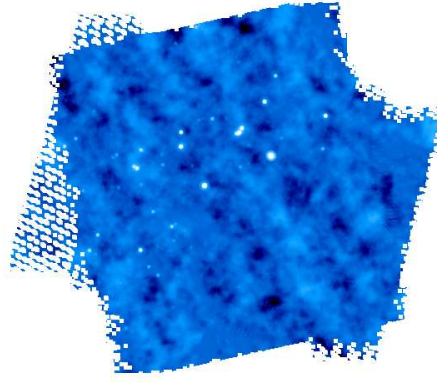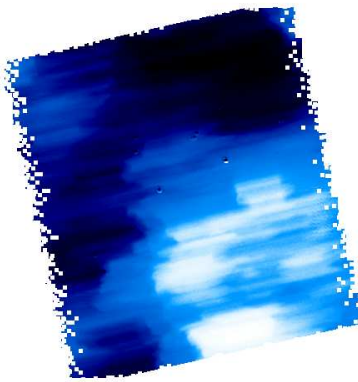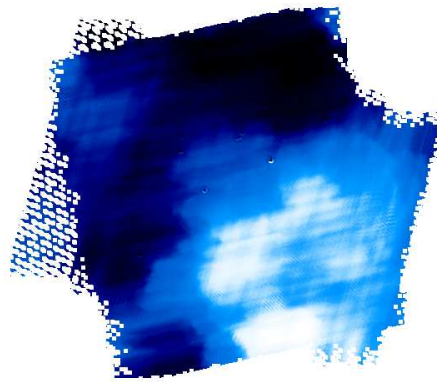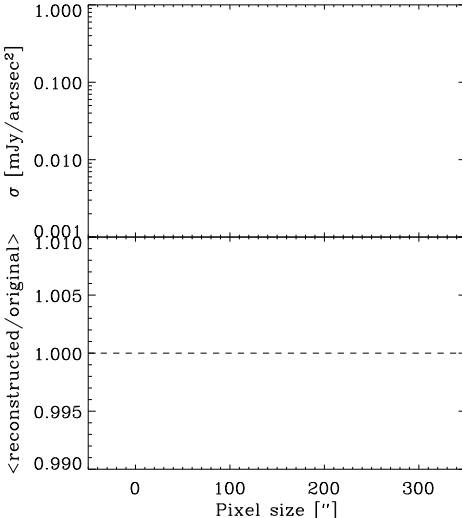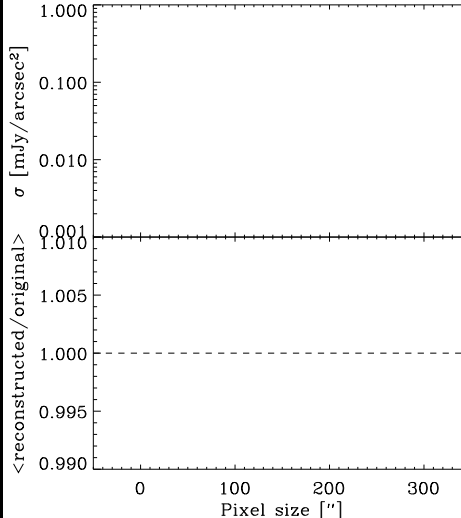
| Single scan | Cross scan |
|---|---|
| 6″ Reconstructed maps (log scale) | |



| Residuals (histogram-equalized) | |
|---|---|





| $\sigma$ [mJy/pixel] | 94.2407 | 93.8885 |
|---|---|---|
| <reconstructed/original> | 0.0002 | -0.0007 |
| Execution time | 16m44s | 1h22m54s |

Table 50: Galics Simulation – Bolocam
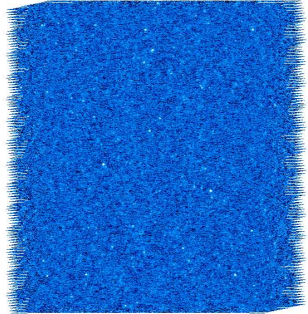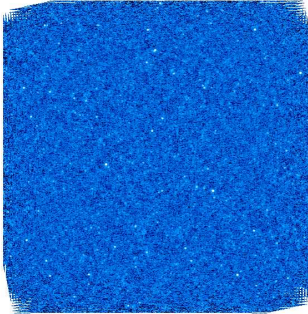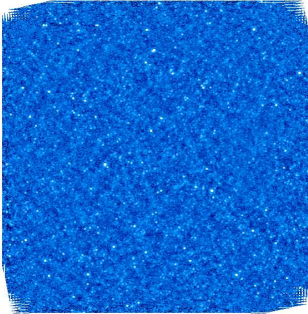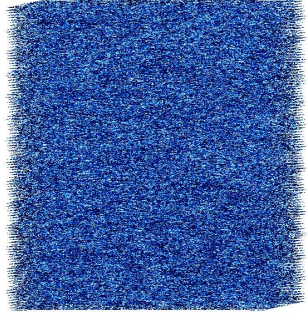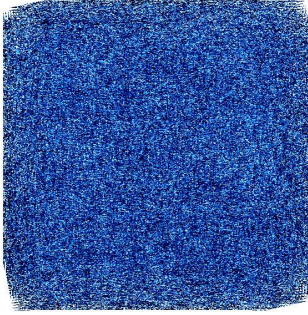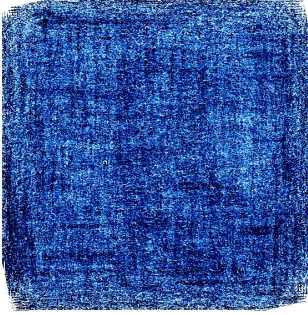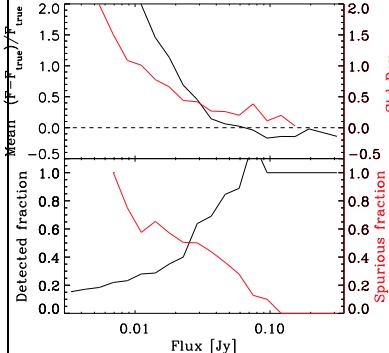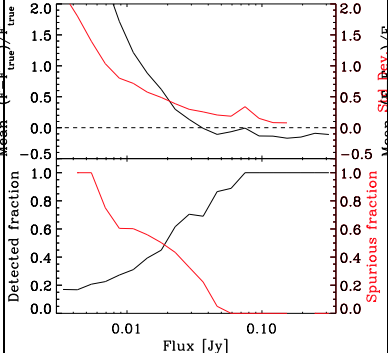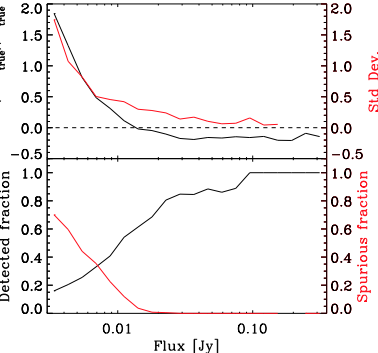
| Single scan | Cross scan | 10 cross scans |
|---|---|---|
| 6″ Reconstructed maps (log scale) | | |
|  |  |  |
| Residuals (histogram-equalized) | | |
|  |  |  |
|  |  |  |
| $\sigma$ [mJy/pixel]   1.2538 | 0.8526 | 0.3063 |
| $N_{crossid.}$   2868 | 3171 | 4105 |
| $N_{spurious}$   2465 | 2282 | 1023 |
| Execution time   15.3s | 25.6s | 4m05s |

Table 51: Grid of Point Sources – Bolocam
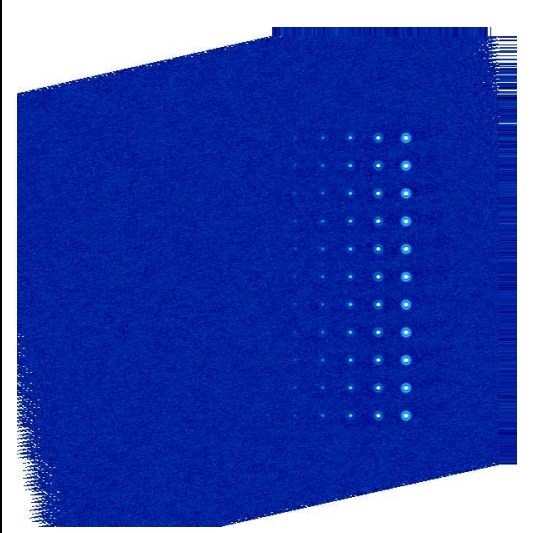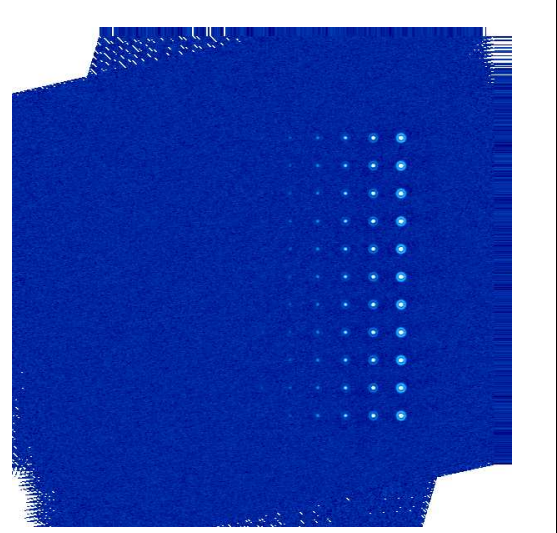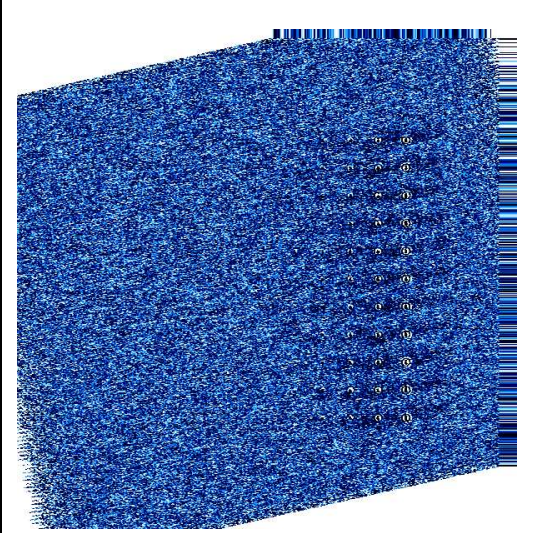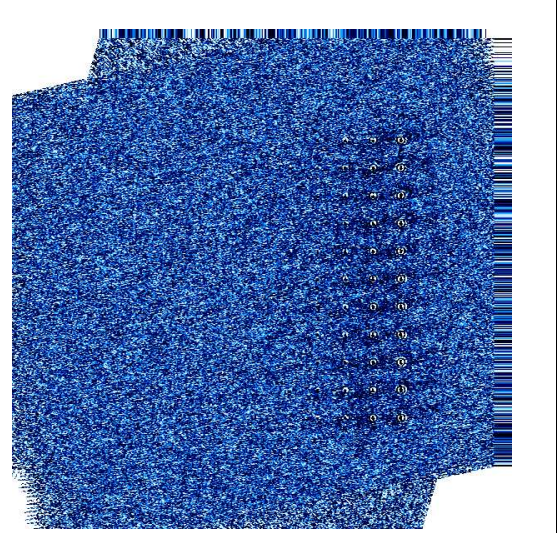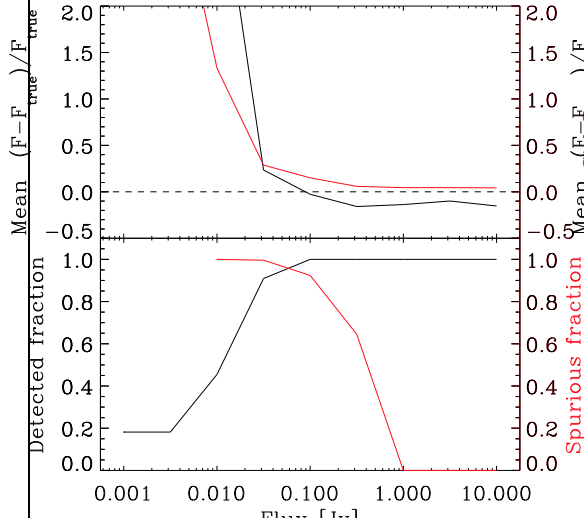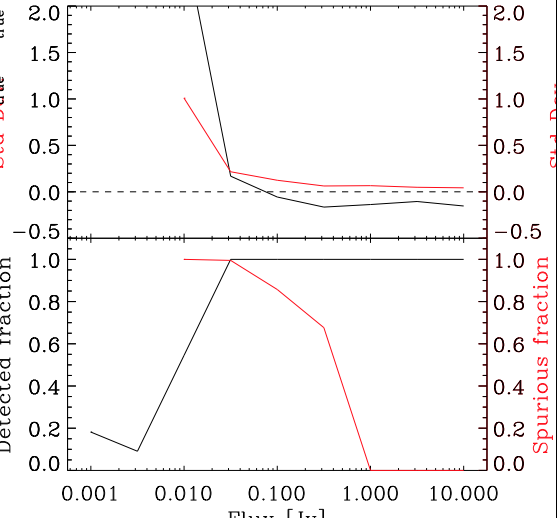
| Single scan | Cross scan |
|---|---|
| 6″ Reconstructed maps (log scale) | |



| Residuals (histogram-equalized) | |



| $\sigma$ [mJy/pixel] | 2.7995 | 2.7674 |
|---|---|---|
| $N_{crossid.}$ | 76 | 78 |
| $N_{spurious}$ | 5079 | 5094 |
| Execution time | 5.1s | 7.2s |

Table 52: NGC 5194 – Bolocam
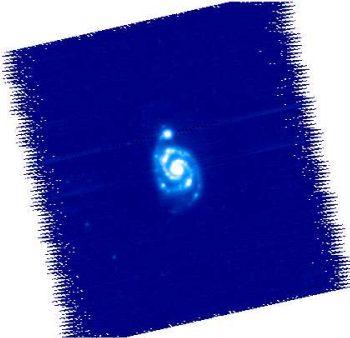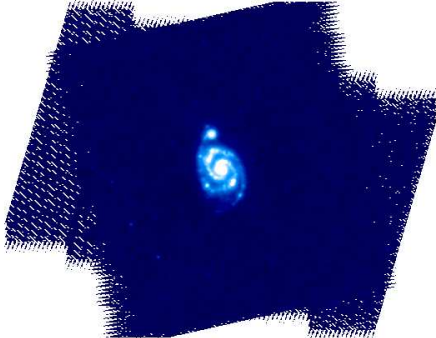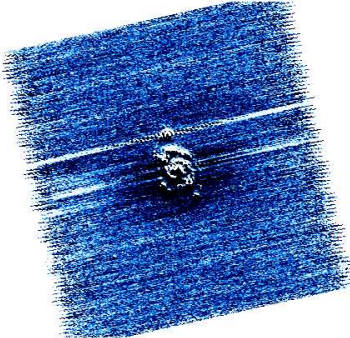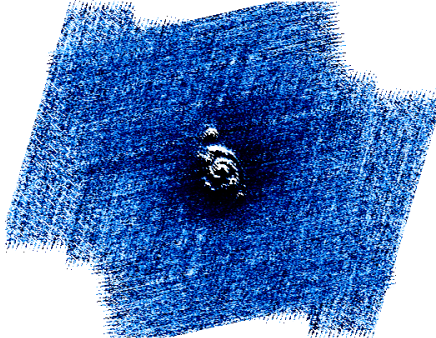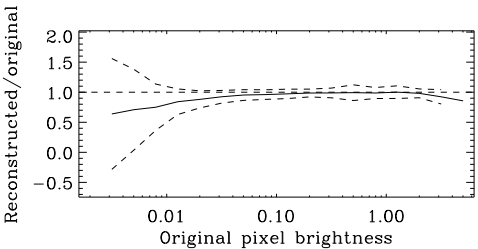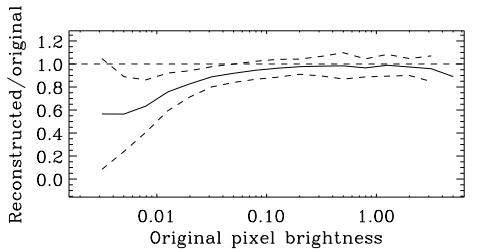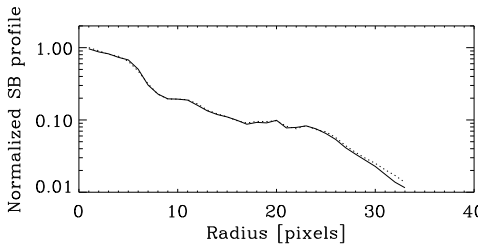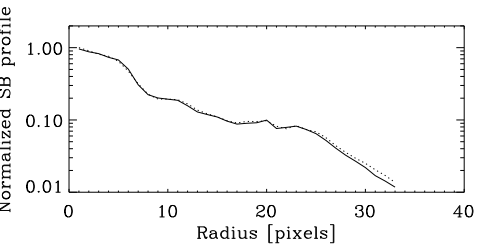
| Single scan | Cross scan |
|---|---|
| 6″ Reconstructed maps (log scale) | |



| Residuals (histogram-equalized) | |
|---|---|





| $\sigma$ [mJy/pixel] | 26.9189 | 25.1206 |
|---|---|---|
| Total flux ratio | 0.9754 | 0.9629 |
| Mean profile ratio | 0.9676 | 0.9603 |
| Std. Dev. profile ratio | 0.0548 | 0.0574 |
| Execution time | 3m34s | 5m06s |

84

Table 53: IC 4710 – Bolocam
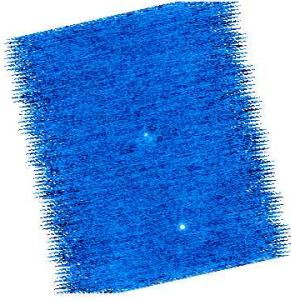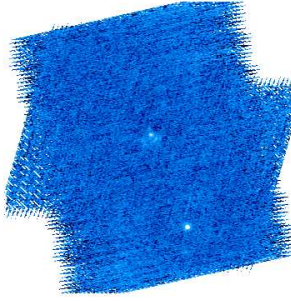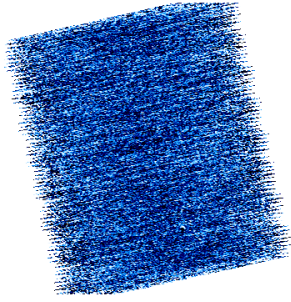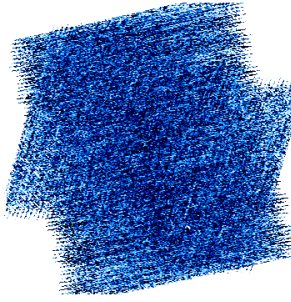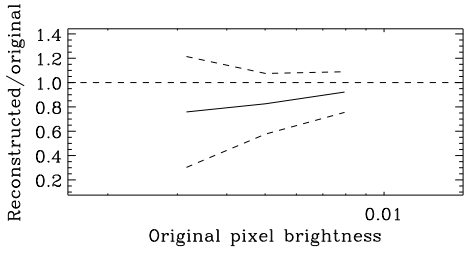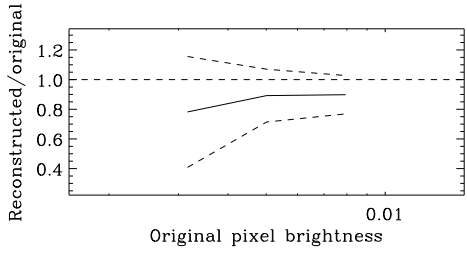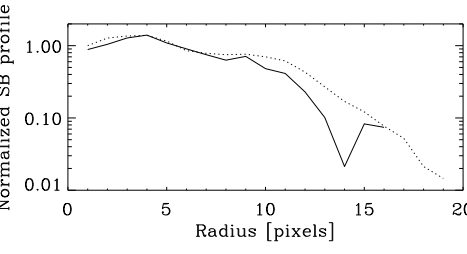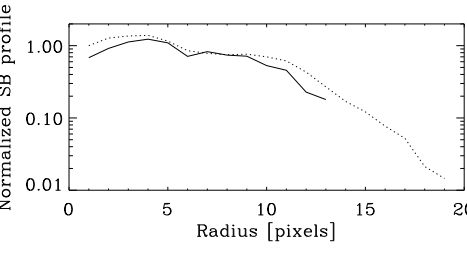
| Single scan | Cross scan |
|---|---|
| 6″ Reconstructed maps (log scale) | |



| Residuals (histogram-equalized) | |
|---|---|





| | Single scan | Cross scan |
|---|---|---|
| $\sigma$ [mJy/pixel] | 1.3629 | 1.1360 |
| Total flux ratio | 0.5899 | 0.7032 |
| Mean profile ratio | 0.2651 | 0.0455 |
| Std. Dev. profile ratio | 1.8116 | 2.2801 |
| Execution time | 13m17s | 18m54s |

Table 54: Small Exponential Disk – Bolocam
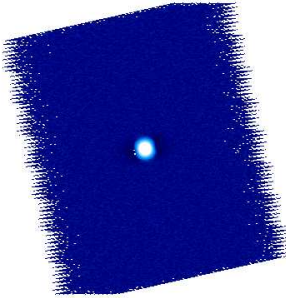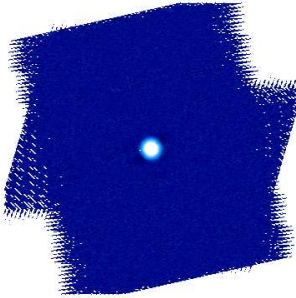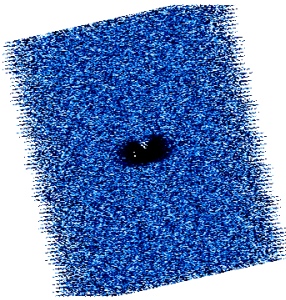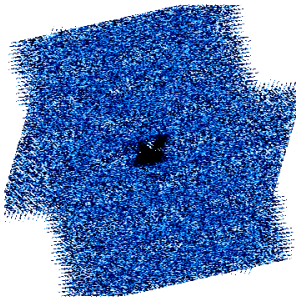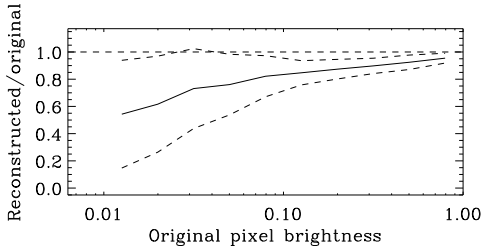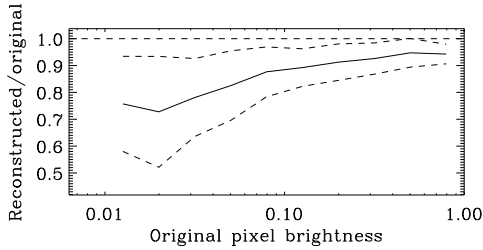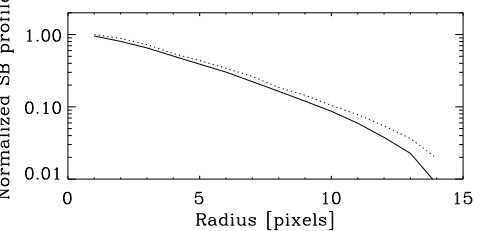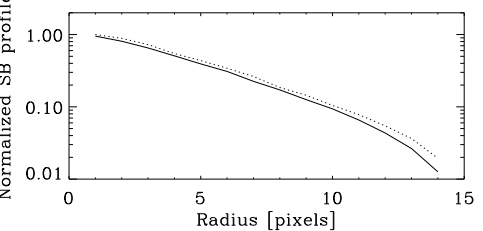
| Single scan | Cross scan |
|---|---|
| 6″ Reconstructed maps (log scale) | |



| Residuals (histogram-equalized) | |
|---|---|



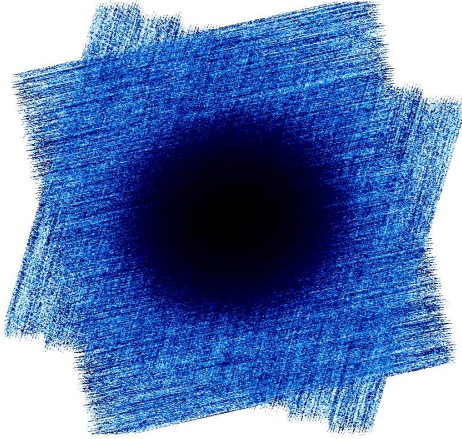| $\sigma$ [mJy/pixel] | 16.7789 | 16.2205 |
|---|---|---|
| Total flux ratio | 0.8794 | 0.9065 |
| Mean profile ratio | 0.8119 | 0.8609 |
| Std. Dev. profile ratio | 0.1406 | 0.0845 |
| Execution time | 5.1s | 7.2s |

Table 55: Large Exponential Disk – Bolocam
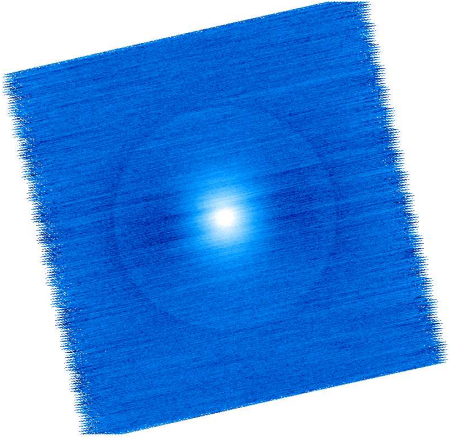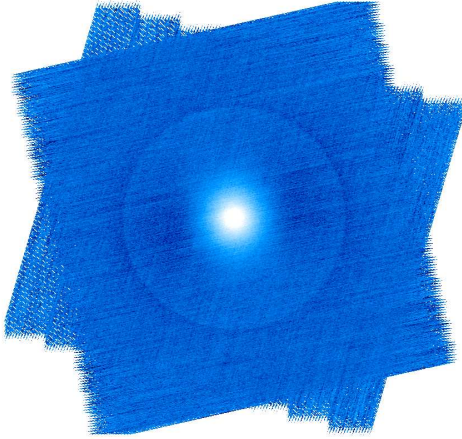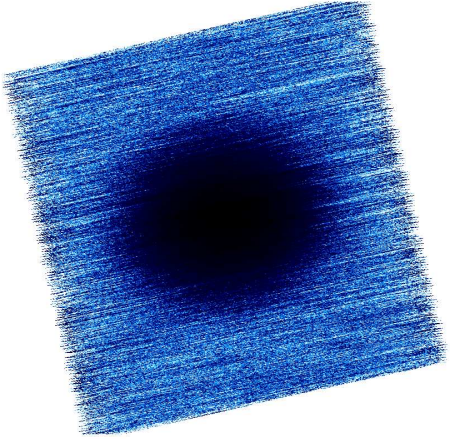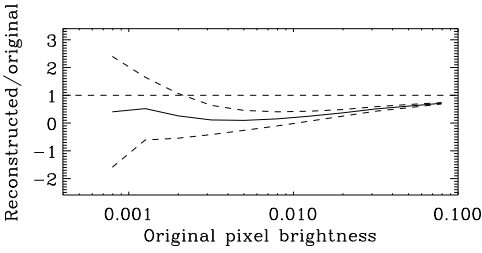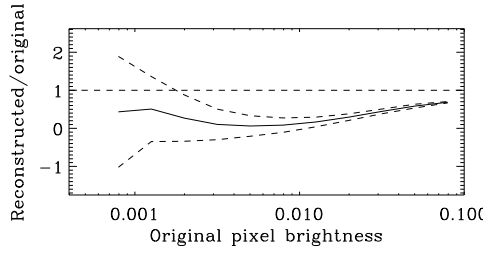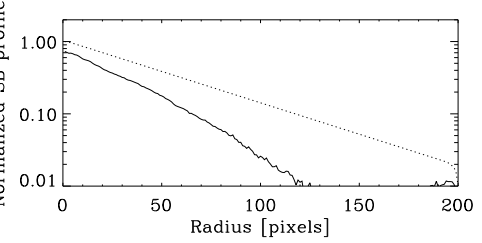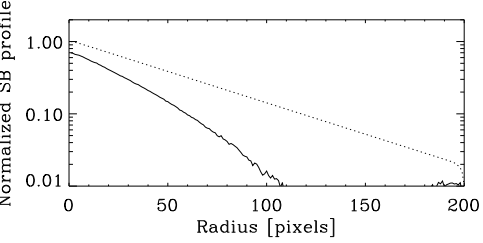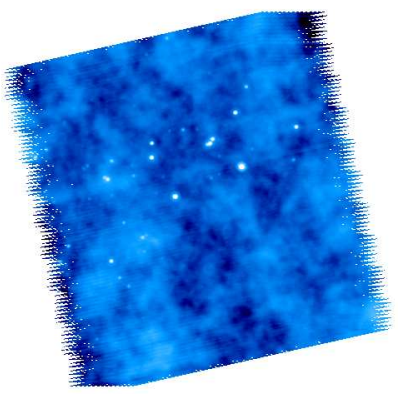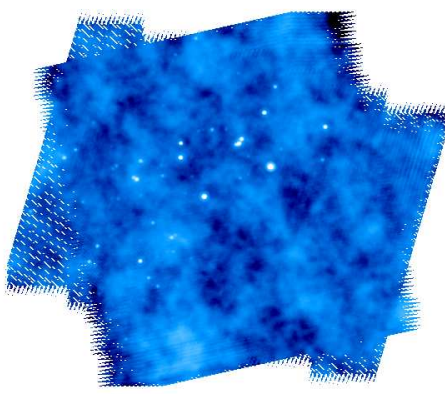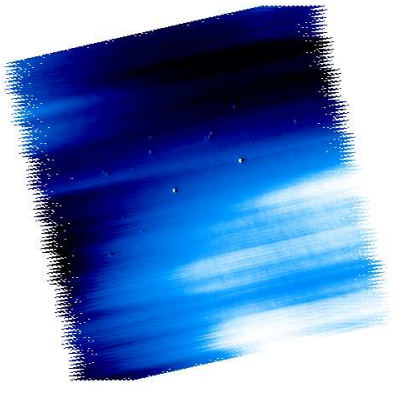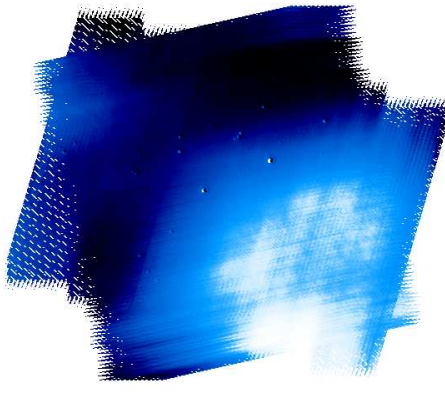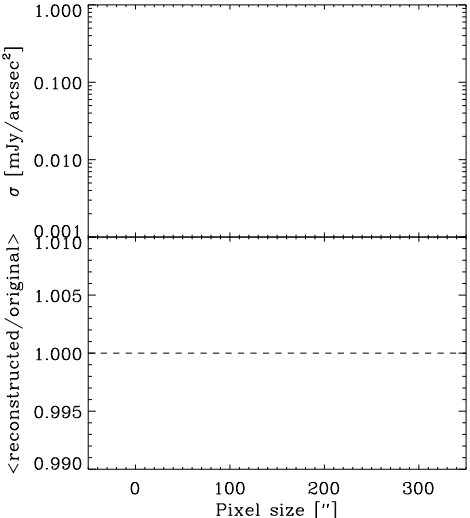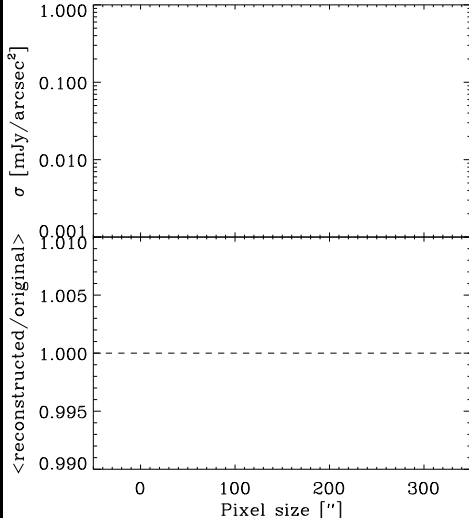
| Single scan | Cross scan |
|---|---|
| 6″ Reconstructed maps (log scale) | |



| Residuals (histogram-equalized) | |
|---|---|





| $\sigma$ [mJy/pixel] | 4.8942 | 5.2480 |
|---|---|---|
| Total flux ratio | 0.3255 | 0.2745 |
| Mean profile ratio | 0.3210 | 0.2793 |
| Std. Dev. profile ratio | 0.1969 | 0.1990 |
| Execution time | 7m40s | 10m44s |

Table 56: Cirrus with Compact Sources – Bolocam

| Single scan | Cross scan |
|:---:|:---:|
| 6″ Reconstructed maps (log scale) | |
|  |  |
| Residuals (histogram-equalized) | |
|  |  |
|  |  |

| | Single scan | Cross scan |
|:---|:---:|:---:|
| $\sigma$ [mJy/pixel] | 86.5302 | 84.8289 |
| <reconstructed/original> | 0.0595 | 0.0571 |
| Execution time | 3m24s | 5m06s |